THE USE OF A THYROID UPTAKE SYSTEM FOR ASSAYING INTERNAL CONTAMINATION FOLLOWING A RADIOACTIVE DISPERSAL EVENT

A Thesis
Presented to
The Academic Faculty

By

Sarah Brashear Scarboro

In Partial Fulfillment
Of the Requirements for the Degree
Master of Science in the
School of Nuclear and Radiological Engineering and Medical Physics

Georgia Institute of Technology

May 2008

THE USE OF A THYROID UPTAKE SYSTEM FOR ASSAYING INTERNAL CONTAMINATION FOLLOWING A RADIOACTIVE DISPERSAL EVENT

Approved by:

Dr. Nolan E Hertel, Advisor
School of Nuclear and Radiological Engineering
and Medical Physics
Georgia Institute of Technology

Dr. Chris Wang
School of Nuclear and Radiological Engineering
and Medical Physics
Georgia Institute of Technology

Dr. Armin Ansari
Radiation Studies Branch
Centers for Disease Control and Prevention

Dr. Rebecca Howell
Assistant Professor, Radiation Physics
University of Texas-Houston
MD Anderson Cancer Center

Date Approved: March 28, 2008

ACKNOWLEDGEMENTS

I must give all credit for this work to God. I have learned that with Him all things are possible, and without Him, nothing. I have learned to lean on His Word and trust His love, knowing that He will also guide me through all my future endeavors.

I want to thank my thesis committee, Dr. Chris Wang, Dr. Armin Ansari, and Dr. Rebecca Howell. Your time and feedback were invaluable and I appreciate everything you have taught me. I want to acknowledge the Radiation Studies Branch of the Centers for Disease Control and Prevention for funding this research. I must also thank Mary Anne Dell from Capintec for loaning Georgia Tech a Captus 3000 Thyroid Uptake System. Without her generosity, this project could not have been completed.

I want to thank Dr. Hertel for being my advisor and mentor. I have learned a great deal from you, both inside and outside the classroom, and have truly enjoyed being one of your students. I also want to thank the rest of Team Hertel for all your contributions to this project. I especially want to thank Eric Burgett and Rebecca Howell. Eric for patiently teaching me MCNP and being my constant support desk, and Rebecca for facilitating all the time I have spent at Emory and for inspiring me to pursue medical physics.

I want to thank my family – especially Mom, Dad, and Laura. You have given more of yourselves than I could ever ask for, and I am who I am because of you. And finally, I want to thank my husband, PJ, for everything you do and everything you are. I cherish your love and support. Thank you for encouraging me through this long process, for sitting with me during late nights of data collection, for discussing this project with me ad nauseaum, for reading countless drafts, and for always loving me. I couldn't have done this without you.

TABLE OF CONTENTS

LIST OF TABLES

LIST OF FIGURES

SUMMARY

This work investigated the use of a common medical device, a thyroid uptake system or thyroid probe, in assessing internal contamination in individuals. In the event of a terrorist act involving a radiological agent, there will be a need to effectively and rapidly screen a large number of people for internal contamination. Using the methodology outlined in this work, those needing further medical assistance can be identified and separated from uncontaminated or very lightly contaminated people. Additionally, this information could be stored in a registry to track population contamination.

A series of measurements and models were used to estimate the response of the thyroid probe to radioactive isotopes in various human phantoms. First, benchmark measurements were made using a polymethyl methacrylate (PMMA) slab phantom and a variety of gamma-ray emitting isotopes. The experimental setup was recreated in a computational model using the Los Alamos Monte Carlo N-Particle Transport Code, MCNP5. [45] The thyroid uptake collimator was also modeled using this code and simulations were completed for each laboratory measurement. A comparison of these results validated the computational model of the thyroid uptake collimator and provided any required normalization factors.

Six anthropomorphic phantoms of varying age and body type were then used in conjunction with the thyroid uptake collimator. These phantoms are based on the Medical Internal Radiation Dose (MIRD) phantoms [7], originally developed at Oak Ridge National Laboratory. Uniformly distributed isotopic sources were placed in all the affected organs according to biokinetic models generated by the Dose and Risk Calculation Software (DCAL). [9]

The results of this work demonstrate that the thyroid uptake probe is a viable tool for assessing internal contamination due to Cs-137, Co-60, I-131, and Ir-192, even at relatively high levels of background. However, this work found that a collimated thyroid uptake probe could not be used to assess individuals internally contaminated with Am-241. The Decision Level (DL) count rate for Am-241 exceeds the expected count rate due to an intake of one Clinical Decision Level (1 CDL is approximately 25 rem) by several orders of magnitude. The most effective location of the thyroid probe for Co-60 and Ir-192 is on the back over the right lung. Two of the isotopes investigated, I-131 and Cs-137, have a recommended lung absorption type of fast. This results in a higher uptake to various tissues, and a smaller fraction of the isotope remaining in the lungs. Thus, for these isotopes, positioning the detector against the neck produces the highest count rate. In general, an increase in body mass index (BMI) adversely affects the count rate per becquerel of activity intake.

CHAPTER 1

INTRODUCTION

After the events of September 11, 2001, the threat of a terrorist act involving chemical, biological, or radiological agents has demanded the attention of government officials and public health agencies. While the ultimate consequence of such an event is difficult to predict, the psychological and economic impact on the United States could be devastating.

With regard to radiological terrorism, weapons are no longer limited to atomic bombs or nuclear devices, such as those used at Hiroshima and Nagasaki. The dispersal of radioactive material into the environment – with or without an associated explosion – is now considered a principal threat. [6] A Radiological Dispersal Device (RDD) is a particular concern due to the widespread use of radioactive materials in foreign and domestic industries. [2]

Radioactive materials are used in the petroleum industry, in health care for diagnostic and therapeutic applications, and in electric power generation. The applications of these materials are as diverse as the isotopes themselves. A work conducted at Sandia National Laboratories examined radioactive materials at facilities licensed by the Nuclear Regulatory Commission (NRC) and controlled and managed by the Department of Energy (DOE). The purpose of the analysis was to determine the relative availability of several nuclear materials and to identify those of greatest concern, or those thought to be most likely used in a RDD. The materials identified by Sandia National Laboratories include Am-241, Cs-137, Co-60, and Ir-192. [36]

One principal health threat resulting from a RDD is internal contamination due to inhalation. Radioactive dust or smoke resulting from an associated explosion or particulate

radioactive materials dispersed into the air could be inhaled and subsequently spread throughout the individual's body. Depending on the isotope, a significant fraction of the intake could remain in the lungs up to several days. This is the optimal window of time to assay internal contamination and make determinations of the need for further medical care to ameliorate the health impact.

Recent publications have examined the feasibility of using a thyroid uptake system to monitor personal internal contamination due to inhalation. [24, 1] As a common nuclear medicine apparatus, the thyroid uptake system is readily available in hospital Nuclear Medicine departments, and is a functional tool for use in an emergency scenario. The ultimate choice in assaying internal contamination, particularly for trace amounts of internal contamination, is a whole body counter (WBC) such as those found at nuclear power facilities. WBCs are highly sensitive, and this level of sensitivity is more than what is needed for emergency triage. In addition, these devices are rarely found in major cities, and in the absence of WBCs, other common radiation detectors have been considered for the rapid and effective triage of potentially contaminated victims.

This work attempts to determine count rates corresponding to various Clinical Decision Levels (CDLs) using Monte Carlo simulation techniques for the Captus 3000 Thyroid Uptake System. For the purpose of this work, one CDL is defined as the intake that results in 25 rem of committed effective dose. [34] This unit was recommended by the Centers for Disease Control and Prevention to be used to quantify count rate thresholds for emergency procedure protocols. Six Medical Internal Radiation Dose (MIRD) phantom types were also examined to estimate the effects of body type and body mass index on the count rates.

CHAPTER 2

LITERATURE REVIEW

In addition to many individuals and organizations, the Centers for Disease Control and Prevention (CDC) and the Nuclear Regulatory Commission (NRC) have published several recent documents concerning emergency medical response to a RDD. These documents include feasibility reports, guidelines, and evaluations of current levels of preparedness. One such document, published by the Belgian Nuclear Research Center, discussed the direct and indirect effects of a radiological attack on a populous area. The direct and immediate effects could include death, injury, contamination, and societal chaos. Delayed effects regarding contamination of food or water supplies and the economic ramifications of such a disaster also present a unique problem. [39] The principal concern is a need for preparedness – both in emergency response and in addressing the long-term effects of such an event.

Several studies have addressed the risk and potential dose to healthcare providers treating contaminated victims following a radiological terrorist event. According to surveys conducted among medical personnel, there exists a significant concern about the risk associated with treating a radioactively-contaminated patient. Despite these concerns, medical guidelines state that the treatment of life-threatening injuries and medical stabilization of a patient should not be delayed for decontamination efforts. [38]

The standard for assessing contamination (both internal and external) in radiation occupations is a Whole Body Counter (WBC). A WBC is generally constructed of an array of NaI(Tl) detectors surrounded by some back-ground reducing material. WBCs can be orientated such that the individual walks into or through the detectors. Numerous studies have been

conducted on the efficiency and sensitivity of WBCs for applications both in emergency response and occupational monitoring. One emergency scenario in which a WBC was employed was following the Cs-137 accident in Goiania, Brazil. This system was constructed in the field using a 20 cm NaI(Tl) mounted approximately 2 m off the ground in a small room. This detector was used to successfully assay over 300 people following the accident. [33]

Internal contamination is a primary cause of committed effective dose to the victim following an RDD. The development of instruments and protocols to estimate internal contamination is the topic of recent studies conducted at the Georgia Institute of Technology. These studies have examined a variety of instruments for both their feasibility and efficiency in detecting internal contamination due to inhalation of radioactive material.

A study conducted by S. Cohen and Associates [1] evaluated the feasibility of using various hospital radiation detectors to assess internal contamination from inhaled radionuclides. The detection systems included in this study are commonly found in hospitals, especially those performing nuclear medicine studies. Based on simulations using an acrylic slab phantom and a water filled phantom, the SC&A study concluded that the gamma camera, thyroid uptake system, and waste monitor are each capable of detecting low levels of radiation and can potentially be used in the aftermath of a terrorist event.

With regard to the thyroid uptake system, the SC&A investigation looked specifically at the Atomlab 950 Thyroid Uptake System. The Atomlab 950 consists of a 2" by 2" NaI crystal with a lead collimator extending approximately six inches from the detector face. This is the same thyroid uptake system that was the primary focus of a thesis completed by Ryan Lorio. [24] The Lorio work also sought to examine the feasibility of using a thyroid uptake system for

estimating dose to individuals following a terrorist event; and furthermore, it sought to develop a validated Monte Carlo model of this probe to estimate uptake to the lungs.

While the work completed by Lorio proved that the use of this system is feasible following an RDD, the models considered did not include the movement of an isotope through the body, or the fraction remaining in various organs over time. To further refine the conclusions, this work will include biokinetic modeling while determining the detector response for internal contamination from various phantom types.

CHAPTER 3

METHODOLOGY

3.1 Captus 3000 Thyroid Uptake System Overview

The Captus 3000 Thyroid Uptake System is manufactured by Capintec, Inc, and is a fully automated, PC-based system which is typically used to perform thyroid uptake tests, bioassay tests, and other lab tests. The system includes two 2" Sodium-Iodide (NaI) detectors mounted on articulating spring arms, a 1024-channel multi-channel analyzer (MCA), and several modules for calibration, measurements, and reporting. Both detectors are collimated with a lead-antimony composite material. The thyroid uptake collimator is longer, extending approximately 16 centimeters from the detector face. The bioassay collimator is shorter, extending only approximately six centimeters from the detector. All Captus 3000 thyroid uptake systems include the thyroid uptake collimator while the bioassay collimator is an optional feature. The focus of this work is on the standard thyroid uptake collimator. The system stores patient information and demographics as well as all collected spectral or counting data. These features are very useful for generating detailed thyroid uptake reports and staff bioassays; reports can be saved and printed as individual reports or as a cumulative history. The Captus 3000 system is shown in Figure 3.1.1.

Figure 3.1.1 Capintec Captus 3000 Thyroid Uptake System with thyroid uptake collimator.

As specified in the user's manual, the Captus 3000 must be auto-calibrated using two calibration sources (Cs-137 and Eu-152, included with system) daily before measurements are collected or tests are performed. In addition, the chi-squared calibration test must be performed before initial use, and then quarterly. All calibration tests were performed successfully at Georgia Tech prior to data collection.

The manual MCA interface was used for all measurements in this work. The MCA calibration is set to 2 keV per channel, allowing it to bin pulse-height data for gamma energies up to 2 MeV. The MCA system is equipped to automatically identify the regions of interest (ROI) based on an isotope selection. It is unrealistic to expect emergency operators to manually adjust the ROIs in the field. Therefore, the system default ROIs set on photopeaks were used in both the data collection and the model validation. Each MCA spectrum report was exported as a spreadsheet and saved, allowing background correction and data analysis.

3.2 Measurements using PMMA Slab Phantom

The thyroid uptake collimator was used to make a series of benchmark measurements with various isotopes. The measurements were made using a slab phantom composed of polymethyl methacrylate (PMMA) and virtual water. PMMA was chosen for its attenuation properties, which are similar to those of human tissue. Virtual Water™ (MED-CAL, Inc., Verone, WI) [43] was used as backscatter material, placed furthest from the detector face and behind the source. The thickness of the backscatter material was 10-cm for all measurements. A 6-mm thick PMMA 'source holder' was placed flush against the virtual water. A cylindrical hole in the center of the source holder contained the source, preventing the source from shifting during measurements. Slabs of PMMA were placed in front of the source holder to increase or decrease the thickness of attenuating material between the source and the detector. The experimental set-up used for measurements with the PMMA slab phantom is shown in Figure 3.2.1.

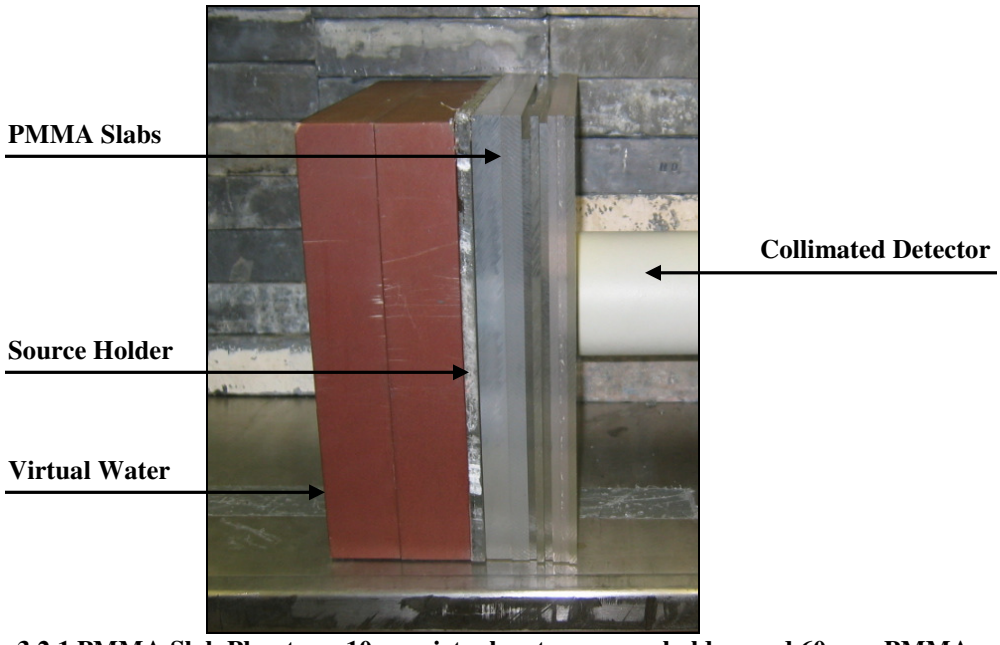

Figure 3.2.1 PMMA Slab Phantom: 10 cm virtual water, source holder, and 60 mm PMMA

The source was centered on the opening of the collimator, and taped in place to prevent movement during a set of measurements. The source position relative to the detector face is shown in Figure 3.2.2. The position of the source holder relative to the PMMA, Virtual Water, and detector is shown above in Figure 3.2.1.

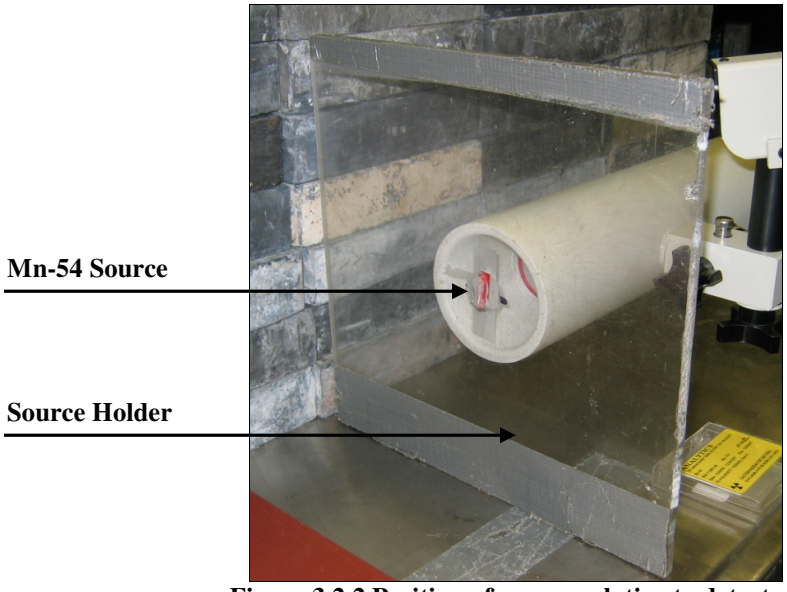

Figure 3.2.2 Position of source relative to detector.

Some of the isotopes of greatest concern for use in a RDD are Co-60, Cs-137, and Am-241. These isotopes, along with three others, were used to encompass a broad range of gamma-ray energies. This selection was based largely on the availability of the sources. The isotopes that were used in detector characterization and their associated photon energies and intensities (Rad Toolbox) [8] are shown in Table 3.2.1

Table 3.2.1 Selected isotopes and photon energies for benchmark measurements and detector validation

Isotope	Photon Energy, MeV	Photon Emission Intensity
Am-241	0.059, 0.026, 0.021, 0.0179, 0.0177, 0.017, 0.0168, 0.0139, 0.0137	0.357, 0.024, 0.045, 0.019, 0.188, 0.022, 0.058, 0.219, 0.024
Ba-133	0.384, 0.356, 0.303, 0.276, 0.081, 0.035, 0.031, 0.030	0.089, 0.622, 0.184, 0.071, 0.338, 0.122, 0.631, 0.341
Cs-137	0.662	0.853
Co-60	1.332, 1.173	0.999, 0.999
Mn-54	0.8348	0.999
Na-22	1.275, 0.511	0.999, 1.798

For each measured isotope, a spectrum was collected for PMMA thicknesses ranging from 0-mm to 108-mm in six millimeter increments. Counting time was determined based on counting in the ROI. A minimum of 10,000 counts before background subtraction (corresponding to 1% counting error under the peak) was specified for each thickness.

Background corrections were applied to the spectra outside of the Capintec software. Before each set of measurements, a ten minute background spectrum was acquired and then subtracted from each of the measured spectra. No other corrections were made to the raw data.

3.3 Detector Model and Validation

The benchmark measurements were used to validate a computational model of the thyroid uptake collimator and detector. The purpose of this model was to accurately represent the detector so that simulations on contaminated 'people' could be performed using computer models. Details concerning the detector and slab phantom computational model are discussed in Chapter 4.

The detector response was calculated for the same PMMA thicknesses as the benchmark measurements. Also, the response to each isotope was calculated separately to ensure that the detector model was validated over a range of gamma-ray energies.

The measured pulse-height spectra were individually integrated over the entire spectrum, and over each photopeak. These values were compared to the corresponding calculated detector response for each isotope and each thickness of PMMA. Validation of the model requires that the ratio of calculated to measured count rate is constant over the range of attenuation thicknesses.

3.4 Development of Emergency Screening Protocols

The validated detector model was used to simulate the detector response on an internally contaminated human. Medical Internal Radiation Dose (MIRD) male and female phantoms based on the reference man were used. These phantoms were originally developed at Oak Ridge National Laboratory. [7] The MCNP models of the reference male and female phantoms were developed at the Pacific Northwest National Laboratory in the late 1980's. These phantoms have been used and further refined at the Georgia Institute of Technology in dose conversion coefficient studies in recent years. One of the major works at Georgia Tech on these phantoms was the addition of adipose tissue to the reference male and female phantoms to create three additional phantoms: Adipose Male, Adipose Female, and Post-Menopausal Adipose Female. [37] Other modifications made to the phantoms include the addition of an esophagus and a walled colon. A child phantom was created using the Bodybuilder Phantom [44] and included in the simulations. In total, six anthropomorphic phantoms were used: Male, Female, Adipose Male, Adipose Female, Post-Menopausal Adipose Female, and a 10-year-old Child.

Five sources were chosen based on those noted by the Nuclear Regulatory Commission as being "isotopes of greatest concern.' [6] These sources (Cs-137, Co-60, Am-241, I-131, and Ir-192) have distributions in various organs in the human body as a function of time when inhaled. To fully characterize the isotopes behavior in the body, the isotopes were distributed throughout the organs based on biokinetic models for inhalation. Details concerning biokinetic modeling are further described in Chapter 5. Table 3.4.1 shows the energy and intensity for the five isotopes of concern used in conjunction with the anthropomorphic phantoms.

Table 3.4.1 Selected isotopes and photon energies for use with anthropomorphic phantoms

Isotope	Photon Energy, MeV	Photon Emission Intensity
Am-241	0.059, 0.026, 0.021, 0.0179, 0.0177, 0.017, 0.0168, 0.0139, 0.0137	0.357, 0.024, 0.045, 0.019, 0.188, 0.022, 0.058, 0.219, 0.024
Cs-137	0.662	0.853
Co-60	1.332, 1.173	0.999, 0.999
I-131	0.364, 0.637, 0.284, 0.723	0.812, 0.727, 0.606, 0.018
Ir-192	0.317, 0.468, 0.308, 0.296, 0.604, 0.612, 0.589, 0.485	0.828, 0.478, 0.297, 0.290, 0.0818, 0.0533, 0.0452, 0.0316

The detector was placed in four locations on the male phantom: front right lung, the back right lung, the front of the neck, and the outer left thigh. The other four adult phantoms have significantly more breast tissue than the male phantom. Thus, the front right lung position was excluded for these phantom types (due to the attenuation caused by breast tissue).

Computer simulations were completed for each combination of phantom and isotope, yielding 30 combinations. The completed simulations are shown in Table 3.4.2.

Table 3.4.2 Anthropomorphic Phantom Simulations Completed

Phantom Type	Isotope
Male	Cs-137
Male	Co-60
Male	Am-241
Male	I-131
Male	Ir-192
Female	Cs-137
Female	Co-60
Female	Am-241
Female	I-131
Female	Ir-192
Adipose Male	Cs-137
Adipose Male	Co-60
Adipose Male	Am-241
Adipose Male	I-131
Adipose Male	Ir-192
Adipose Female	Cs-137
Adipose Female	Co-60
Adipose Female	Am-241
Adipose Female	I-131
Adipose Female	Ir-192
Post Menopausal Adipose Female	Cs-137
Post Menopausal Adipose Female	Co-60
Post Menopausal Adipose Female	Am-241
Post Menopausal Adipose Female	I-131
Post Menopausal Adipose Female	Ir-192
Child	Cs-137
Child	Co-60
Child	Am-241
Child	I-131
Child	Ir-192

3.5 Considerations of the Decision Level and Minimum Detectable Activity

The minimum detectable activity (MDA) for each isotope was considered to establish count rate thresholds for the thyroid uptake collimator. First, a decision level (DL) is defined as the net count rate indicating the presence of radioactive material with some predetermined confidence level. A general expression for this limit is shown in Equation 3.5.1. [40]

$$\text{DL (counts per minute)} = 1.645\sqrt{\mathbf{R_b}\left(\frac{1}{\mathbf{t_b}}+\frac{1}{\mathbf{t_g}}\right)} \qquad \text{[Eqn 3.5.1]}$$

In this expression,

R_b = background count rate

t_b = background counting time

t_g = gross counting time

The MDA is a value of activity that would result in a count rate less than the DL a certain fraction of the time. This occurrence is a false negative, because there is actual activity present, but the system does not identify it based on the set decision level. It is generally accepted to specify a 5% false negative rate. An expression for the MDA is shown in Equation 3.5.2. [40]

$$\text{MDA in } \mu\text{Ci} = \frac{3+3.29\sqrt{R_b t_g\left(1+\frac{t_g}{t_b}\right)}}{Kt_g} \qquad \text{[Eqn 3.5.2]}$$

In this expression,

K = counting yield, or counting efficiency.

The MDA should not be compared to the measured count rate as it is a performance indicator for the counting system. Instead, the determined DL should be compared to the count rate as an indicator for the presence of activity in the sample. For this work, the calculated count rates were compared to the DL count rate for various counting times and background levels. These results are described in Chapter 6, Section 3.

3.6 Considerations of the Minimum Detectable Dose

The minimum detectable dose (MDD) is a valuable quantity for bioassay applications. The MDD is directly proportional to the MDA and takes into account the biological half-life and

retention fraction of a particular isotope. An expression for the MDD is shown in Equation 3.6.1. [40]

$$MDD = \frac{MDA}{Y_{RC} V_{bio} IRF_u(\Delta t)} \times h_{E,50} \qquad \text{[Eqn 3.6.1]}$$

In this expression,

Y_{RC} = radiochemical yield of the isotope of interest

V_{bio} = biological variability in excretion rates and volumes

IRF_n = intake retention fraction, or the fraction of the intake that remains in any bioassay compartment

Δt = time between intake and the bioassay measurement

$h_{E,50}$ = 50-year committed effective dose per unit inhake (ICRP 1994)

MDD values are not directly relevant to the intent of this work, therefore they were not calculated.

CHAPTER 4

COMPUTATIONAL MODELS

Computational models were developed to accurately represent the response of various detection systems to internal contamination in humans. The Los Alamos Code, MCNP Version 5 [45], was used to simulate the photon transport essential to replicating the response of the thyroid uptake collimator and detector. The results of these simulations allow validation of the methodology by comparison with experimental measurements. These computational models can also be used for comparison to other studies involving thyroid uptake counters. A summary of the computational models used in this research is included below, including the use of various human phantoms internally contaminated with the five selected isotopes.

4.1 Thyroid Uptake Collimator Model

The thyroid uptake collimator was modeled using the Los Alamos N-Particle Transport Code MCNP5. [45] Specifications from Capintec were used to model the critical components of the detector and collimator. The NaI detector crystal was manufactured by Saint Gobain [35] and is surrounded by 0.508 mm of Aluminum. The photomultiplier tube is mounted directly against the back of the crystal, and was represented by an enclosed cylindrical vacuum in the model. A detector side shield (3.175 mm thick lead) wraps around the detector and connects to the collimator. The 2" x 2" Ø NaI crystal and photomultiplier tube are housed in a lead and antimony collimator, which extends approximately 16 cm from the face of the crystal. The entire collimator is enclosed in an outer steel layer that is painted. The layer of paint was not included in the model. A cross-sectional view generated with the VisEd program [46] of the model and a side view of the actual collimator is shown in Figure 4.1.1.

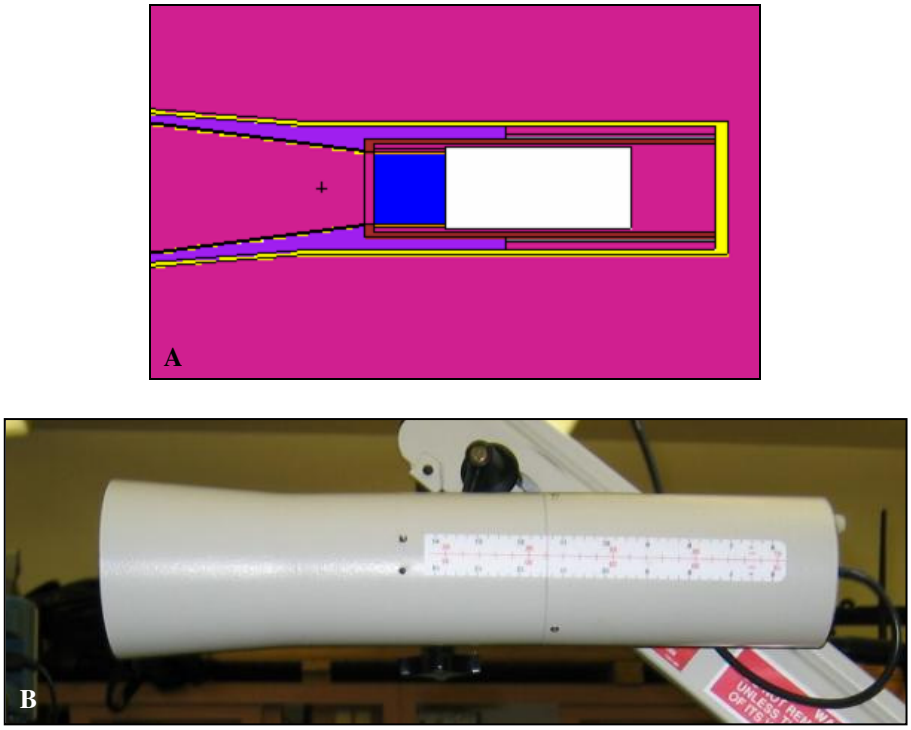

Figure 4.1.1 (A) MCNP model of thyroid uptake collimator as displayed in VisEd; (B) Captus 3000 thyroid uptake collimator

The material compositions of the various components were either obtained from the Capintec drawings, or were selected based on industry standards. The exact material compositions used in the thyroid uptake collimator model are shown in Table 4.1.1 and Table 4.1.2.

Table 4.1.1 Material composition of steel used in Thyroid Uptake Collimator model by atom fraction

	Density	Carbon	Oxygen	Phosphorus	Manganese	Iron
AISI 1000 [26]	7.82 g/cc	0.002786	8.687E-5	7.1946E-5	0.003549	0.9935

Table 4.1.2 Material compositions of materials used in Thyroid Uptake Collimator model by atom fraction

	Density	Aluminum	Copper	Zinc	Antimony	Lead
Brass	8.4 g/cc		0.65	0.35		
Antimonal Lead	11.4 g/cc				0.04	0.96
Lead	11.4 g/cc					1
Aluminum	2.7 g/cc	1				

4.2 Slab Phantom Model

The slab phantom was modeled in MCNP5 for the purpose of simulating the benchmark measurements made in the laboratory. Variations of the slab phantom were created to represent each thickness of PMMA used in laboratory measurements. The compositions of the PMMA and Virtual Water are shown in Table 4.2.1.

Table 4.2.1 Material compositions of PMMA and Virtual Water by weight percent

	Density	Hydrogen	Carbon	Nitrogen	Oxygen	Chlorine	Calcium
PMMA [24]	1.19 g/cc	0.5333	0.3333		0.1333		
Virtual Water [43]	1.03 g/cc	0.08056	0.6733	0.02149	0.2000	0.001406	0.02320

Each source was modeled and placed at the same position in the PMMA source holder. The single isotope sources were fully encapsulated with activities ranging from 1.813×10^5 Bq to 2.775×10^5 Bq. Each source was approximately 2.3-cm in length and 0.4-cm in diameter. Figure 4.2.1 illustrates the source position relative to the collimator in the computational model.

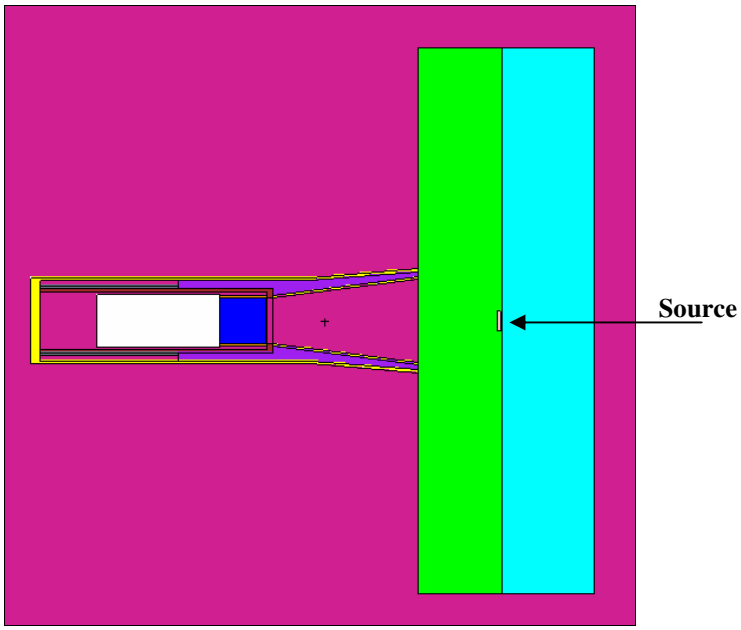

Figure 4.2.1 Cross-sectional VisEd representation of the slab phantom and thyroid uptake probe with source positioning.

A pulse height tally (MCNP F8 tally) was performed over the NaI crystal volume for the photons (shown in Table 3.2.1) emitted by the sources. MCNP tallies are normalized by the code to an emission of one source particle. The tally output must then be multiplied by the exact activity of the laboratory source and branching ratios for a direct comparison. For four of the isotopes used in the detector validation (Co-60, Am-241, Ba-133, Na-22), multiple gamma-rays are emitted for every particle disintegration. In this case, the sum of the branching ratios (or the total number of photons emitted per decay) is used. The branching ratios used are shown in Table 4.2.2.

Table 4.2.2 Total branching ratio for each isotope used in slab phantom calculations

Isotope	Branching Ratio
Am-241	0.9592
Ba-133	2.3966
Cs-137	0.8528
Co-60	1.9988
Mn-54	0.9997
Na-22	2.7974

A VisEd generated simulation of the emissions from the source and collisions in the surrounding materials as sampled in MCNP is shown in Figure 4.2.2.

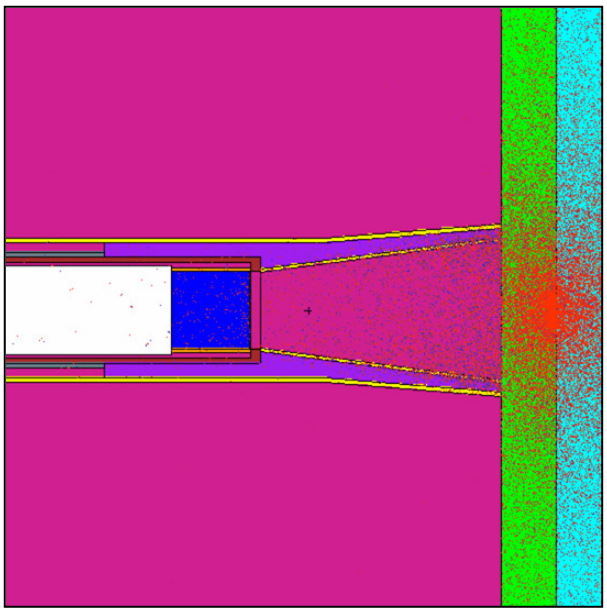

Figure 4.2.2 VisEd representation of the emissions from the source and collisions in surrounding materials

A Gaussian Energy Broadening (GEB) smoothing function available as an option in MCNP was used to simulate the detector resolution. The GEB function is intended to provide a simple analytical function that represents the full width at half maximum of the physical detector to broaden the MCNP computed pulse-height spectrum to simulate the energy resolution of the detector. In the raw MCNP tally, all photoelectric interactions lead to a single energy electron rather than a resolution broadened photopeak. To illustrate the effect of the GEB smoothing function, a comparison of the raw MCNP tally, a GEB smoothed MCNP tally, and a measured spectrum for Cs-137 are shown in Figure 4.2.3.

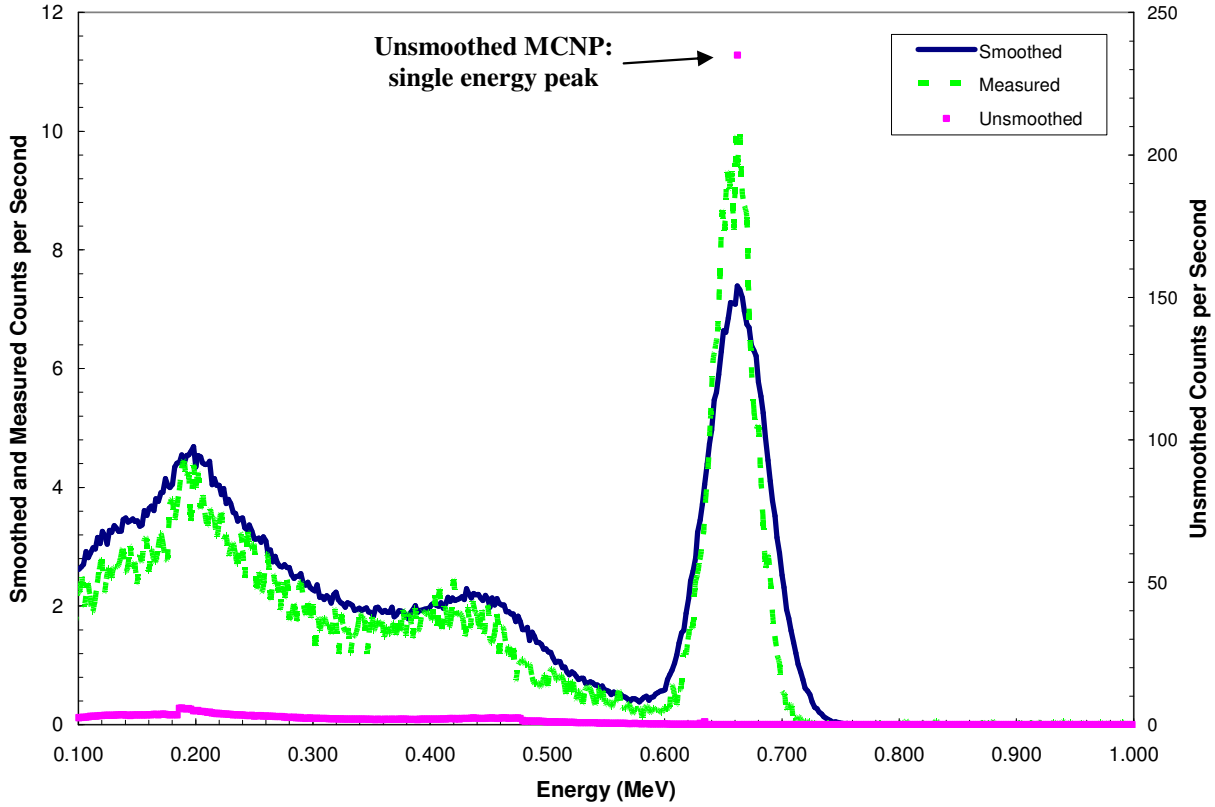

Figure 4.2.3 Comparison of Measured Spectrum with Smoothed and Unsmoothed Calculated Spectra

The parameters required for the GEB function (***a***, ***b***, and ***c***) were calculated based on the measured detector response for Co-60 (1.17 MeV and 1.33 MeV) and Na-22 (0.511 MeV). The expression used to determine these three parameters is shown in Eqn 4.2.1

$$FWHM = a + b\sqrt{E + cE^2} \qquad \text{[Eqn. 4.2.1]}$$

In this expression,

E = the energy of the particle

FWHM = Full Width at Half Maximum for the photopeak

The GEB parameters ***a***, ***b***, and ***c*** were determined iteratively using a fitting routine in Mathematica. [28] Figure 4.2.4 shows a plot of the detector resolution verse energy for the energies selected.

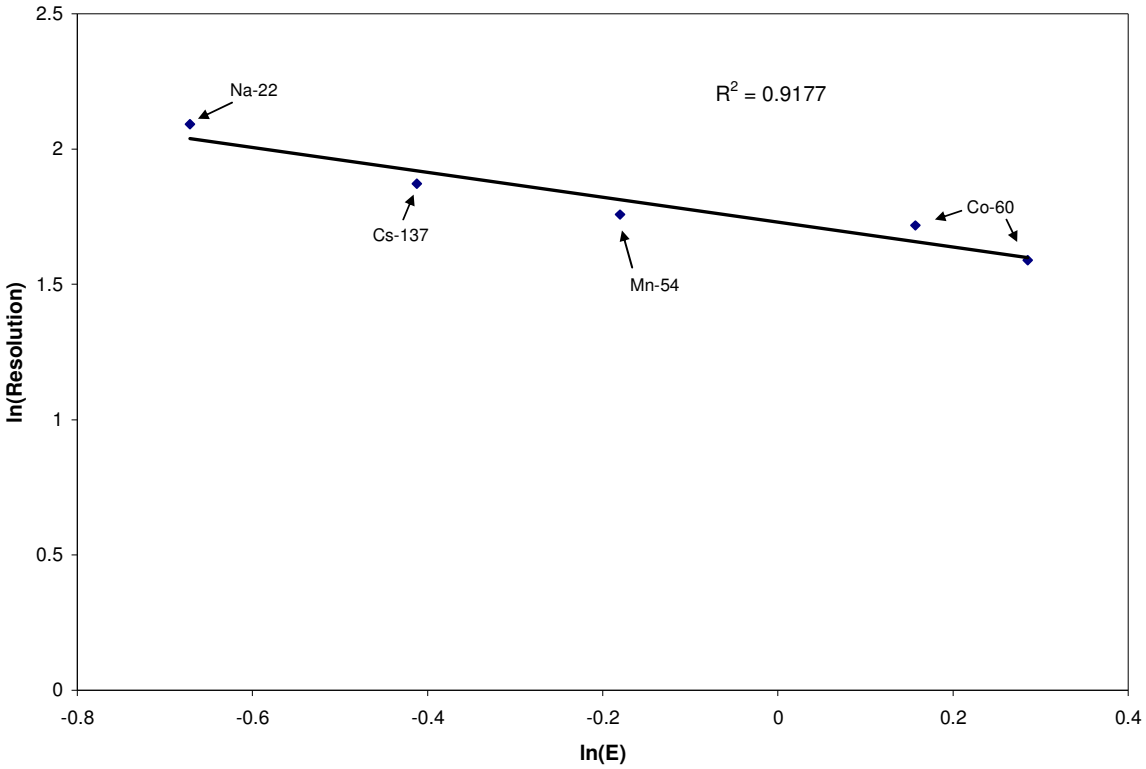

Figure 4.2.4: Detector resolution verse energy for the isotopes chosen to calculate the GEB parameters

4.3 MIRD Phantom Models

To simulate the response of the thyroid uptake collimator on internally contaminated individuals, a series of Monte Carlo models was used. Six anthropomorphic phantoms, of varying ages and body sizes, were used in conjunction with the MCNP5 model of the thyroid uptake collimator. These phantoms can be described by their height and body mass and the mass of adipose tissue. The Body Mass Index (BMI) is a useful tool for characterizing human body size as well. The BMI is calculated by dividing the mass (kg) by the square of the height (m), and is only valid for adults older than 17 years. In general, a BMI greater than 30 indicates obesity. [37] Table 4.3.1 shows the characteristics of each human phantom used in this work.

Table 4.3.1 Characteristics of human phantoms used in MCNP simulations

	Height (cm)	Mass (kg)	BMI	Adipose Mass (kg)
Reference Male	179	73.1	23	11
Reference Female	168	56.5	20	15
Adipose Male	179	93.7	30	22
Adipose Female	168	73.9	26	15
Post-Menopausal Adipose Female	168	85.9	30	27
10-year Androgynous Child	140	32.7	n/a	n/a

The position of the thyroid uptake collimator can greatly influence the detection efficiency of internally deposited radionuclides. Previous MCNP modeling studies showed that the back right lung and the front right lung are the most optimal chest locations for the thyroid uptake counter. [24] In our current model, the detector was placed at both the back right and front right chest positions for the male phantom, as well as on the outer left thigh and the front of the neck. For each of the other phantom types, the front right chest position was excluded. A VisEd generated representation of the male phantom with each of the thyroid uptake probe positions is shown in Figure 4.3.1.

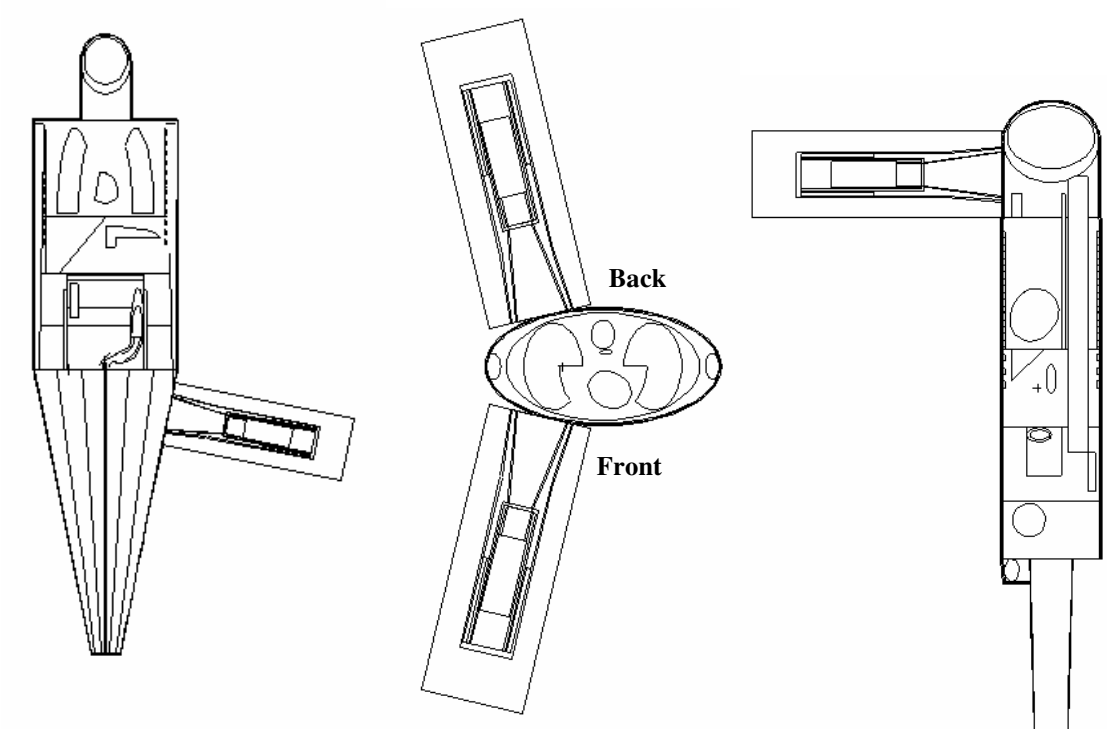

Figure 4.3.1 Thyroid uptake collimator positions on the Male anthropomorphic phantom

A uniformly distributed unit source of each isotope of interest (Am-241, Cs-137, Co-60, I-131, and Ir-192) was distributed in various organs throughout the phantoms. The organs selected are based on the ICRP models for inhaled dose, and include the gastro-intestinal tract and several body tissues. These organs vary slightly depending on the gender of the phantom and the presence of adipose tissue. The organs in which unit sources were distributed in the male phantom are shown in Table 4.3.2.

Table 4.3.2 Organs where unit sources were distributed in MCNP model

Isotope	Organs
Cs-137	Left Lung, Right Lung, Stomach, Small Intestines, Heart, Ascending Colon Wall, Sigmoid Colon Wall, Transverse Colon Wall, Descending Colon Wall, Bladder, Body Tissue (Torso, Head, Shoulder, Left Leg, Right Leg, Genitalia)
Co-60	Left Lung, Right Lung, Stomach, Small Intestines, Heart, Ascending Colon Wall, Sigmoid Colon Wall, Transverse Colon Wall, Descending Colon Wall, Bladder, Body Tissue (Torso, Shoulder, Abdomen, Head, Left Leg, Right Leg, Genitalia), Liver
I-131	Left Lung, Right Lung, Stomach, Small Intestines, Heart, Ascending Colon Wall, Sigmoid Colon Wall, Transverse Colon Wall, Descending Colon Wall, Bladder, Body Tissue (Torso, Shoulder, Abdomen, Head, Left Leg, Right Leg, Genitalia), Thyroid
Ir-192	Left Lung, Right Lung, Stomach, Small Intestines, Heart, Ascending Colon Wall, Sigmoid Colon Wall, Transverse Colon Wall, Descending Colon Wall, Bladder, Body Tissue (Torso, Shoulder, Abdomen, Head, Left Leg, Right Leg, Genitalia), Liver, Left Kidney, Right Kidney, Spleen
Am-241	Left Lung, Right Lung, Stomach, Small Intestines, Heart, Ascending Colon Wall, Sigmoid Colon Wall, Transverse Colon Wall, Descending Colon Wall, Bladder, Body Tissue (Torso, Shoulder, Abdomen, Head, Right Leg, Left Leg), Liver, Ribs, Pelvis, Spine, Skull, Left Leg bones, Right Leg bones, Left Arm bones, Right Arm bones, Left Kidney, Right Kidney, Left Testicle, Right Testicle, Left Clavicle, Right Clavicle, Left Scapula, Right Scapula

The difference between the organs in the male phantom and the female phantom is the addition of the right and left breast tissue included in the body tissue category. Also, the female phantom includes the right and left ovaries rather than the testicles. The adipose phantoms include the addition of adipose tissue on the abdomen, subcutaneous adipose tissue, and adipose tissue on the upper legs. All adipose tissue is included in the body tissue grouping. A unit source is distributed in the child phantom within the same organs as the male phantom.

A source contribution tally modifier (SCX card) was used in conjunction with a pulse height tally (MCNP F8 tally) to determine the counts in the detector per a unit source distributed in each organ. The tally modifier records the origin (in this case, the source organ) of each particle that reaches the detector. This value is essentially the detector efficiency for a unit source in each organ for each isotope of concern.

Once the detector efficiency for each organ and each isotope has been computed using the MCNP model, these values were multiplied by the biokinetic modeling results. The biokinetic modeling provides the fractional organ concentration as a function of time per becquerel of intake. By summing the contributions from each source organ, the total count rate from the modeled detector was determined per becquerel of intake.

As previously mentioned, count rates are reported per becquerel of intake and per Clinical Decision Level (CDL). The MCNP input file for the male phantom with a unit source of Cs-137 in each organ is provided in Appendix C as an example.

CHAPTER 5

BIOKINETIC MODELING USING DCAL

Biokinetic modeling describes the movement of a particular isotope through the human body as a function of time. Depending on the characteristics of the isotope, it can concentrate in various organs or it can equally distribute itself throughout the body tissue.

The Dose and Risk Calculation System (DCAL) software [9] was used to determine the movement of an isotope through the human body as a function of time. Activity Calculations (ACTACAL) is part of the DCAL software, and it provides the activity as a function of time for various body compartments. The DCAL biokinetic libraries include the ICRP-66 lung model [17]. the ICRP-30 gastro-intestinal tract model [12], and the ICRP-67 urinary bladder voiding model [16]. DCAL was originally created under the sponsorship of the Environmental Protection Agency (EPA) for estimating tissue dose and associated health risks associated with different environmental exposures. DCAL has been used in the development of several International Commission on Radiation Protection (ICRP) publications, in particular those with age-specific dose coefficients. [ICRP 1989, 1993, 1995a, 1995b, 1996]

DCAL was used to estimate the retention fraction in affected organs as a function of time following initial uptake. Six isotopes (Cs-137, Co-60, Am-241, I-131, Ir-192, and Sr/Y-90) were modeled using this method. DCAL calls for several parameters in generating the compartmental activities. For each isotope, inhalation was specified as the intake pathway, from an environmental source (as opposed to occupational), and activity median aerodynamic diameter (AMAD) of 1 micrometer was used. The default lung absorption type (fast, moderate, or slow) was specified for each isotope according to the International Commission on Radiological

Protection (ICRP) recommended defaults. [21] These absorption types correspond broadly to the inhalation classes D, W, and Y from the ICRP Publication 30 model. [12] This classification refers to the length of time the radioactive materials are retained in the pulmonary region. Class-D materials have a 'half-time' in the lungs of less than 10 days, Class-W materials have a pulmonary half-time of 10 to 100 days, and Class-Y materials have a pulmonary half-time of greater than 100 days. [41] For the nuclides Cobalt and Americium, the ICRP default absorption type for particulate aerosol is moderate. For Iodine and Cesium, the default type is fast. A default type is not specified for Iridium, so moderate was selected. The default types are summarized in Table 5.1.

Table 5.1 Default Lung Absorption Type for each nuclide

Nuclide	Default Lung Absorption Type
Cobalt	M
Strontium	M
Yttrium	n/a
Iodine	F
Cesium	F
Iridium	n/a
Americium	M

A comparison of the total fraction retained for each selected isotope for the first 30 days following intake is shown in Figure 5.1. The retention of an isotope in the body is a function of both the clearance class, and the isotope's radioactive half life. As seen in the figure, Cs-137 has the highest retention rate in the body, and I-131 leaves the body with the fastest rate.

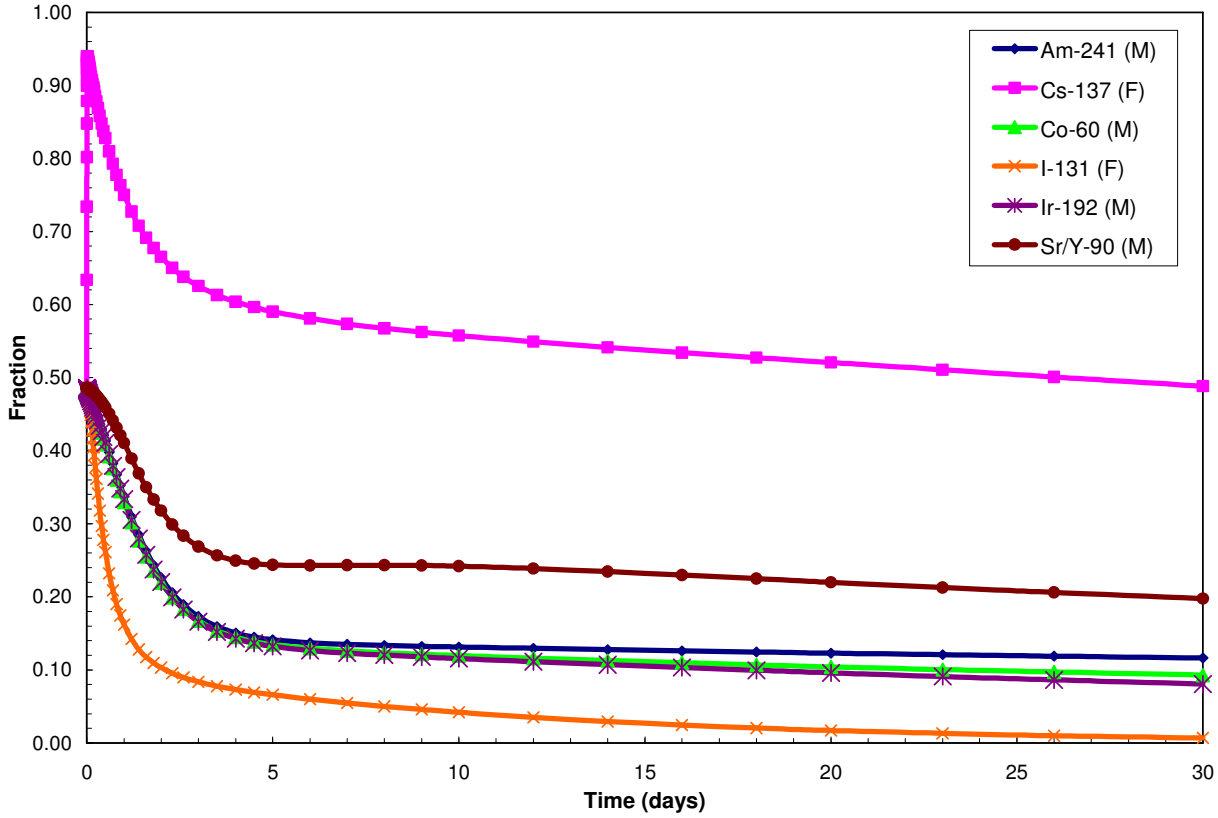

Figure 5.1 Comparison of Total Fraction Retained for each selected isotope.

DCAL shows that more than half of the initially inhaled activity is exhaled with the first breath for each of the isotopes with a moderate lung absorption class. The main organs of interest for each isotope include the lungs, stomach, small and large intestines, and urinary bladder. According to DCAL, these organs are of particular interest because large fractions of the amount originally inhaled move through the pulmonary tract and gastro-intestinal tract, depositing dose in these organs. A large fraction is retained in the intestinal tract and body tissue. The body tissue is composed of mostly abdominal tissue, but also includes breast tissue, adipose tissue, muscle tissue in the arms and legs, and genitalia. As expected, certain isotopes collect in specific body tissues – an example is the collection of I-131 in the thyroid gland. The

compartments retaining a significant fraction of the isotope were identified for each selected isotope using DCAL. These compartments are shown in Table 5.2.

Table 5.2 Body Compartments identified by DCAL for each selected isotope, bolded items are specific to that isotope

Isotope	Body Compartments identified by DCAL
Cs-137	Lungs, Stomach Content, Small Intestine Content, Upper Large Intestine Content, Lower Large Intestine Content, Blood, Body Tissue, Bladder Content
Co-60	Lungs, Stomach Content, Small Intestine Content, Upper Large Intestine Content, Lower Large Intestine Content, Blood, Body Tissue, **Liver**, Bladder Content
I-131	Lungs, Stomach Content, Small Intestine Content, Upper Large Intestine Content, Lower Large Intestine Content, Blood, Body Tissue, **Thyroid**, Bladder Content
Ir-192	Lungs, Stomach Content, Small Intestine Content, Upper Large Intestine Content, Lower Large Intestine Content, Blood, Body Tissue, **Liver, Kidneys, Spleen**, Bladder Content
Am-241	Lungs, Stomach Content, Small Intestine Content, Upper Large Intestine Content, Lower Large Intestine Content, Blood, Body Tissue, **Cortical Bone, Trabecular Bone, Liver, Kidneys, Testes/Ovaries, Red Marrow**, Bladder Content
Sr/Y-90	Lungs, Stomach Content, Small Intestine Content, Upper Large Intestine Content, Lower Large Intestine Content, Blood, Body Tissue, **Cortical Bone, Trabecular Bone,** Bladder Content

A graphical comparison of the lungs, body tissue, and any special organs for each isotope is shown in Figures 5.2 through 5.7. The lungs and body tissue were selected due to the high fraction retained in each of these body compartments. The total retention fraction is also included on each of these figures.

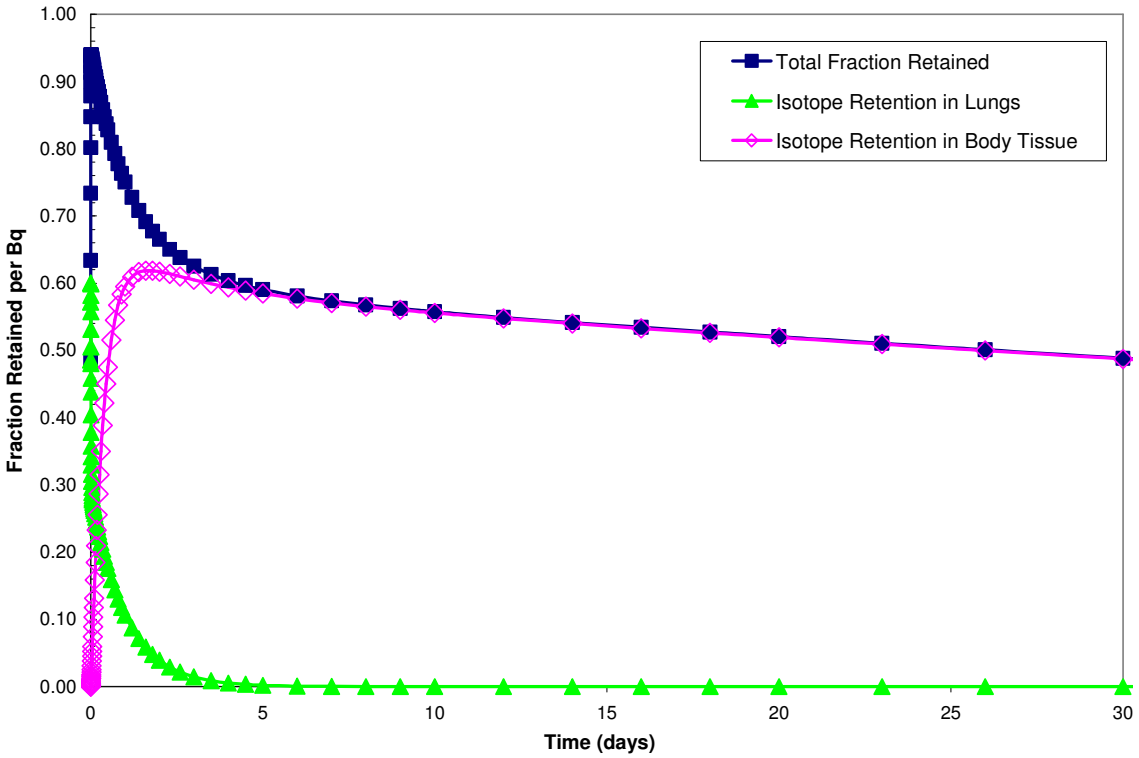

Figure 5.2 Retention of Cs-137(fast) in the lungs and body tissue and total fraction retained over first 30 days following intake.

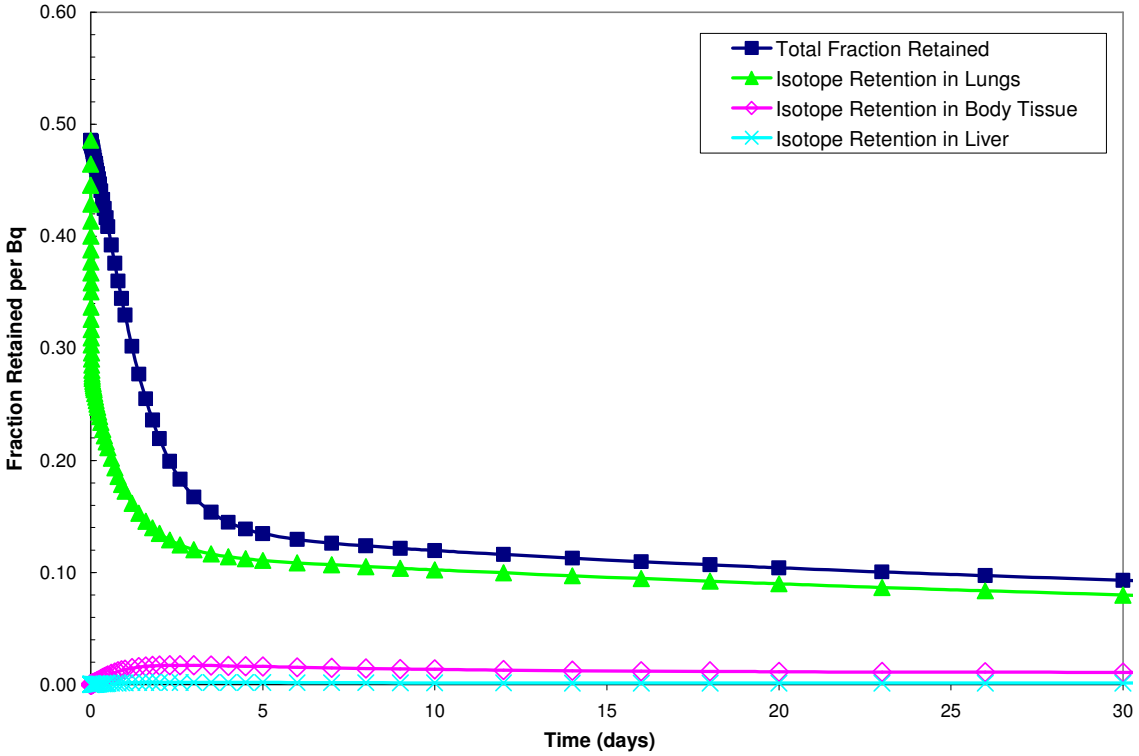

Figure 5.3 Retention of Co-60 (moderate)in the lungs, body tissue, and liver and total fraction retained over first 30 days following intake.

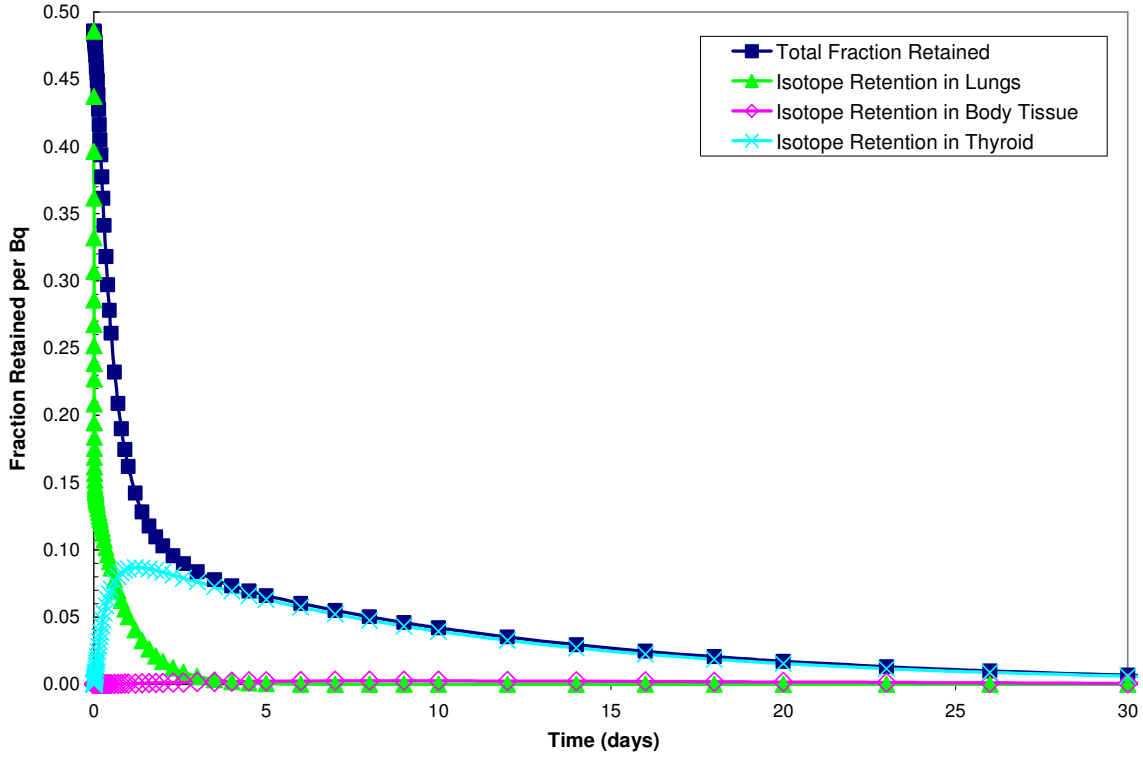

Figure 5.4 Retention of I-131 (fast) in the lungs, body tissue, and thyroid and total fraction retained over first 30 days following intake.

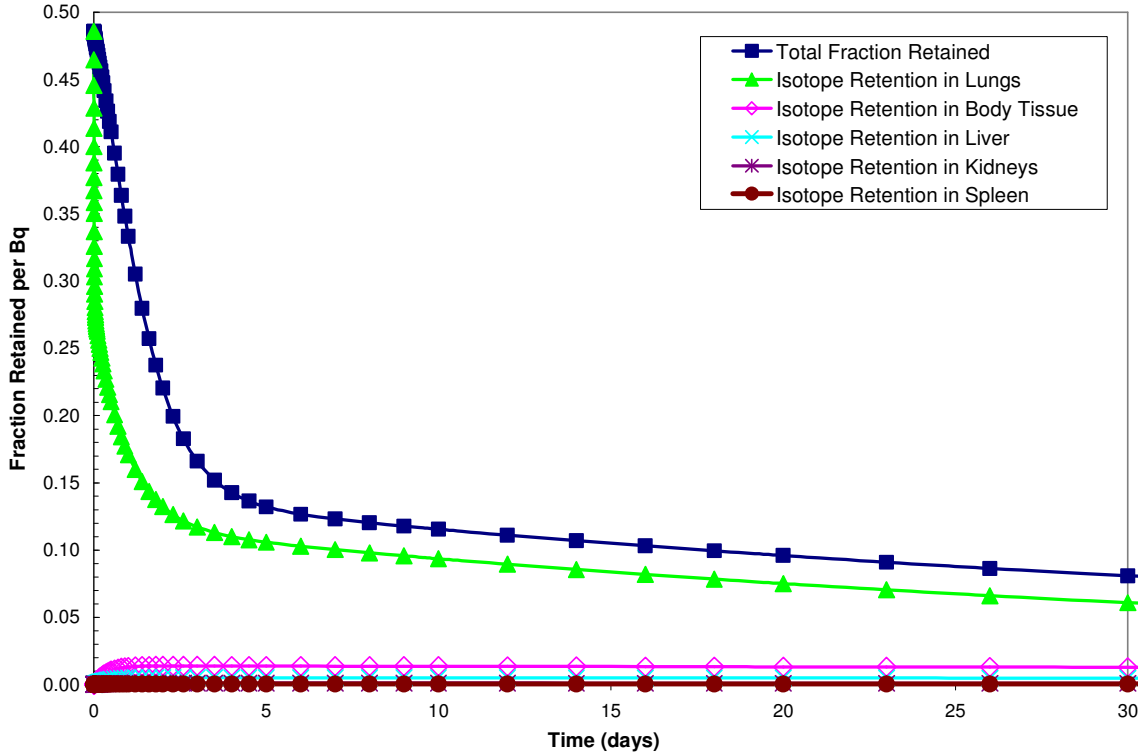

Figure 5.5 Retention of Ir-192 (moderate) in the lungs, body tissue, liver, kidneys, and spleen and total fraction retained over first 30 days following intake.

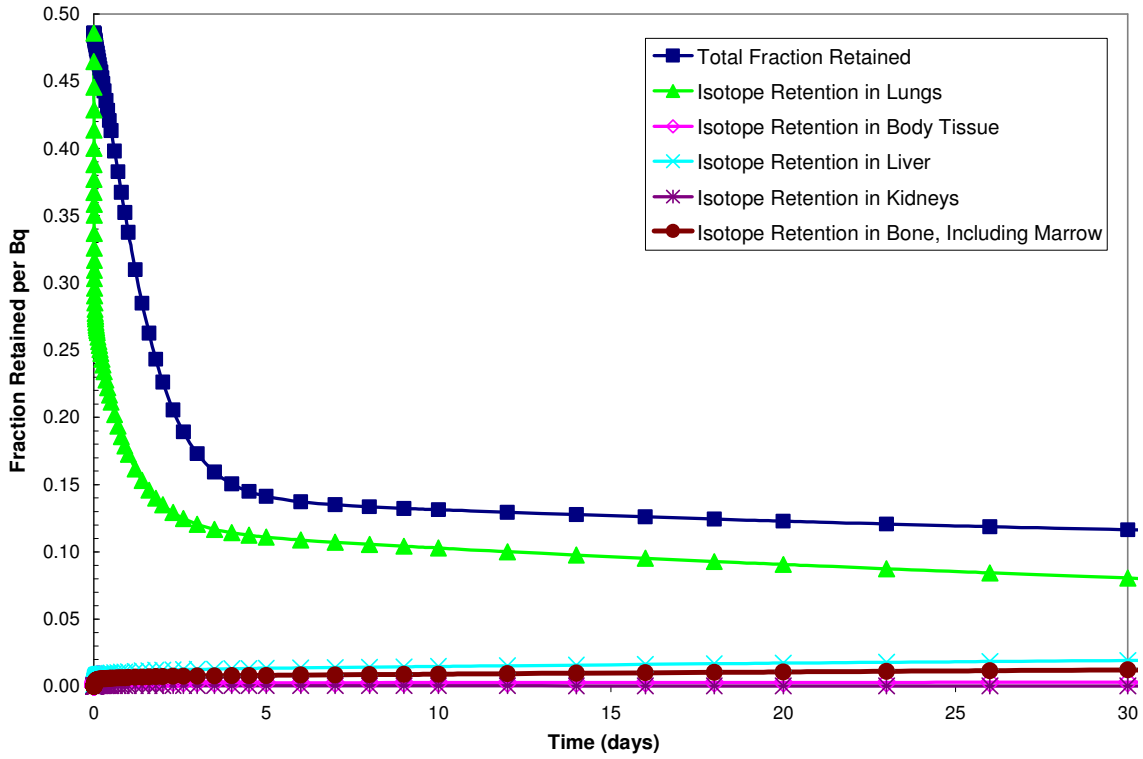

Figure 5.6 Retention of Am-241 (moderate) in the lungs, body tissue, liver, kidneys, and bone (including red bone marrow) and total fraction retained over first 30 days following intake.

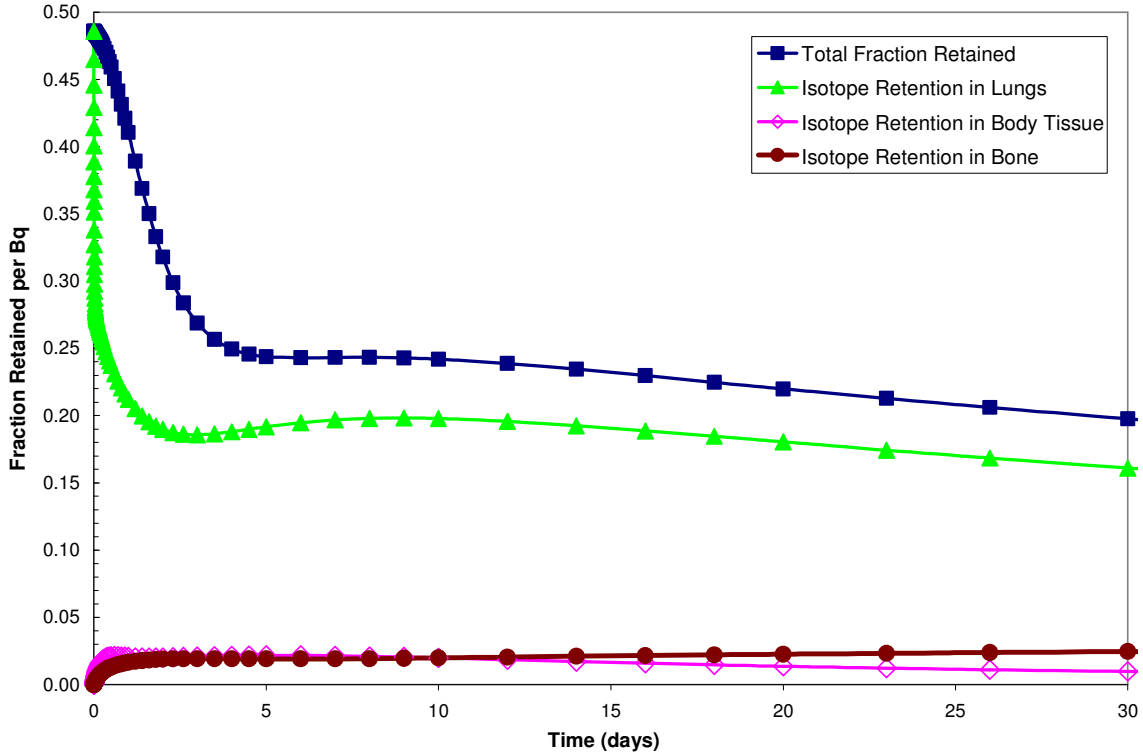

Figure 5.7 Retention of Sr/Y-90 (moderate) in the lungs, body tissue, and bone and total fraction retained over first 30 days following intake.

A fundamental component in assaying internal contamination is understanding the movement of an isotope through the body. Accordingly, the DCAL predicted organ activities are folded with the detector response for each organ and summed for each detector location. The convolution provides count rates for each detector location per unit of inhaled activity as a function of time following initial exposure.

CHAPTER 6

RESULTS

6.1 Model Validation

The MCNP model of the thyroid uptake collimator was validated in a comparison between the measured data and the MCNP calculated data. The measured slab phantom spectra for the six isotopes described in Table 3.2.1 were compared to the MCNP model prediction to check the representation of the actual detector response over a broad gamma-ray energy range. Both the total spectra and the selected Regions of Interest (ROI) around each photopeak were examined. This process was also used to create a scaling factor between the measured and calculated spectra, if needed. A representative comparison between the measured and calculated spectra for each measured isotope is shown in Figures 6.1.1 through 6.1.6. These spectra were measured with a thickness of 60mm of PMMA between the collimator and the source. Spectra for 0mm, 60mm, and 108mm for each isotope are contained in Appendix B.

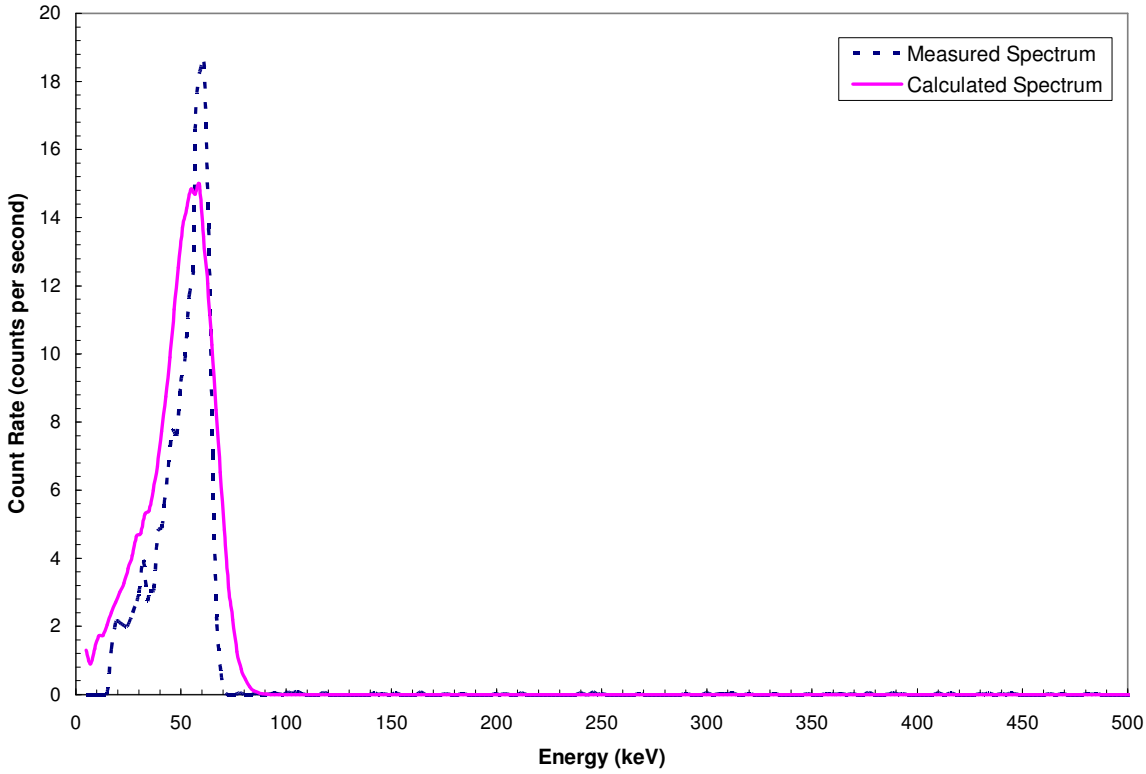

Figure 6.1.1 Measured and calculated spectra for Am-241 with 60 mm PMMA

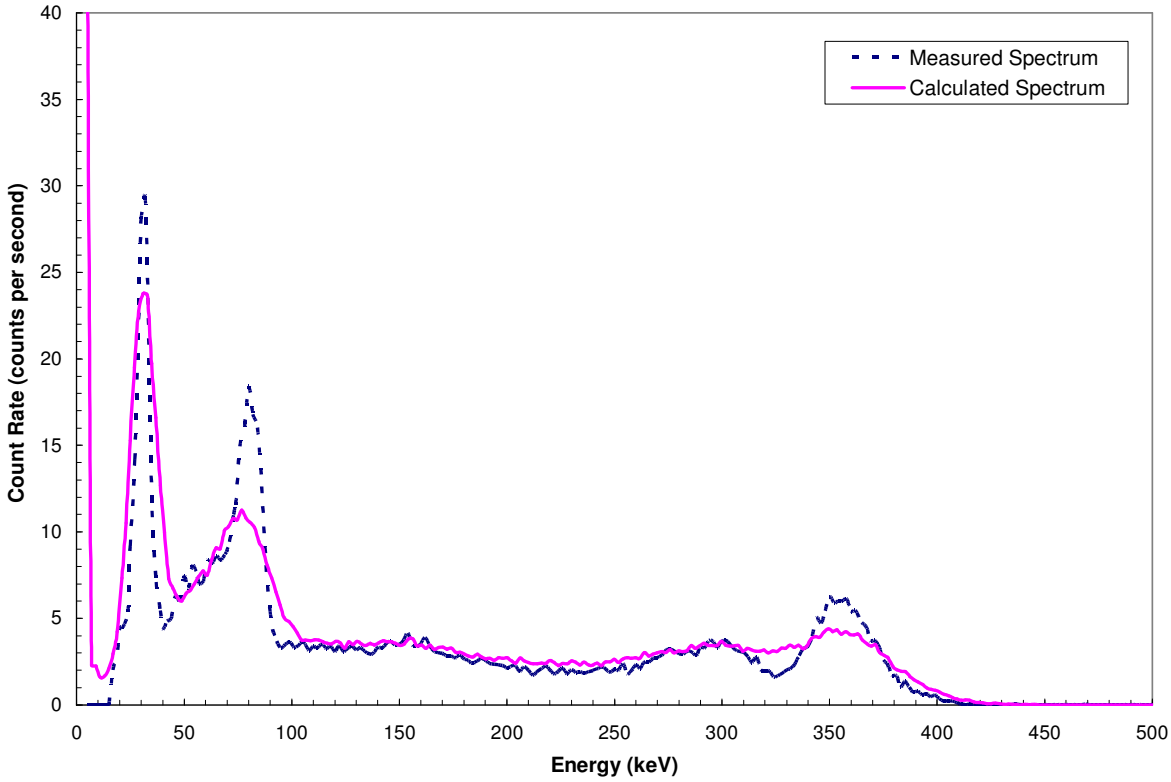

Figure 6.1.2 Measured and calculated spectra for Ba-133 with 60 mm PMMA

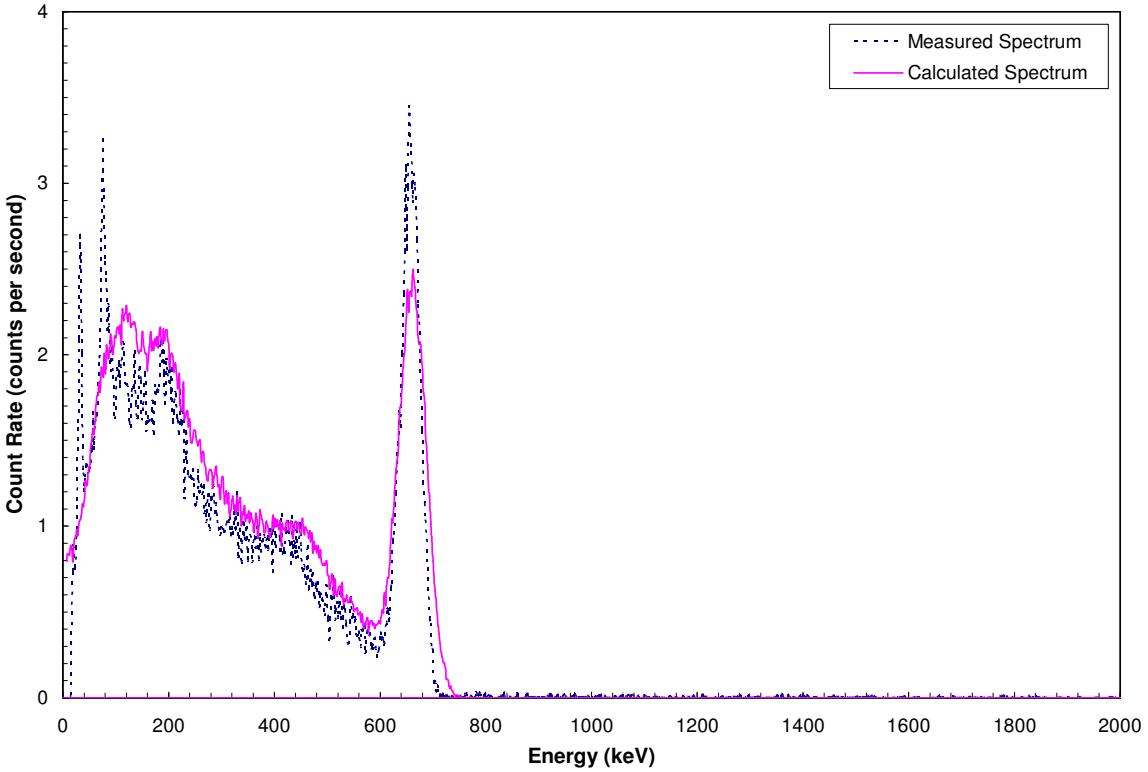

Figure 6.1.3 Measured and calculated spectra for Cs-137 with 60 mm PMMA

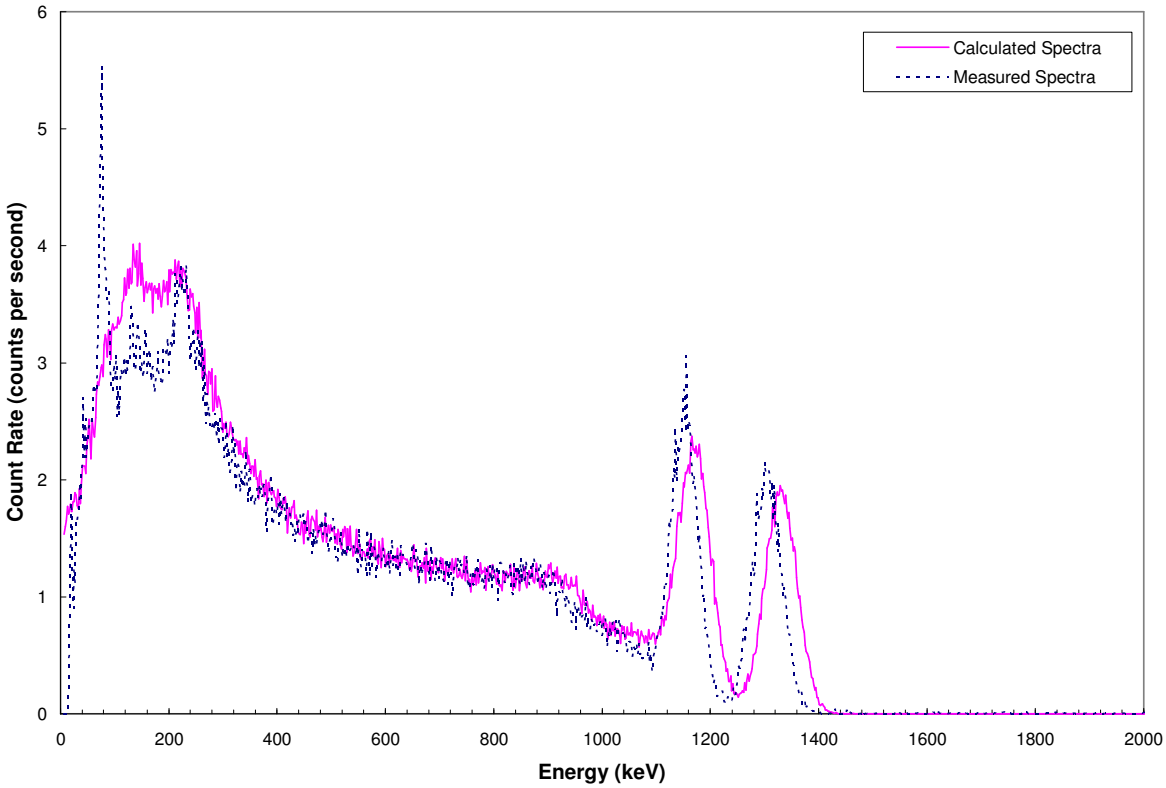

Figure 6.1.4 Measured and calculated spectra for Co-60 with 60 mm PMMA

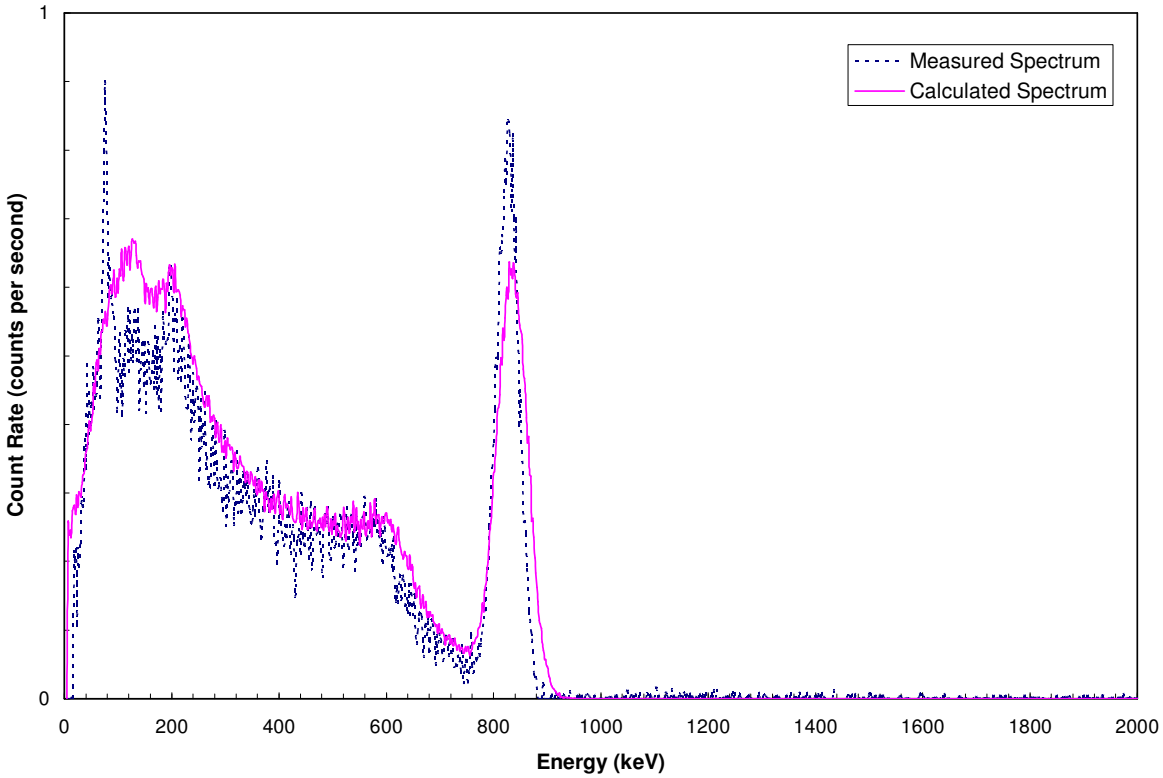

Figure 6.1.5 Measured and calculated spectra for Mn-54 with 60 mm PMMA

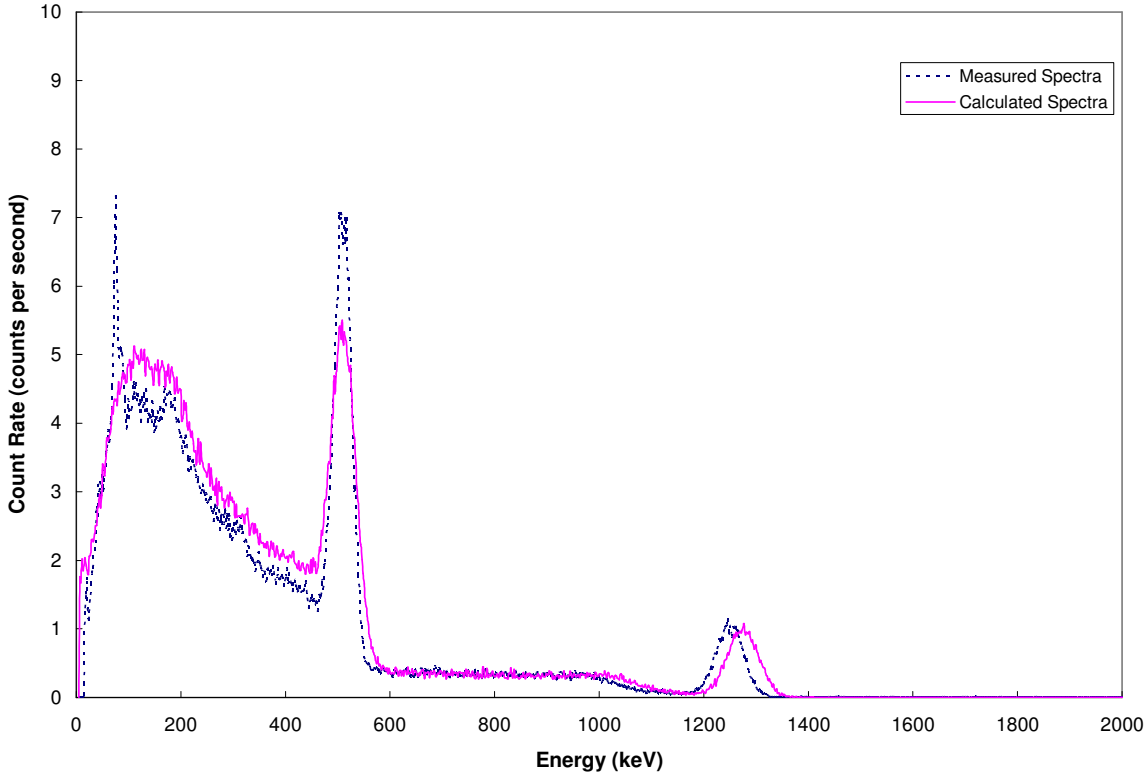

Figure 6.1.6 Measured and calculated spectra for Na-22 with 60 mm PMMA

The gamma-ray photopeaks for the benchmark measurements were automatically selected using the thyroid uptake system nuclide identification software. The default calibration is set to 2keV/channel, and the nuclide selection tool calls upon preset values in the data library for each isotope. For consistency, the same ROI was used for the calculated spectra. The default ROI values for each isotope are shown in Table 6.1.1.

Table 6.1.1: Capintec default ROI values used in measured and calculated spectra

Isotope	Default ROI (keV)
Am-241	49-70
Ba-133	70-100, 334-384
Cs-137	627-697
Co-60	1126-1382
Mn-54	792-878
Na-22	480-546, 1220-1328

The ratio of the calculated (MCNP) count rate to the measured count rate for the gamma-ray photopeak(s) of each isotope are shown in Figures 6.1.7 through 6.1.12. The solid line in these figures show the mean ratio for the Capintec selected ROI around the photopeak.

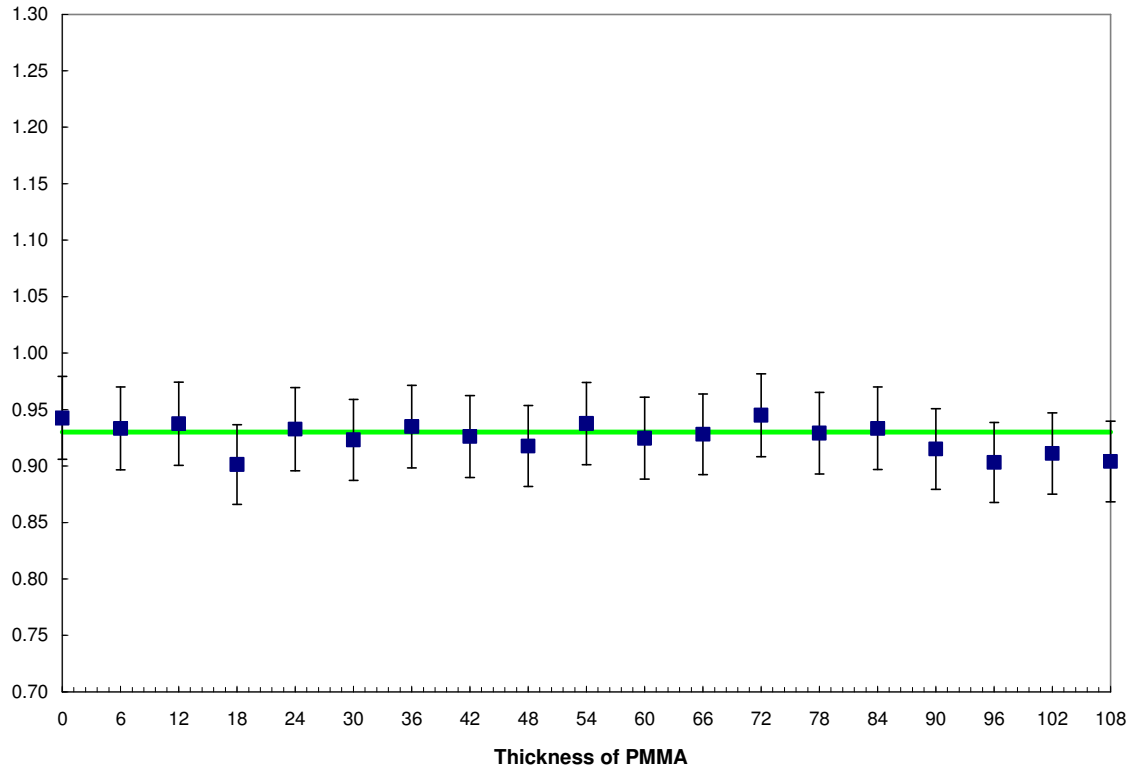

Figure 6.1.7 Ratio of MCNP results to measured data for the 662 keV photopeak from Cs-137, with mean of 0.93

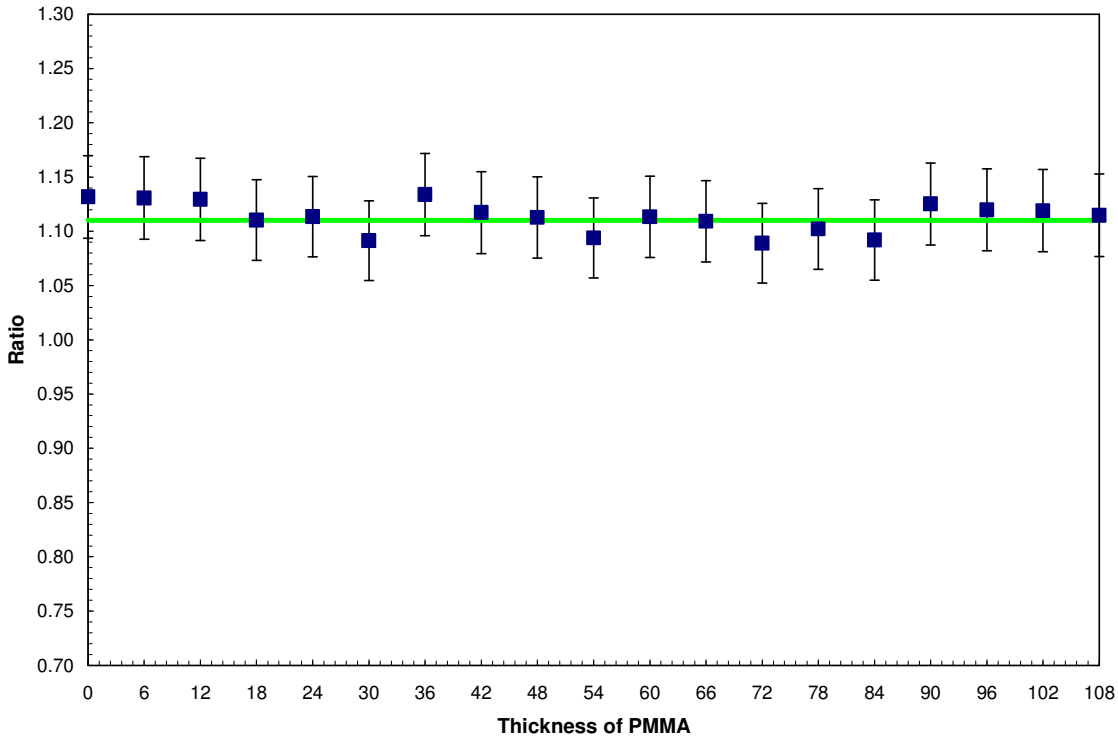

Figure 6.1.8 Ratio of MCNP results to measured data for the sum of the 1.17 and 1.33 MeV photopeaks from Co-60, with mean of 1.11

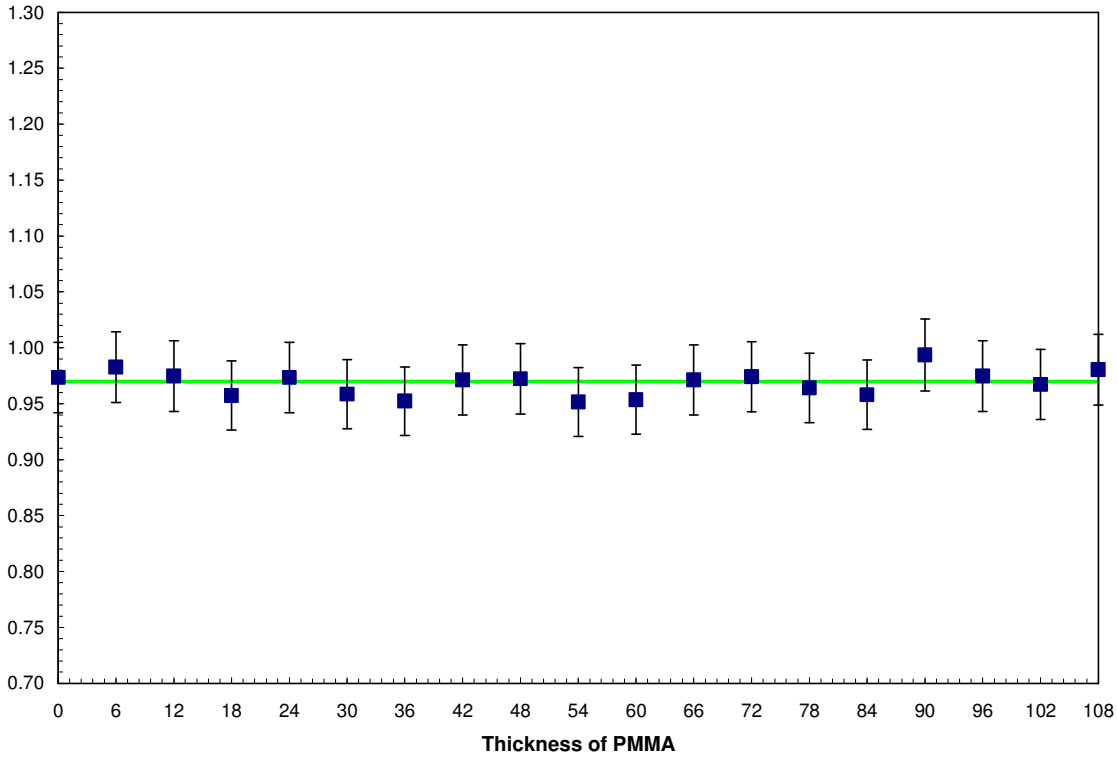

Figure 6.1.9 Ratio of MCNP results to measured data for the sum of the 0.511 and 1.27 MeV photopeaks from Na-22, with mean of 0.97

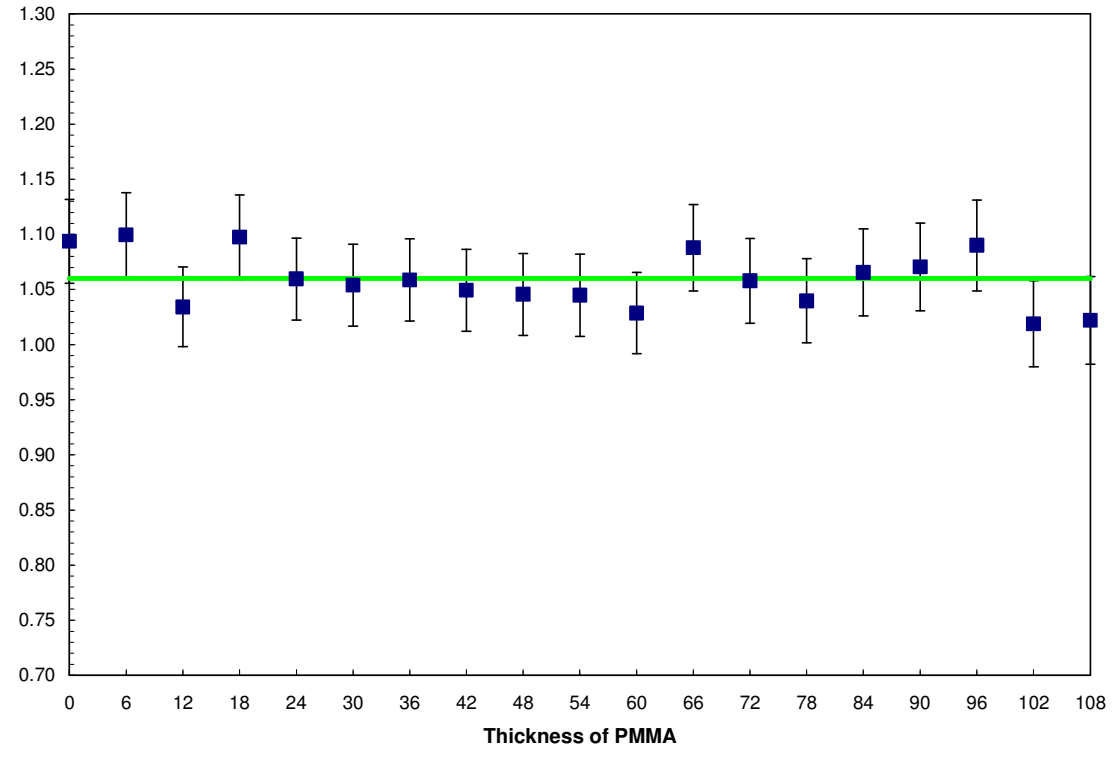

Figure 6.1.10 Ratio of MCNP results to measured data for the 835 keV photopeak from Mn-54, with mean of 1.06

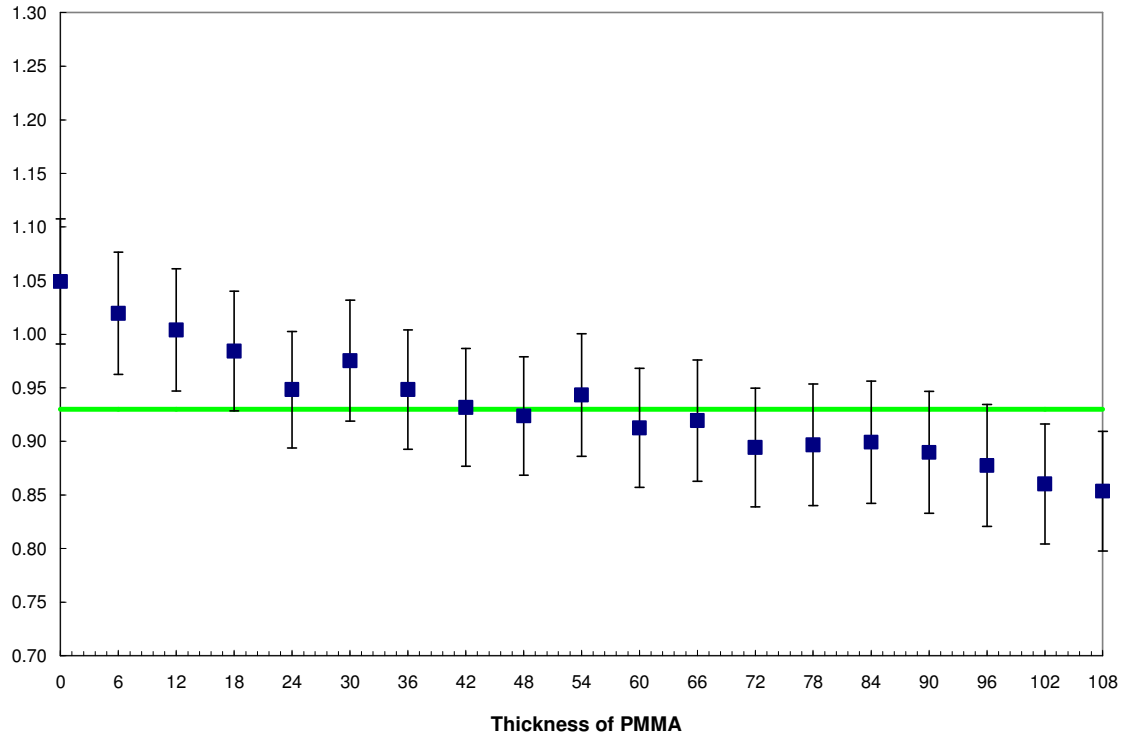

Figure 6.1.11 Ratio of MCNP results to measured data for the sum of the 31, 80, and 356 keV photopeaks from Ba-133, with mean of 0.93

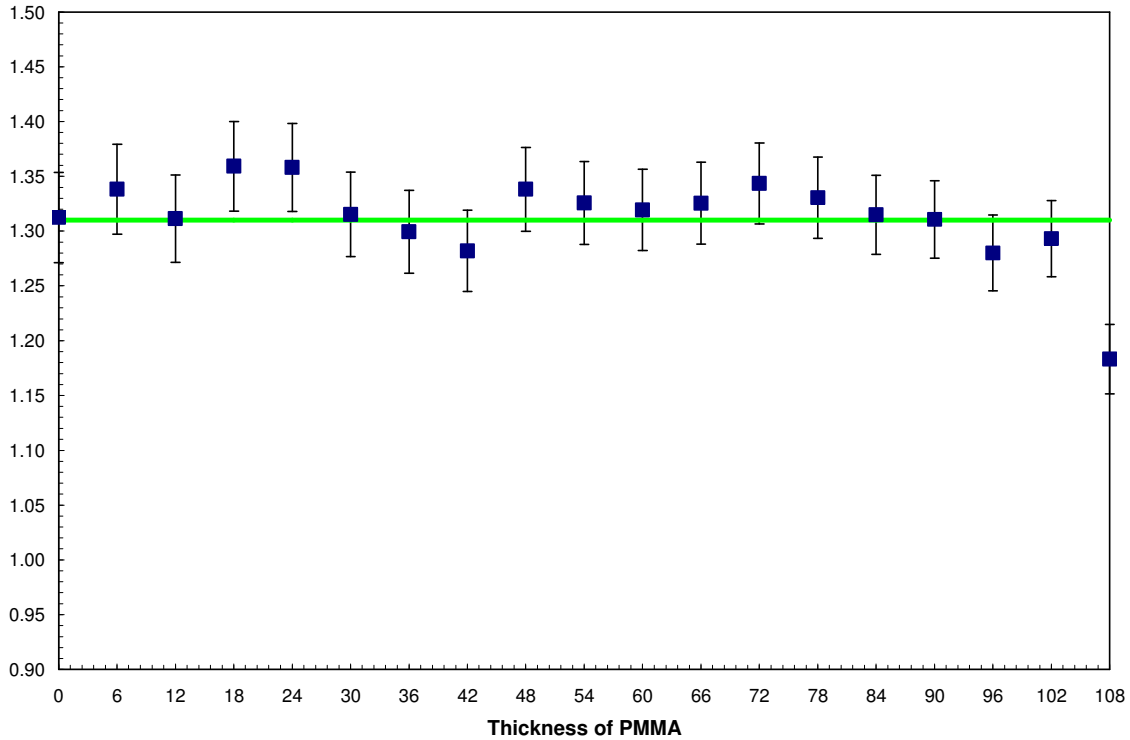

Figure 6.1.12 Ratio of MCNP results to measured data for the 59.5 keV photopeak from Am-241, with mean of 1.31

As seen in the figures, the ratio of the calculated spectra to measured spectra is essentially constant over all thicknesses for a given isotope. This indicates that the model of the detector is valid regardless of the attenuator thickness. This result provides confidence when using the detector in conjunction with the anthropomorphic phantoms. Any differences in chest-wall thickness between the various phantoms will not affect the detector response in the photopeaks, nor should it.

Ideally, the ratio of the calculated spectra to the measured photopeaks would be one. In actuality, a number of factors introduce error terms into the data. The error on each photopeak is dominated by the reported source activity error of 3.3%. The pulse-height bin error from MCNP and the counting error from the measured spectra were considerably smaller than the source activity error, but were also considered and included in the error calculations, illustrated by the error bars. All data for each isotope fall within 2 standard deviations of the mean.

To compensate for the differences between the measured and calculated spectra, a scaling factor (the mean ratio) is applied to the phantom results. This 'converts' the measured pulse-height tally to an equivalent count rate on the actual probe. The scaling factors for each isotope that is used for both benchmark measurements and phantom calculations are shown in Table 6.1.2.

Table 6.1.2 Scaling Factors for isotopes used in benchmark measurements and phantom calculations

Isotope	Scaling Factor
Am-241	1.31
Cs-137	0.93
Co-60	1.11

The ratios for Ba-133 and Am-241 show a negative slope as the thickness of PMMA increases. The most probable cause for this is an inappropriate representation of the resolution by the GEB function at these energies. The lowest energy considered in determining the GEB

function was 0.511 MeV (Na-22). Ba-133 and Am-241 both have gamma-ray emissions at energies lower than 0.511 MeV meaning that they have a higher resolution. This is due to the fact that resolution is inversely proportional to the square-root of the gamma ray energy. [Knoll, 2002] A comparison of the spectra shows that indeed, the calculated ROIs are considerably broader than the measured spectra. This can be seen in the Slab Phantom Spectral Data, contained in Appendix B.

With the exception of Am-241, all the isotopes of greatest concern investigated herein have energies higher than 300 keV. Thus, the GEB function is adequate for the purpose and intent of this work and therefore the scaling factor also is valid. The scaling factor corrects for differences between the measured and calculated data, and provides a validated estimate of the actual detector response.

6.2 MIRD Phantom Results

In the event of an actual emergency requiring the use of this screening procedure, the operators are not expected to visually inspect the spectra to select an optimal ROI. Instead, they will simply use the Capintec nuclide identification tool, which selects the ROI channels based on data stored in the Captus 3000 data library. Thus, the following results use the scaling factor based on the Captus system default ROI selection, which was discussed in the previous section. Two of the isotopes (I-131 and Ir-192) used in the phantom simulations were not included in the benchmark measurements and validation process. As a result, scaling factors were not calculated for these two isotopes; Capintec system default ROIs were used throughout the analysis for these two isotopes.

Each of the six isotopes listed in Table 3.4.1 were uniformly distributed in the six phantom types. The results for the Male phantom contaminated with Cs-137 are shown in Table

6.2.1. The values are given in count rate (counts per minute) per becquerel of intake activity. Results for the remaining phantom types contaminated with Cs-137 and each of the other four isotopes are provided in Appendix D.

Table 6.2.1 Count rate per Bq calculated for the Male phantom contaminated with Cs-137

		Back Right Lung	Front Right Lung	Neck	Thigh
		cpm per Bq	cpm per Bq	cpm per Bq	cpm per Bq
Days following exposure	0	1.85E-04	1.77E-04	1.51E-05	1.31E-06
	1	4.29E-04	4.63E-04	5.07E-04	2.47E-04
	2	4.11E-04	4.48E-04	5.20E-04	2.54E-04
	3	3.94E-04	4.30E-04	5.08E-04	2.49E-04
	4	3.83E-04	4.19E-04	4.99E-04	2.44E-04
	5	3.76E-04	4.11E-04	4.91E-04	2.40E-04
	6	3.71E-04	4.05E-04	4.84E-04	2.37E-04
	7	3.66E-04	4.00E-04	4.79E-04	2.35E-04
	8	3.63E-04	3.97E-04	4.74E-04	2.32E-04
	9	3.60E-04	3.93E-04	4.70E-04	2.30E-04
	10	3.57E-04	3.90E-04	4.66E-04	2.28E-04
	20	3.33E-04	3.64E-04	4.36E-04	2.13E-04
	30	3.13E-04	3.42E-04	4.09E-04	2.00E-04

As discussed, the fast absorption type of Cs-137 rapidly distributes itself through the body tissue and is quickly out of the lung cavities. Analysis of the data for Cs-137 shows that after one day, the neck provides a higher count rate per becquerel than the front and back lung positions. The thigh shows a lower count rate; however, it is the same order of magnitude as the lung and neck count rates.

In the case of Cs-137, the variability between body type and detector response is much more pronounced than for the other isotopes. Figure 6.2.1 shows a graphical comparison of the count rates resulting from each phantom type contaminated with Cs-137 with the detector on the

neck. The other detector positions (back right lung and thigh) show a similar distribution, with a lower count rate.

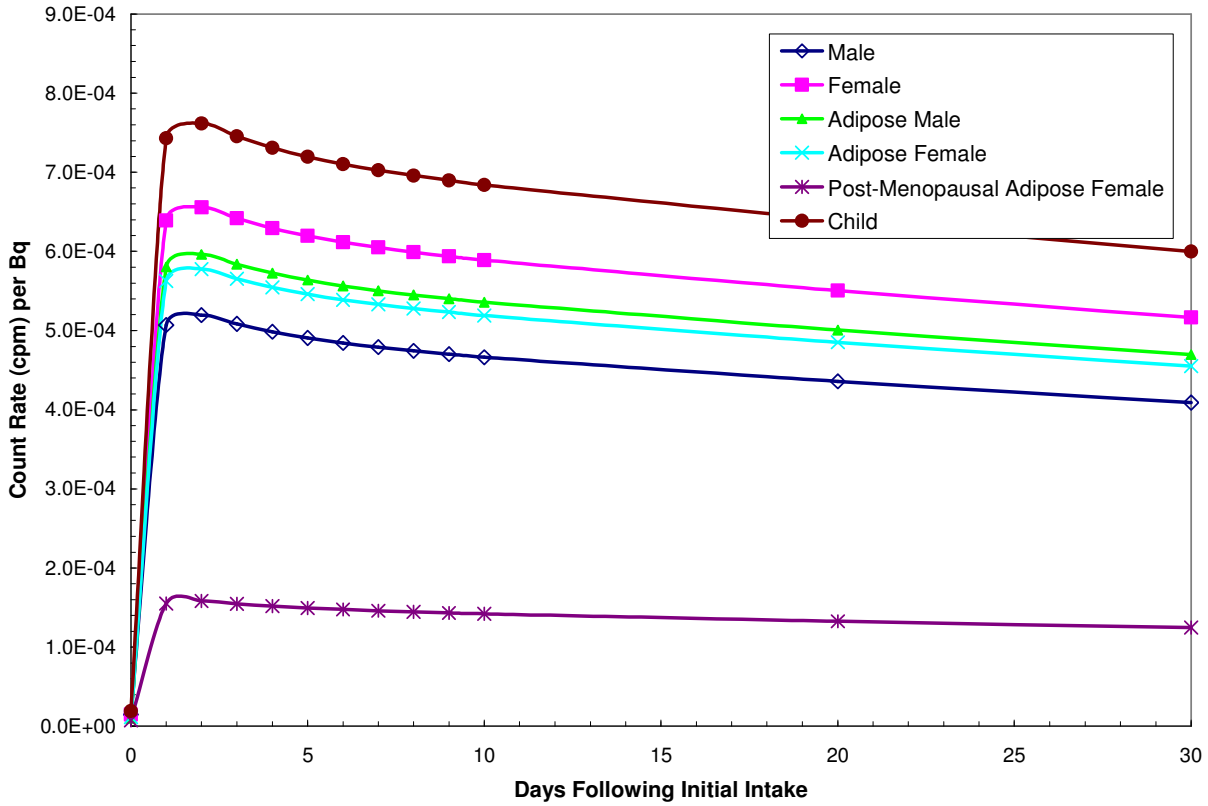

Figure 6.2.1 Comparison of count rate per phantom type for Cs-137, with detector positioned on the neck

An analysis of the various phantom results shows that in general, the highest count rate is found in the child. This is expected as the child has the least amount of tissue, or attenuating material, between the isotope and the detector. The lowest count rate is found in one of the adipose phantoms, usually the Post-Menopausal Adipose Female. The Post-Menopausal Adipose Female has more tissue, resulting in more attenuation and absorption of the gamma ray photons before they reach the detector crystal. While it is tempting to make such generalities about the effects of body type on the detector response, in actuality the isotope has just as much impact on the count rate.

For the case of I-131, the count rates are more similar between the phantom types, and in fact, the child shows the lowest count rate per becquerel. As discussed, I-131 is rapidly absorbed by the thyroid gland. A child has a smaller thyroid gland than an adult, causing it to become saturated with I-131 before an adult's thyroid. [42] Figure 6.2.2 shows the increasing count rate per Bq for the neck detector position one, three, and ten days following the initial intake.

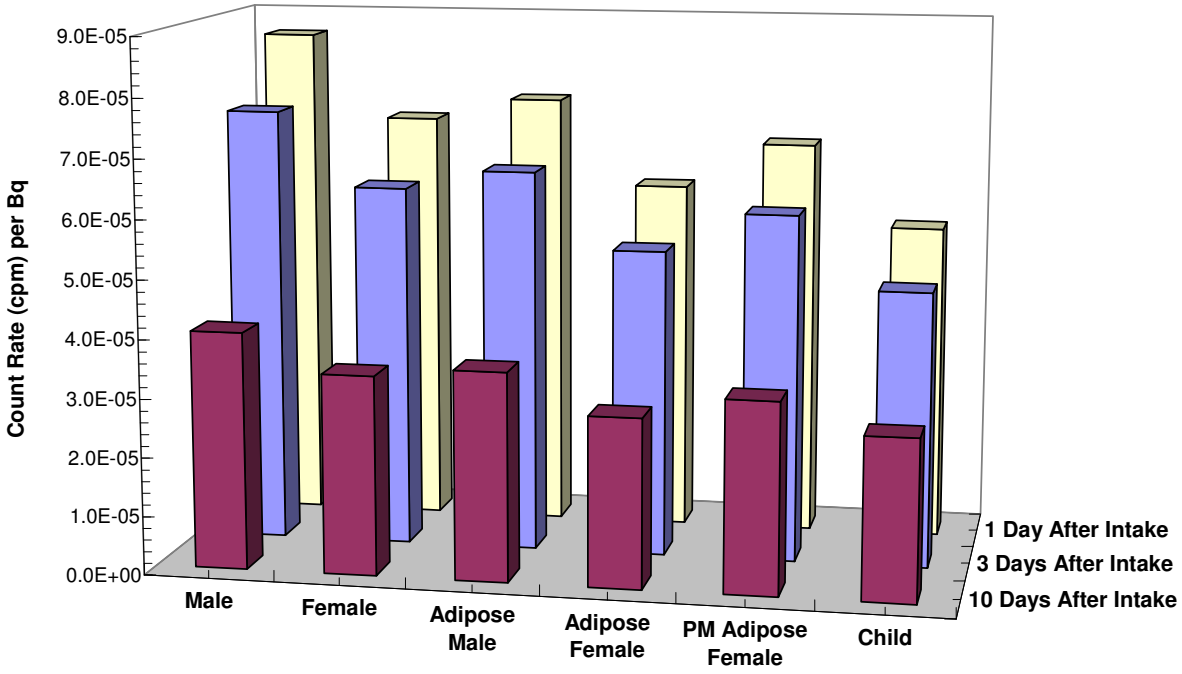

Figure 6.2.2 Count Rate per Bq of intake of I-131 for the neck position

A large fraction of Co-60 intake remains in the lungs, and this is reflected in the higher count rate found at the back right lung position of the detector. In addition, there is little variation between phantom types for Co-60. The Reference Male and Reference Female phantoms have similar response, as do the adipose phantoms. A comparison of the detector position and phantom type for Co-60 is shown in Figure 6.2.3.

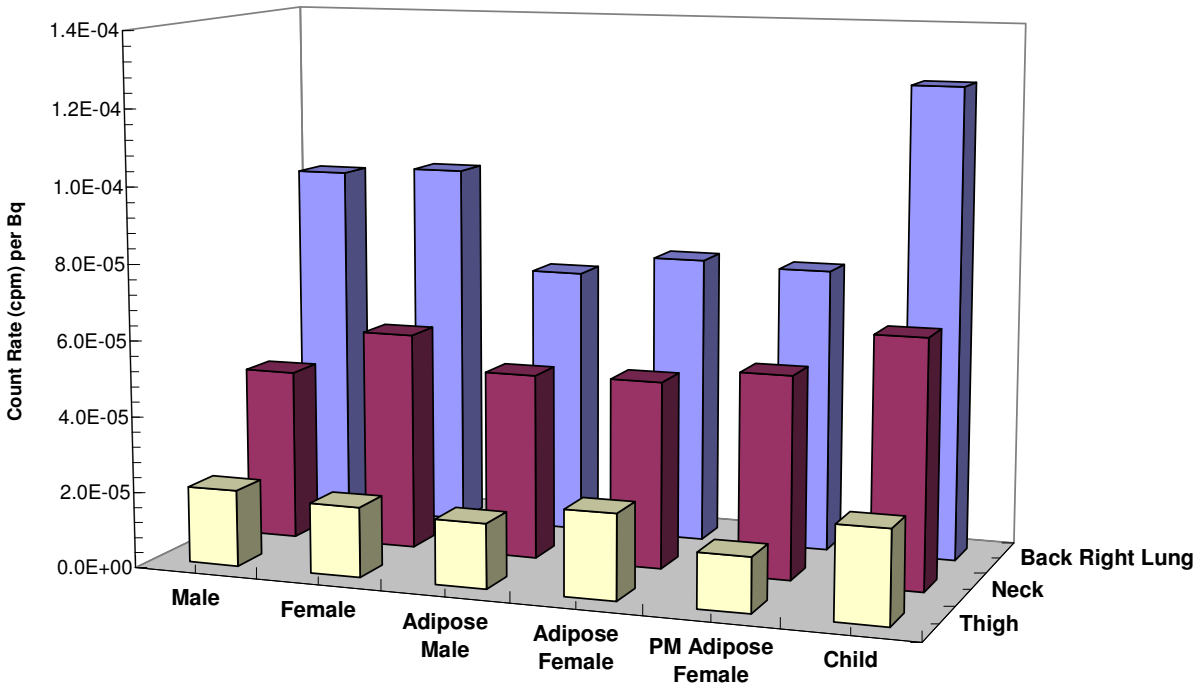

Figure 6.2.3 Comparison of detector position and phantom type for Co-60, 3 days after intake

Ir-192 is similar to Co-60 in that they both have moderate lung absorption types; consequently, the most efficient measurement location is the back right lung for each phantom type. A significant portion of the uptake of Ir-192 goes to the blood and as a result, the majority of the counts originate in the liver, heart, and body tissue. The count rate as a function of time for the various phantom types contaminated with Ir-192 is shown in Figure 6.2.4.

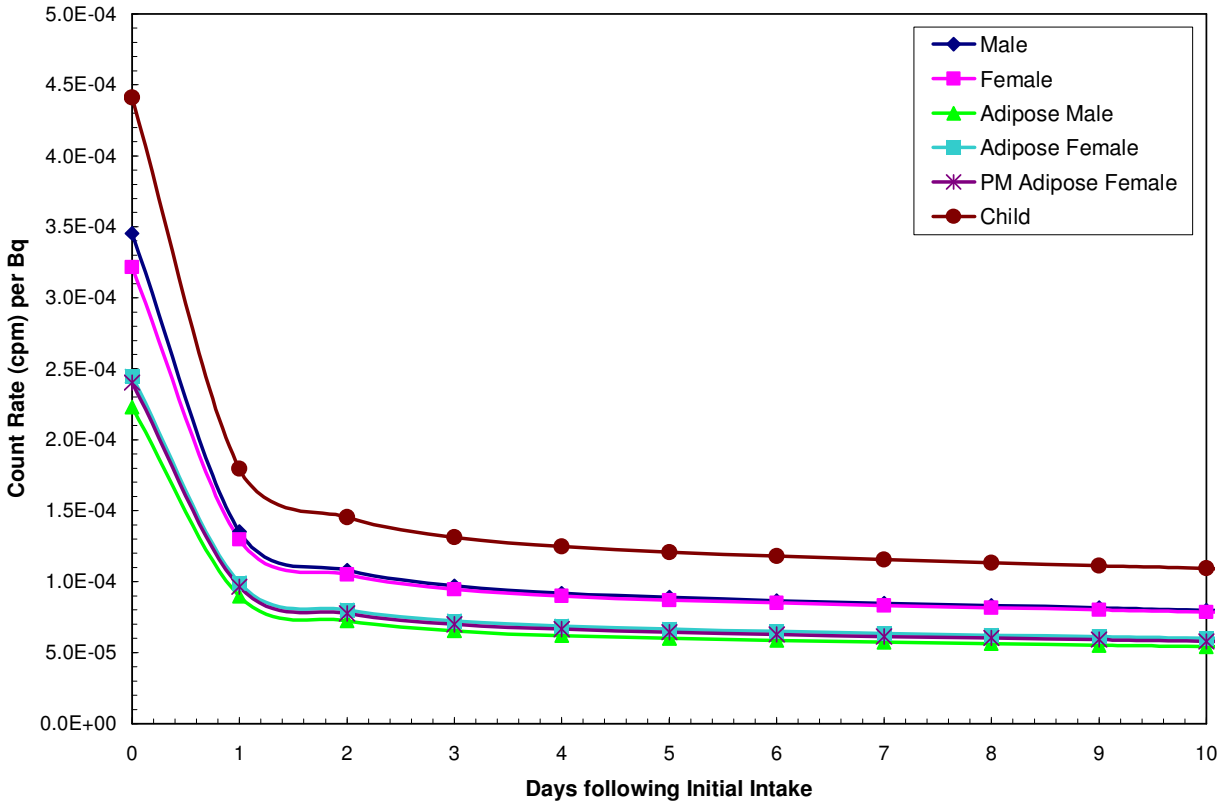

Figure 6.2.4 Count rate as a function of time for each phantom type contaminated with Ir-192

The effects of body type on the detector response are also similar between Co-60 and Ir-192. Similar phantom types display similar count rates: the adipose phantoms show the lowest count rate, but there is little variability between each adipose phantom. The reference male and reference female show similar count rates. Also, as seen in Cs-137 and Co-60, the highest count rate for Ir-192 was exhibited in the child phantom.

Am-241 showed the lowest count rate per Bq of activity. Due to the low energy of the gamma-ray emission (59.5keV) only a small fraction of the particles travel to the detector. Due to this, the count rate per Bq is several orders of magnitude less than the other isotopes. In addition, the dose coefficient for Am-241 is much lower than the other isotopes investigated in this work. As a result, the count rate due to an intake of Am-241 that would result in a 25 rem committed effective dose by inhalation is less than one count per minute for the male phantom

for the back lung position and less than 0.01 counts per minute for the neck and thigh position in the male phantom for all times modeled.

The statistical error of the computational models was the main source of error for each of the phantom results. The total bin error for each tally was generally less than 1%.

Monte Carlo simulations were also performed using Strontium-90 and the male phantom type. Strontuim-90 emits a beta spectrum with an average beta energy of 934 keV and exists in secular equilibrium with Yttrium-90 which emits a beta spectrum with an average beta energy of 196 keV. [8] Electrons were generated in the source organs, and were also transported in the model. Bremmsstrahlung photons were also generated and tracked, and both electrons and photons were tallied in the detector crystal. The results of the simulation showed that the thyroid uptake collimator was unable to detect significant amounts of Sr/Y-90, and on the basis of these results the other phantom types were not simulated.

6.3 Consideration of Background Spectra

Thyroid Uptake Systems are built with collimators for the purpose of shielding background and obtaining a spectrum from a fairly localized area. In the event of a RDD, there could be widespread contamination surrounding the measurement areas. In an emergency situation, it is possible, though not likely, that external contamination may still be present on the skin or clothing of individuals being assessed. In this case, the collimator provides a basic advantage by attenuating a significant amount of radiation emitted from external contamination. For this work, external contamination on the victims was not considered and not included in the phantom models. The only source of background is assumed to originate from the surroundings,

not the individual. To thoroughly understand the effect that high background rates might have on assessing internal contamination, the following analysis was performed.

Several background measurements were collected at the Emory University Hospital Nuclear Medicine Injection Room in Atlanta, Georgia. In this room, nuclear medicine procedures involving various isotopes are conducted. The room has a relatively high background rate since contaminated objects (needles, towels, gloves, etc) are disposed of in a lead shielded box stored in the room. A Captus 2000 Thyroid Uptake System was housed in this room, and background count rate levels were collected using this machine. The Captus 2000 and the Captus 3000 are very similar in that each includes a thyroid uptake collimator with a 2" by 2" NaI crystal and a lead and antimony collimator. One major difference between the two systems is that the Captus 2000 does not include the nuclide identification tool. As a result, background rates were collected for the entire spectrum only.

The average background rate in this room was 2846 counts per minute. Counts were taken for 10 minutes of live time. In the Georgia Tech laboratory that held the Captus 3000 Thyroid Uptake System, the background rate was significantly lower. The average background rate was approximately 1700 counts per minute, recorded over 10 minutes of live time. One background spectrum collected in the Georgia Tech laboratory is shown in Figure 6.3.1. The spectrum has been scaled up by a factor of two to approximate a more realistic hospital background. This scaled spectrum was used in the calculations of MDA and the DLs.

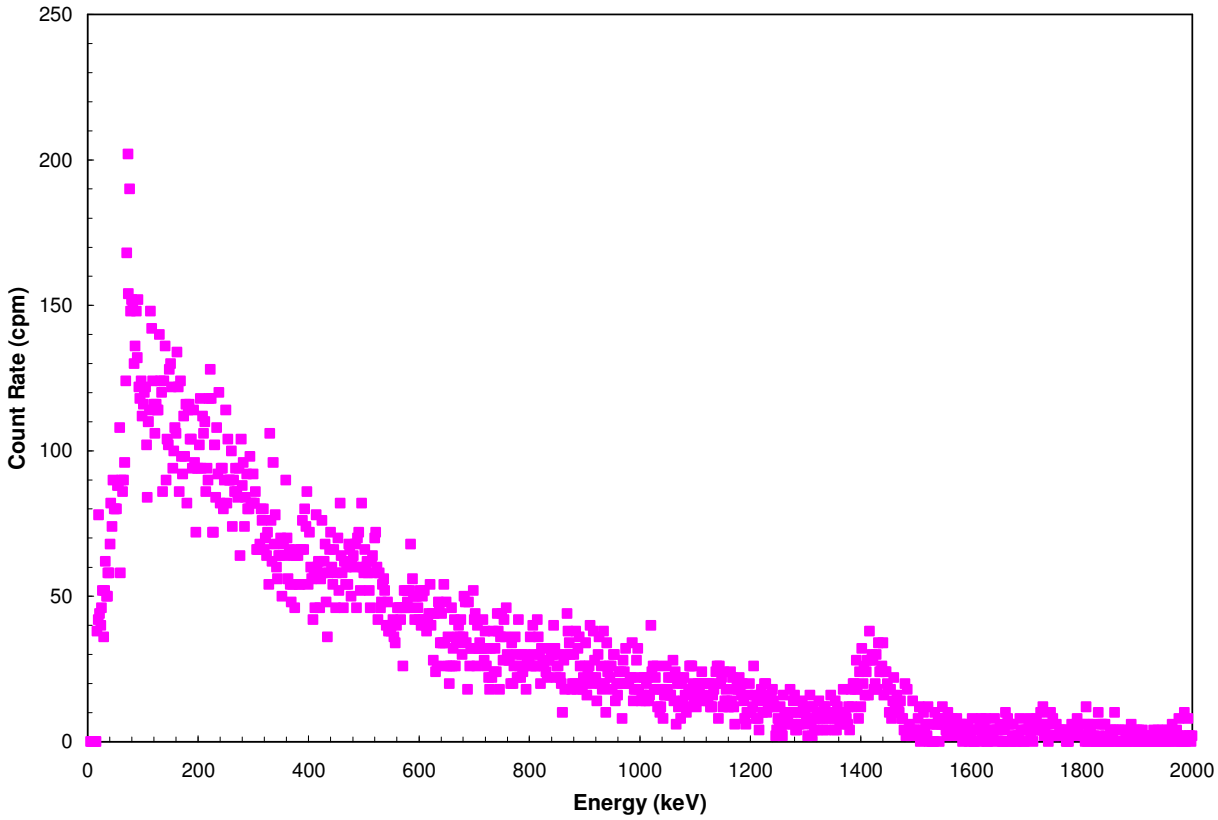

Figure 6.3.1 Background spectrum collected at Georgia Tech laboratory

6.4 Decision Levels

The DL for determining whether activity is present was calculated for the thyroid uptake collimator. The DL is a function of the background rate and counting times; thus is is dependent on the isotope. The background rate in the Capintec ROI was used for each isotope. The DL values represent the minimum count rates above background to assume that activity is present. Table 6.4.1 shows the DL necessary for a one minute counting time for a factor of five times the scaled up Georgia Tech background spectrum (this is essentially 10 times the average background count rate). This table also includes the default ROI values for each isotope used in conjunction with the phantoms, and the background count rate within that ROI.

Table 6.4.1 Decision Levels for one minute counting times for the thyroid uptake collimator

Isotope	Default ROI (keV)	5 x background count rate in ROI	Decision Level for one minute counting time (Count rate above background)
Am-241	49-70	5340	40
Cs-137	627-697	6430	44
Co-60	1126-1382	5120	39
Ir-192	287-335	9230	52
I-131	338-391	8500	50

As anticipated, the minimum count rate required to determine the presence of activity with 95% confidence increases as the background rate increases, and decreases as counting time increases. In the event of an RDD, the minimum counting time will be desired to maximize the number of people assessed in a given amount of time. By comparing the decision level to the calculated count rate due to an intake of one CDL for the male phantom, it has been determined that one minute is more than adequate to detect Cs-137, Co-60, or Ir-192 from the back right lung position. I-131 can be detected from the back right lung position with a one minute counting time for the first two days following intake. Subsequent to that, the neck is a more optimal position. If the detector is placed over the neck, a one minute counting time is sufficient to detect one CDL of Cs-137 and I-131 as well. The thigh is not an adequate position for assaying I-131 or Am-241. For Co-60, Cs-137, and Ir-192, a one minute counting time is sufficient to detect an intake of one CDL or greater for the thigh position. Am-241 is not detectable above background at any of the studied detector positions. A comparison of the count rate per CDL and the DL for a one minute counting time is shown in Table 6.4.2 for each isotope and the optimal detector position. From this comparison, it is clear that Am-241 is undetectable, and the other four isotopes exceed the decision level by at least two orders of magnitude.

Table 6.4.2 Count rate per CDL for optimal detector position on male phantom, 3 days following initial intake

Isotope	Detector Position	Count Rate (cpm) per CDL	Decision Level for one minute counting time (Count rate above background)
Am-241	Back Right Lung	0.146	40
Cs-137	Neck	27600	44
Co-60	Back Right Lung	2390	39
Ir-192	Back Right Lung	4670	52
I-131	Neck	2530	50

With 27 kg of adipose tissue, the Post-Menopausal Adipose Female phantom contains the most adipose tissue, and as a result generally shows the lowest count rates per Bq of intake. By examining the Post-Menopausal Adipose Female, an upper limit to the minimum necessary counting time can be estimated. A counting time of one minute is sufficient to detect one CDL of Co-60, Ir-192, and Cs-137 when the detector is placed over the back right lung. For I-131 and Cs-137, the detector should be placed over the front neck to achieve maximum efficiency. One minute is a sufficient amount of time to detect I-131 and Cs-137 when the detector is placed on the front neck of the Post-Menopausal Adipose Female phantom.

6.5 Personal Contamination Screening Threshold Determination

As previously discussed, one Clinical Decision Level is assumed to be an intake which leads to 25 rem committed effective dose. The actual use of the Clinical Decision Level will be made by governing bodies at the time of an event. The dose coefficients for inhalation for each isotope are from ICRP 72 and were determined using Rad Toolbox [8]. The dose coefficients are shown in Table 6.5.1.

Table 6.5.1 Dose coefficients for inhalation for one CDL

	Adult (Bq/CDL)	10 year Child (Bq/CDL)
Cs-137 F	5.43E+07	1.25E+08
Co-60 M	2.50E+07	1.67E+07
I-131 F	3.38E+07	1.32E+07
Ir-192 M	4.81E+07	3.29E+07
Am-241 M	5.95E+03	6.25E+03

Count rates per CDL are given for each isotope and phantom type in Tables 6.5.2 through 6.5.31.

Table 6.5.2 Count rate per CDL for the Male phantom contaminated with Cs-137

		Back Right Lung	**Front Right Lung**	**Neck**	**Thigh**
		cpm per CDL	**cpm per CDL**	**cpm per CDL**	**cpm per CDL**
Days following exposure	0	1.01E+04	9.65E+03	8.20E+02	7.11E+01
	1	2.33E+04	2.52E+04	2.76E+04	1.34E+04
	2	2.24E+04	2.43E+04	2.82E+04	1.38E+04
	3	2.14E+04	2.34E+04	2.76E+04	1.35E+04
	4	2.08E+04	2.27E+04	2.71E+04	1.33E+04
	5	2.04E+04	2.23E+04	2.67E+04	1.31E+04
	6	2.01E+04	2.20E+04	2.63E+04	1.29E+04
	7	1.99E+04	2.18E+04	2.60E+04	1.27E+04
	8	1.97E+04	2.16E+04	2.58E+04	1.26E+04
	9	1.95E+04	2.14E+04	2.56E+04	1.25E+04
	10	1.94E+04	2.12E+04	2.54E+04	1.24E+04
	20	1.81E+04	1.98E+04	2.37E+04	1.16E+04
	30	1.70E+04	1.86E+04	2.22E+04	1.09E+04

Table 6.5.3 Count rate per CDL for the Female phantom contaminated with Cs-137

		Back Right Lung	Neck	Thigh
		cpm per CDL	cpm per CDL	cpm per CDL
Days following exposure	0	9.38E+03	8.10E+02	8.62E+01
	1	2.94E+04	3.47E+04	1.29E+04
	2	2.87E+04	3.56E+04	1.32E+04
	3	2.77E+04	3.49E+04	1.30E+04
	4	2.70E+04	3.42E+04	1.27E+04
	5	2.65E+04	3.37E+04	1.25E+04
	6	2.62E+04	3.32E+04	1.24E+04
	7	2.59E+04	3.29E+04	1.22E+04
	8	2.56E+04	3.26E+04	1.21E+04
	9	2.54E+04	3.23E+04	1.20E+04
	10	2.52E+04	3.20E+04	1.19E+04
	20	2.35E+04	2.99E+04	1.11E+04
	30	2.21E+04	2.81E+04	1.04E+04

Table 6.5.4 Count rate per CDL for the Adipose Male phantom contaminated with Cs-137

		Back Right Lung	Neck	Thigh
		cpm per CDL	cpm per CDL	cpm per CDL
Days following exposure	0	6.64E+03	5.59E+02	3.49E+01
	1	2.00E+04	3.15E+04	1.25E+04
	2	1.95E+04	3.24E+04	1.28E+04
	3	1.88E+04	3.17E+04	1.26E+04
	4	1.83E+04	3.11E+04	1.23E+04
	5	1.80E+04	3.06E+04	1.21E+04
	6	1.77E+04	3.02E+04	1.20E+04
	7	1.75E+04	2.99E+04	1.19E+04
	8	1.73E+04	2.96E+04	1.17E+04
	9	1.72E+04	2.94E+04	1.16E+04
	10	1.70E+04	2.91E+04	1.15E+04
	20	1.59E+04	2.72E+04	1.08E+04
	30	1.49E+04	2.55E+04	1.01E+04

Table 6.5.5 Count rate per CDL for the Adipose Female phantom contaminated with Cs-137

		Back Right Lung	Neck	Thigh
		cpm per CDL	cpm per CDL	cpm per CDL
Days following exposure	0	7.00E+03	6.21E+02	5.13E+01
	1	2.29E+04	3.06E+04	1.79E+04
	2	2.24E+04	3.14E+04	1.85E+04
	3	2.16E+04	3.07E+04	1.81E+04
	4	2.11E+04	3.01E+04	1.77E+04
	5	2.07E+04	2.97E+04	1.75E+04
	6	2.04E+04	2.93E+04	1.72E+04
	7	2.02E+04	2.90E+04	1.71E+04
	8	2.00E+04	2.87E+04	1.69E+04
	9	1.98E+04	2.84E+04	1.67E+04
	10	1.96E+04	2.82E+04	1.66E+04
	20	1.84E+04	2.64E+04	1.55E+04
	30	1.72E+04	2.47E+04	1.46E+04

Table 6.5.6 Count rate per CDL for the Post-Menopausal Adipose Female phantom contaminated with Cs-137

		Back Right Lung	Neck	Thigh
		cpm per CDL	cpm per CDL	cpm per CDL
Days following exposure	0	1.14E+03	4.12E+02	4.57E+01
	1	5.98E+03	8.43E+03	3.01E+03
	2	5.97E+03	8.61E+03	3.09E+03
	3	5.79E+03	8.42E+03	3.03E+03
	4	5.66E+03	8.25E+03	2.97E+03
	5	5.56E+03	8.12E+03	2.92E+03
	6	5.49E+03	8.02E+03	2.88E+03
	7	5.43E+03	7.93E+03	2.85E+03
	8	5.37E+03	7.85E+03	2.82E+03
	9	5.33E+03	7.78E+03	2.80E+03
	10	5.28E+03	7.72E+03	2.78E+03
	20	4.94E+03	7.21E+03	2.59E+03
	30	4.63E+03	6.77E+03	2.43E+03

Table 6.5.7 Count rate per CDL for the Child phantom contaminated with Cs-137

		Back Right Lung	Neck	Thigh
		cpm per CDL	cpm per CDL	cpm per CDL
Days following exposure	0	2.85E+04	2.37E+03	0.00E+00
	1	8.75E+04	9.29E+04	4.83E+04
	2	8.53E+04	9.52E+04	4.98E+04
	3	8.21E+04	9.32E+04	4.88E+04
	4	8.01E+04	9.14E+04	4.79E+04
	5	7.87E+04	9.00E+04	4.71E+04
	6	7.76E+04	8.88E+04	4.65E+04
	7	7.67E+04	8.78E+04	4.60E+04
	8	7.59E+04	8.70E+04	4.56E+04
	9	7.53E+04	8.62E+04	4.52E+04
	10	7.47E+04	8.55E+04	4.48E+04
	20	6.98E+04	7.99E+04	4.19E+04
	30	6.55E+04	7.50E+04	3.93E+04

Table 6.5.8 Count rate per CDL calculated for the Male phantom contaminated with Co-60

		Back Right Lung	Front Right Lung	Neck	Thigh
		cpm per CDL	cpm per CDL	cpm per CDL	cpm per CDL
Days following exposure	0	6.91E+03	6.63E+03	1.60E+03	1.64E+02
	1	3.24E+03	3.32E+03	1.31E+03	5.09E+02
	2	2.66E+03	2.69E+03	1.21E+03	5.04E+02
	3	2.39E+03	2.41E+03	1.13E+03	4.59E+02
	4	2.26E+03	2.27E+03	1.08E+03	4.25E+02
	5	2.18E+03	2.19E+03	1.03E+03	4.01E+02
	6	2.12E+03	2.13E+03	9.98E+02	3.83E+02
	7	2.08E+03	2.08E+03	9.69E+02	3.69E+02
	8	2.03E+03	2.04E+03	9.43E+02	3.57E+02
	9	2.00E+03	2.00E+03	9.19E+02	3.47E+02
	10	1.96E+03	1.96E+03	8.98E+02	3.37E+02
	20	1.70E+03	1.70E+03	7.69E+02	2.85E+02
	30	1.54E+03	1.54E+03	7.10E+02	2.68E+02

Table 6.5.9 Count rate per CDL calculated for the Female phantom contaminated with Co-60

		Back Right Lung	Neck	Thigh
		cpm per CDL	cpm per CDL	cpm per CDL
Days following exposure	0	6.59E+03	1.61E+03	1.92E+02
	1	3.21E+03	1.58E+03	5.21E+02
	2	2.69E+03	1.52E+03	5.10E+02
	3	2.44E+03	1.44E+03	4.62E+02
	4	2.31E+03	1.37E+03	4.27E+02
	5	2.23E+03	1.32E+03	4.03E+02
	6	2.17E+03	1.27E+03	3.85E+02
	7	2.12E+03	1.23E+03	3.71E+02
	8	2.08E+03	1.20E+03	3.59E+02
	9	2.04E+03	1.17E+03	3.49E+02
	10	2.00E+03	1.14E+03	3.39E+02
	20	1.73E+03	9.72E+02	2.87E+02
	30	1.57E+03	9.02E+02	2.69E+02

Table 6.5.10 Count rate per CDL calculated for the Adipose Male phantom contaminated with Co-60

		Back Right Lung	Neck	Thigh
		cpm per CDL	cpm per CDL	cpm per CDL
Days following exposure	0	4.79E+03	1.18E+03	9.96E+01
	1	2.32E+03	1.28E+03	4.53E+02
	2	1.95E+03	1.28E+03	4.63E+02
	3	1.78E+03	1.22E+03	4.28E+02
	4	1.68E+03	1.17E+03	3.98E+02
	5	1.62E+03	1.12E+03	3.77E+02
	6	1.58E+03	1.08E+03	3.61E+02
	7	1.54E+03	1.05E+03	3.47E+02
	8	1.51E+03	1.02E+03	3.36E+02
	9	1.48E+03	9.93E+02	3.25E+02
	10	1.46E+03	9.68E+02	3.17E+02
	20	1.26E+03	8.25E+02	2.67E+02
	30	1.14E+03	7.68E+02	2.52E+02

Table 6.5.11Count rate per CDL calculated for the Adipose Female phantom contaminated with Co-60

		Back Right Lung	Neck	Thigh
		cpm per CDL	cpm per CDL	cpm per CDL
Days following exposure	0	4.95E+03	1.27E+03	1.29E+02
	1	2.48E+03	1.31E+03	5.58E+02
	2	2.10E+03	1.30E+03	5.93E+02
	3	1.91E+03	1.24E+03	5.63E+02
	4	1.81E+03	1.18E+03	5.31E+02
	5	1.74E+03	1.13E+03	5.06E+02
	6	1.70E+03	1.10E+03	4.85E+02
	7	1.66E+03	1.06E+03	4.67E+02
	8	1.62E+03	1.03E+03	4.52E+02
	9	1.59E+03	1.00E+03	4.38E+02
	10	1.56E+03	9.79E+02	4.26E+02
	20	1.35E+03	8.34E+02	3.60E+02
	30	1.22E+03	7.76E+02	3.39E+02

Table 6.5.12 Count rate per CDL calculated for the Post-Menopausal Adipose Female phantom contaminated with Co-60

		Back Right Lung	Neck	Thigh
		cpm per CDL	cpm per CDL	cpm per CDL
Days following exposure	0	5.07E+03	1.33E+03	1.24E+02
	1	2.47E+03	1.40E+03	3.98E+02
	2	2.07E+03	1.40E+03	3.96E+02
	3	1.88E+03	1.34E+03	3.61E+02
	4	1.78E+03	1.28E+03	3.35E+02
	5	1.72E+03	1.23E+03	3.17E+02
	6	1.67E+03	1.18E+03	3.03E+02
	7	1.63E+03	1.15E+03	2.92E+02
	8	1.60E+03	1.11E+03	2.82E+02
	9	1.57E+03	1.08E+03	2.74E+02
	10	1.54E+03	1.06E+03	2.66E+02
	20	1.33E+03	9.01E+02	2.25E+02
	30	1.21E+03	8.38E+02	2.12E+02

Table 6.5.13 Count rate per CDL calculated for the Child phantom contaminated with Co-60

		Back Right Lung	Neck	Thigh
		cpm per CDL	cpm per CDL	cpm per CDL
Days following exposure	0	5.60E+03	1.11E+03	3.19E+02
	1	2.75E+03	1.22E+03	5.00E+02
	2	2.30E+03	1.16E+03	4.59E+02
	3	2.08E+03	1.09E+03	4.07E+02
	4	1.97E+03	1.03E+03	3.74E+02
	5	1.90E+03	9.88E+02	3.52E+02
	6	1.85E+03	9.53E+02	3.37E+02
	7	1.81E+03	9.23E+02	3.26E+02
	8	1.77E+03	8.96E+02	3.16E+02
	9	1.73E+03	8.72E+02	3.07E+02
	10	1.70E+03	8.51E+02	2.99E+02
	20	1.48E+03	7.25E+02	2.54E+02
	30	1.34E+03	6.74E+02	2.37E+02

Table 6.5.14 Count rate per CDL calculated for the Male phantom contaminated with Am-241

		Back Right Lung	Front Right Lung	Neck	Thigh
		cpm per CDL	cpm per CDL	cpm per CDL	cpm per CDL
Days following exposure	0	4.26E-01	4.07E-01	2.83E-03	0.00E+00
	1	1.90E-01	1.54E-01	8.60E-03	3.86E-03
	2	1.58E-01	1.21E-01	6.05E-03	2.63E-03
	3	1.46E-01	1.08E-01	5.10E-03	1.99E-03
	4	1.42E-01	1.03E-01	4.76E-03	1.73E-03
	5	1.40E-01	1.00E-01	4.65E-03	1.63E-03
	6	1.39E-01	9.85E-02	4.63E-03	1.61E-03
	7	1.38E-01	9.72E-02	4.64E-03	1.61E-03
	8	1.38E-01	9.60E-02	4.66E-03	1.62E-03
	9	1.38E-01	9.49E-02	4.69E-03	1.63E-03
	10	1.37E-01	9.39E-02	4.71E-03	1.64E-03
	20	1.34E-01	8.46E-02	4.96E-03	1.76E-03
	30	1.33E-01	7.71E-02	5.13E-03	1.85E-03

Table 6.5.15 Count rate per CDL calculated for the Female phantom contaminated with Am-241

		Back Right Lung	Neck	Thigh
		cpm per CDL	cpm per CDL	cpm per CDL
Days following exposure	0	3.87E-01	3.36E-03	0.00E+00
	1	1.95E-01	9.10E-03	4.16E-03
	2	1.68E-01	6.41E-03	2.83E-03
	3	1.59E-01	5.41E-03	2.10E-03
	4	1.56E-01	5.05E-03	1.80E-03
	5	1.55E-01	4.93E-03	1.69E-03
	6	1.54E-01	4.91E-03	1.66E-03
	7	1.55E-01	4.92E-03	1.65E-03
	8	1.55E-01	4.94E-03	1.66E-03
	9	1.55E-01	4.97E-03	1.67E-03
	10	1.55E-01	4.99E-03	1.69E-03
	20	1.58E-01	5.23E-03	1.81E-03
	30	1.62E-01	5.40E-03	1.90E-03

Table 6.5.16 Count rate per CDL calculated for the Adipose Male phantom contaminated with Am-241

		Back Right Lung	Neck	Thigh
		cpm per CDL	cpm per CDL	cpm per CDL
Days following exposure	0	2.47E-01	2.69E-03	2.69E-03
	1	1.25E-01	8.20E-03	8.20E-03
	2	1.08E-01	5.77E-03	5.77E-03
	3	1.02E-01	4.86E-03	4.86E-03
	4	1.00E-01	4.54E-03	4.54E-03
	5	9.95E-02	4.43E-03	4.43E-03
	6	9.94E-02	4.41E-03	4.41E-03
	7	9.95E-02	4.42E-03	4.42E-03
	8	9.96E-02	4.44E-03	4.44E-03
	9	9.98E-02	4.47E-03	4.47E-03
	10	1.00E-01	4.49E-03	4.49E-03
	20	1.02E-01	4.72E-03	4.72E-03
	30	1.04E-01	4.89E-03	4.89E-03

Table 6.5.17 Count rate per CDL calculated for the Adipose Female phantom contaminated with Am-241

		Back Right Lung	Neck	Thigh
		cpm per CDL	cpm per CDL	cpm per CDL
Days following exposure	0	3.06E-01	3.13E-03	7.94E-06
	1	1.52E-01	8.49E-03	6.94E-03
	2	1.31E-01	5.98E-03	4.77E-03
	3	1.23E-01	5.05E-03	3.80E-03
	4	1.20E-01	4.71E-03	3.43E-03
	5	1.20E-01	4.60E-03	3.30E-03
	6	1.19E-01	4.58E-03	3.27E-03
	7	1.19E-01	4.59E-03	3.28E-03
	8	1.19E-01	4.61E-03	3.30E-03
	9	1.19E-01	4.63E-03	3.33E-03
	10	1.20E-01	4.66E-03	3.36E-03
	20	1.21E-01	4.88E-03	3.61E-03
	30	1.24E-01	5.04E-03	3.80E-03

Table 6.5.18 Count rate per CDL calculated for the Post-Menopausal Adipose Female phantom contaminated with Am-241

		Back Right Lung	Neck	Thigh
		cpm per CDL	cpm per CDL	cpm per CDL
Days following exposure	0	2.67E-01	3.41E-03	0.00E+00
	1	1.36E-01	8.98E-03	3.14E-03
	2	1.18E-01	6.33E-03	2.14E-03
	3	1.12E-01	5.35E-03	1.59E-03
	4	1.10E-01	4.99E-03	1.35E-03
	5	1.09E-01	4.87E-03	1.27E-03
	6	1.09E-01	4.85E-03	1.24E-03
	7	1.09E-01	4.86E-03	1.24E-03
	8	1.09E-01	4.88E-03	1.25E-03
	9	1.09E-01	4.90E-03	1.26E-03
	10	1.09E-01	4.93E-03	1.27E-03
	20	1.12E-01	5.16E-03	1.36E-03
	30	1.15E-01	5.33E-03	1.43E-03

Table 6.5.19 Count rate per CDL calculated for the Child phantom contaminated with Am-241

		Back Right Lung	Neck	Thigh
		cpm per CDL	cpm per CDL	cpm per CDL
Days following exposure	0	6.92E-01	1.17E-02	0.00E+00
	1	3.14E-01	2.12E-02	7.19E-03
	2	2.61E-01	1.51E-02	4.71E-03
	3	2.42E-01	1.28E-02	3.23E-03
	4	2.34E-01	1.19E-02	2.59E-03
	5	2.31E-01	1.17E-02	2.35E-03
	6	2.29E-01	1.16E-02	2.27E-03
	7	2.29E-01	1.16E-02	2.25E-03
	8	2.28E-01	1.16E-02	2.26E-03
	9	2.27E-01	1.17E-02	2.27E-03
	10	2.27E-01	1.17E-02	2.29E-03
	20	2.23E-01	1.21E-02	2.45E-03
	30	2.21E-01	1.24E-02	2.57E-03

Table 6.5.20 Count rate per CDL calculated for the Male phantom contaminated with I-131

		Back Right Lung	Front Right Lung	Neck	Thigh
		cpm per CDL	cpm per CDL	cpm per CDL	cpm per CDL
Days following exposure	0	9.67E+03	9.28E+03	8.16E+01	6.41E+00
	1	1.13E+03	1.11E+03	2.91E+03	3.45E+01
	2	3.76E+02	3.91E+02	2.75E+03	2.07E+01
	3	1.58E+02	1.81E+02	2.53E+03	2.73E+01
	4	9.16E+01	1.15E+02	2.32E+03	3.32E+01
	5	7.25E+01	9.53E+01	2.12E+03	3.76E+01
	6	6.82E+01	8.96E+01	1.95E+03	4.06E+01
	7	6.80E+01	8.79E+01	1.78E+03	4.25E+01
	8	6.83E+01	8.67E+01	1.63E+03	4.34E+01
	9	6.82E+01	8.51E+01	1.49E+03	4.37E+01
	10	6.74E+01	8.30E+01	1.37E+03	4.33E+01
	20	4.26E+01	4.93E+01	5.59E+02	2.77E+01
	30	2.06E+01	2.34E+01	2.25E+02	1.34E+01

Table 6.5.21 Count rate per CDL calculated for the Female phantom contaminated with I-131

		Back Right Lung	Neck	Thigh
		cpm per CDL	cpm per CDL	cpm per CDL
Days following exposure	0	8.98E+03	8.03E+01	8.48E+00
	1	1.07E+03	2.42E+03	3.20E+01
	2	3.67E+02	2.28E+03	1.91E+01
	3	1.69E+02	2.10E+03	2.51E+01
	4	1.10E+02	1.93E+03	3.05E+01
	5	9.48E+01	1.77E+03	3.45E+01
	6	9.24E+01	1.63E+03	3.73E+01
	7	9.31E+01	1.49E+03	3.90E+01
	8	9.37E+01	1.37E+03	3.99E+01
	9	9.35E+01	1.25E+03	4.01E+01
	10	9.23E+01	1.15E+03	3.98E+01
	20	5.80E+01	4.74E+02	2.54E+01
	30	2.80E+01	1.92E+02	1.23E+01

Table 6.5.22 Count rate per CDL calculated for the Adipose Male phantom contaminated with I-131

		Back Right Lung	Neck	Thigh
		cpm per CDL	cpm per CDL	cpm per CDL
Days following exposure	0	6.18E+03	5.98E+01	3.62E+00
	1	7.37E+02	2.54E+03	3.05E+01
	2	2.51E+02	2.41E+03	1.83E+01
	3	1.14E+02	2.21E+03	2.43E+01
	4	7.37E+01	2.03E+03	2.96E+01
	5	6.29E+01	1.86E+03	3.36E+01
	6	6.10E+01	1.71E+03	3.63E+01
	7	6.14E+01	1.56E+03	3.80E+01
	8	6.18E+01	1.43E+03	3.88E+01
	9	6.16E+01	1.31E+03	3.91E+01
	10	6.08E+01	1.20E+03	3.88E+01
	20	3.82E+01	4.92E+02	2.48E+01
	30	1.84E+01	1.98E+02	1.20E+01

Table 6.5.23 Count rate per CDL calculated for the Adipose Female phantom contaminated with I-131

		Back Right Lung	Neck	Thigh
		cpm per CDL	cpm per CDL	cpm per CDL
Days following exposure	0	6.73E+03	6.26E+01	5.93E+00
	1	8.09E+02	2.04E+03	4.62E+01
	2	2.77E+02	1.93E+03	2.85E+01
	3	1.28E+02	1.78E+03	3.79E+01
	4	8.36E+01	1.63E+03	4.63E+01
	5	7.20E+01	1.50E+03	5.24E+01
	6	7.00E+01	1.38E+03	5.66E+01
	7	7.04E+01	1.26E+03	5.92E+01
	8	7.08E+01	1.16E+03	6.06E+01
	9	7.05E+01	1.06E+03	6.09E+01
	10	6.96E+01	9.73E+02	6.05E+01
	20	4.35E+01	4.02E+02	3.86E+01
	30	2.10E+01	1.63E+02	1.87E+01

Table 6.5.24 Count rate per CDL calculated for the Post-Menopausal Adipose Female phantom contaminated with I-131

		Back Right Lung	Neck	Thigh
		cpm per CDL	cpm per CDL	cpm per CDL
Days following exposure	0	6.54E+03	6.80E+01	5.52E+00
	1	7.84E+02	2.31E+03	2.33E+01
	2	2.68E+02	2.18E+03	1.37E+01
	3	1.23E+02	2.01E+03	1.79E+01
	4	7.92E+01	1.84E+03	2.17E+01
	5	6.74E+01	1.69E+03	2.45E+01
	6	6.51E+01	1.56E+03	2.64E+01
	7	6.52E+01	1.43E+03	2.76E+01
	8	6.54E+01	1.31E+03	2.83E+01
	9	6.50E+01	1.20E+03	2.84E+01
	10	6.41E+01	1.10E+03	2.82E+01
	20	3.99E+01	4.54E+02	1.80E+01
	30	1.92E+01	1.84E+02	8.71E+00

Table 6.5.25 Count rate per CDL calculated for the Child phantom contaminated with I-131

		Back Right Lung	Neck	Thigh
		cpm per CDL	cpm per CDL	cpm per CDL
Days following exposure	0	4.80E+03	2.92E+01	1.06E+01
	1	5.89E+02	7.15E+02	1.58E+01
	2	2.02E+02	6.66E+02	9.42E+00
	3	9.57E+01	6.20E+02	1.18E+01
	4	6.42E+01	5.76E+02	1.40E+01
	5	5.58E+01	5.34E+02	1.57E+01
	6	5.44E+01	4.95E+02	1.69E+01
	7	5.45E+01	4.59E+02	1.76E+01
	8	5.46E+01	4.24E+02	1.79E+01
	9	5.43E+01	3.92E+02	1.80E+01
	10	5.34E+01	3.62E+02	1.78E+01
	20	3.31E+01	1.57E+02	1.13E+01
	30	1.59E+01	6.55E+01	5.45E+00

Table 6.5.26 Count rate per CDL calculated for the Male phantom contaminated with I-192

		Back Right Lung	Front Right Lung	Neck	Thigh
		cpm per CDL	cpm per CDL	cpm per CDL	cpm per CDL
Days following exposure	0	1.66E+04	1.59E+04	1.47E+02	8.29E+00
	1	6.50E+03	6.26E+03	8.46E+02	4.62E+02
	2	5.20E+03	5.02E+03	8.73E+02	4.54E+02
	3	4.67E+03	4.51E+03	8.65E+02	4.27E+02
	4	4.42E+03	4.27E+03	8.58E+02	4.12E+02
	5	4.27E+03	4.13E+03	8.53E+02	4.06E+02
	6	4.17E+03	4.03E+03	8.49E+02	4.02E+02
	7	4.08E+03	3.94E+03	8.45E+02	4.00E+02
	8	4.00E+03	3.86E+03	8.42E+02	3.98E+02
	9	3.92E+03	3.79E+03	8.38E+02	3.97E+02
	10	3.84E+03	3.72E+03	8.35E+02	3.95E+02
	20	3.19E+03	3.09E+03	8.09E+02	3.85E+02
	30	2.69E+03	2.61E+03	7.82E+02	3.73E+02

Table 6.5.27 Count rate per CDL calculated for the Female phantom contaminated with I-192

		Back Right Lung	Neck	Thigh
		cpm per CDL	cpm per CDL	cpm per CDL
Days following exposure	0	1.55E+04	1.51E+02	1.05E+01
	1	6.24E+03	8.84E+02	4.30E+02
	2	5.04E+03	9.12E+02	4.20E+02
	3	4.55E+03	9.04E+02	3.92E+02
	4	4.32E+03	8.97E+02	3.78E+02
	5	4.18E+03	8.92E+02	3.71E+02
	6	4.08E+03	8.87E+02	3.68E+02
	7	4.00E+03	8.83E+02	3.66E+02
	8	3.92E+03	8.80E+02	3.64E+02
	9	3.85E+03	8.76E+02	3.63E+02
	10	3.78E+03	8.73E+02	3.62E+02
	20	3.17E+03	8.46E+02	3.52E+02
	30	2.69E+03	8.18E+02	3.41E+02

Table 6.5.28 Count rate per CDL calculated for the Adipose Male phantom contaminated with I-192

		Back Right Lung	Neck	Thigh
		cpm per CDL	cpm per CDL	cpm per CDL
Days following exposure	0	1.07E+04	1.16E+02	3.50E+00
	1	4.31E+03	7.67E+02	4.12E+02
	2	3.48E+03	7.95E+02	4.06E+02
	3	3.14E+03	7.89E+02	3.82E+02
	4	2.98E+03	7.84E+02	3.69E+02
	5	2.88E+03	7.79E+02	3.63E+02
	6	2.82E+03	7.75E+02	3.60E+02
	7	2.76E+03	7.72E+02	3.58E+02
	8	2.70E+03	7.69E+02	3.56E+02
	9	2.65E+03	7.66E+02	3.55E+02
	10	2.60E+03	7.64E+02	3.54E+02
	20	2.18E+03	7.41E+02	3.45E+02
	30	1.85E+03	7.16E+02	3.34E+02

Table 6.5.29 Count rate per CDL calculated for the Adipose Female phantom contaminated with I-192

		502 - Back Right Lung	542 - Neck	562 - Thigh
		cpm per CDL	cpm per CDL	cpm per CDL
Days following exposure	0	1.18E+04	1.14E+02	8.11E+00
	1	4.76E+03	7.50E+02	5.98E+02
	2	3.85E+03	7.76E+02	6.08E+02
	3	3.48E+03	7.70E+02	5.90E+02
	4	3.30E+03	7.64E+02	5.79E+02
	5	3.20E+03	7.60E+02	5.73E+02
	6	3.12E+03	7.56E+02	5.70E+02
	7	3.06E+03	7.53E+02	5.67E+02
	8	3.00E+03	7.50E+02	5.65E+02
	9	2.94E+03	7.47E+02	5.63E+02
	10	2.89E+03	7.44E+02	5.61E+02
	20	2.42E+03	7.22E+02	5.47E+02
	30	2.06E+03	6.98E+02	5.30E+02

Table 6.5.30 Count rate per CDL calculated for the Post-Menopausal Adipose Female phantom contaminated with I-192

		Back Right Lung	Neck	Thigh
		cpm per CDL	cpm per CDL	cpm per CDL
Days following exposure	0	1.15E+04	1.28E+02	3.69E+00
	1	4.63E+03	8.43E+02	3.23E+02
	2	3.73E+03	8.74E+02	3.09E+02
	3	3.37E+03	8.67E+02	2.84E+02
	4	3.19E+03	8.61E+02	2.71E+02
	5	3.09E+03	8.56E+02	2.65E+02
	6	3.02E+03	8.52E+02	2.62E+02
	7	2.95E+03	8.48E+02	2.60E+02
	8	2.90E+03	8.45E+02	2.59E+02
	9	2.84E+03	8.42E+02	2.58E+02
	10	2.79E+03	8.39E+02	2.57E+02
	20	2.33E+03	8.13E+02	2.51E+02
	30	1.98E+03	7.86E+02	2.43E+02

Table 6.5.31 Count rate per CDL calculated for the Child phantom contaminated with I-192

		Back Right Lung	Neck	Thigh
		cpm per CDL	cpm per CDL	cpm per CDL
Days following exposure	0	1.45E+04	1.42E+02	1.89E+01
	1	5.91E+03	1.03E+03	3.58E+02
	2	4.78E+03	1.06E+03	3.42E+02
	3	4.32E+03	1.05E+03	3.14E+02
	4	4.10E+03	1.04E+03	3.00E+02
	5	3.98E+03	1.04E+03	2.94E+02
	6	3.88E+03	1.03E+03	2.90E+02
	7	3.80E+03	1.03E+03	2.89E+02
	8	3.73E+03	1.02E+03	2.87E+02
	9	3.66E+03	1.02E+03	2.86E+02
	10	3.59E+03	1.02E+03	2.85E+02
	20	3.02E+03	9.87E+02	2.77E+02
	30	2.57E+03	9.55E+02	2.68E+02

CHAPTER 7

CONCLUSIONS

The Captus 3000 Thyroid Uptake System can be used to assess the internal contamination in an individual following the use of a RDD for some isotopes. These isotopes include Co-60, Cs-137, Ir-192, and I-131. The thyroid uptake system cannot be used to detect internal contamination due to Am-241. The calculated count rate per one CDL of Am-241 is too low to differentiate it from background using this system. This is a consequence of the low dose coefficient and the low energy of the gamma-ray emission of Am-241. Even at a relatively high intake of Am-241 (1 CDL) the count rate from the thyroid uptake collimator is less than one count per minute.

In an emergency scenario, it would be more beneficial to identify the isotope than to spend time determining the BMI or body type of the individuals being scanned. The optimal position for the thyroid uptake collimator depends on the isotope inhaled. If the isotope has not been identified, the most optimal position is the back right lung followed by the neck. The thigh should not be chosen as a detection position for the thyroid uptake collimator unless circumstances prevent use of the other two locations. This is one of the consequences of a high degree of collimation. The detection efficiency is reduced as a result of a smaller angle seen by the detector, and the distance between the detector and the object of interest.

Given the threshold of one CDL, the minimum necessary counting time is one minute. This can be used as a baseline for all isotopes on the back right lung, with the exception of I-131, in which the probe would need to be placed on the neck for this counting time. In a situation

where large numbers of people are potentially contaminated, it is important to use the minimum necessary counting time to achieve efficient results.

CHAPTER 8

FUTURE WORK

Based on the conclusions from this investigation, other methods for detecting Am-241 need to be developed. Possible methods include urinalysis or fecal studies to detect low levels of this isotope. It is likely that these methodologies must retain high efficiency even a high levels of background, otherwise they will not be applicable for this application.

Another feature of the Captus 3000 Thyroid Uptake System is the Bioassay collimator, which was not fully considered in this analysis. With a considerably shorter collimator, it is possible that the bioassay collimator could be used to detect isotopes with a smaller dose coefficient (such as Am-241) following an RDD event. It would also tend to have lower decision levels, allowing it to detect smaller activities in a human.

This work focused on inhalation as the method of intake for each radionuclide. By considering ingestion, the work can be expanded to cover the two main routes of intake. This would require repeating the biokinetic analysis for ingestion and positioning the thyroid uptake collimator over the abdomen rather than the lungs or neck.

Finally, the validated model of the thyroid uptake probe could be used in conjunction with newly developed voxel phantoms. Voxel phantoms are based on digital images captured from studies completed on actual humans using Computed Tomography (CT) or Magnetic Resonance Imaging (MRI). While many of these phantoms are still undergoing development and validation, it is possible that they could provide a more realistic representation of various human body types, thus refining the simulations of internal contamination following a RDD.

APPENDIX A

THYROID UPTAKE COLLIMATOR AND SLAB PHANTOM MCNP INPUT FILE

```
Thyroid Uptake Collimator - 30mmPMMA, Cs-137
c Cell Cards
1    1   -0.0012    1 2 3 17 19 20 -99          imp:p=1 $ Outside Air
2    2   -3.67     -5                           imp:p=1 $ NaI crystal
3    4   -1.19     -1:-2 3 4                    imp:p=1 $ PMMA
4    3   -7.82      (-17 10):(-19 18): -20      imp:p=1 $ Steel
5    5   -1.03     -3 2                         imp:p=1 $ Virtual Water
6    6   -2.7       5 14 -6                     imp:p=1 $ Aluminum
7    7   -1        -4                           imp:p=1 $ Source
8    0             -9 5                         imp:p=1 $ Vacuum
9    1   -0.0012   -7                           imp:p=1 $ Air in coll
10   3   -7.82      (7 -11)                     imp:p=1 $ Inner Steel Liner
11   8   -11.4     (-10 11):(-18 11 12 16 21)   imp:p=1 $ Pb innards
12   1   -.0012     -18 16 -21                  imp:p=1 $ air in back
13   9   -8.4      (-14 15):(-12 13)            imp:p=1 $ Brass Ring
14   1   -0.0012    6 11 -15                    imp:p=1 $ Air ret ring
15   1   -0.0012   -13 6 9 14 15                imp:p=1 $ Air in brass tube
16   10  -11.4     -16 12                       imp:p=1 $ Pure Led sheet
99   0              99                          imp:p=0 $ Universe

c Surface Cards
1       rpp  0 3.0 -30 30 -30 30                $ PMMA slab
2       rpp  3.0 3.6 -30 30 -30 30              $ Source Holder
3       rpp  3.6001 13.6 -30 30 -30 30          $ Virtual Water
4       rcc  3.3001 -1.15 0 0 2.3 0 .2          $ Source
5       rcc -21.5051 0 0 5.08 0 0 2.54          $ NaI Crystal
6       rcc -21.5051 0 0 5.1308 0 0 2.824       $ Al Housing
9       rcc -34.7893 0 0 13.2842 0 0 2.921      $ PMT Tubes space
10      trc -11.5824 0 0 11.5824 0 0 4.445 5.3975   $ Outer Detector Housing ID
17      trc -11.5824 0 0 11.5824 0 0 4.7625 5.715   $ Outer Detector Housing OD
11      trc -15.7393 0 0 15.7393 0 0 2.7344 4.8018  $ Inner Steel Liner
7       trc -15.7393 0 0 15.7393 0 0 2.5344 4.6018  $ Air in collimator
12      rcc -40.8223 0 0 25.083 0 0 3.505       $ Inner Tube OD around PMT
13      rcc -40.8223 0 0 25.083 0 0 3.175       $ Inner Tube ID
14      rcc -16.3743 0 0 0.635 0 0 3.175        $ Retaining Ring OD
15      rcc -16.3743 0 0 0.635 0 0 2.565        $ Retaining Ring ID (air)
16      rcc -40.8223 0 0 14.9225 0 0 3.823      $ Detector Side Shield (Pb)
18      rcc -40.8223 0 0 29.2399 0 0 4.445      $ Cyl Detector Housing ID
19      rcc -40.8223 0 0 29.2399 0 0 4.7625     $ Cyl Detector Housing OD
20      rcc -41.8223 0 0 1.0 0 0 4.7625         $ Back end cap
21      px -25.8998                         $ air plane!
99      rpp -50 50 -50 50 -50 50                $ Universe

c Data Cards
c Material Card for Air (NIST DRY AIR)
m1    8016.          -0.232
      7014.          -0.755
      6012           -1.20E-4
      18000.42c      -1.28E-2
c Material Card for Sodium Iodide
m2    11000.04p      0.5
      53000.04p      0.5
c Material Card for grain controlled mild steel
m3    26054          -0.05821
      26056          -0.9137
      26057          -0.0211    26058          -0.00281
```

```
      6012          -0.0006
     25055          -0.0035
     15031          -0.00004
     16000          -0.00005
c Material Card for PMMA
m4    6000.          0.3333
     8016.          0.1333
     1001.          0.5333
c Material Card for Virtual Water
m5    1001.          0.0802
     6000.          0.6703
     7015.          0.0214
     8016.          0.1991
     17000.          0.0014
     20000.          0.0231
c Material Card for Aluminum
m6    13027.  1
c Material Card for polyester (sources)
m7    6000.          0.333
     1001.          0.533
     8016.          0.133
c Material Card for Antimonial Lead
m8    82000   0.96
     51000   0.04
c Material Card for High Brass
m9    29000    0.65
     30000    0.35
c Material Card for Pure Lead
m10    82000   1
mode  p
phys:p 4j 1
sdef par=2 rad=d1 ext=d2 pos=3.3 0 0 axs=0 1 0 vec=0 0 1 erg=d3
si1 0 0.2
sp1 -21 1
si2 -1.15 1.15
sp2 -21 0
si3 l 0.661645
sp3   .897759
c Two Tallys
f8:p 2  $ volume of crystal
f18:p 2  $ same volume
c energy bins
e0 0 1e-8 0.005 1024i 2.046
c Gaussian Energy Broadening
ft8 GEB -0.00298579 0.0925102 -0.4
print
nps 1E8
```

APPENDIX B

SLAB PHANTOM SPECTRAL DATA

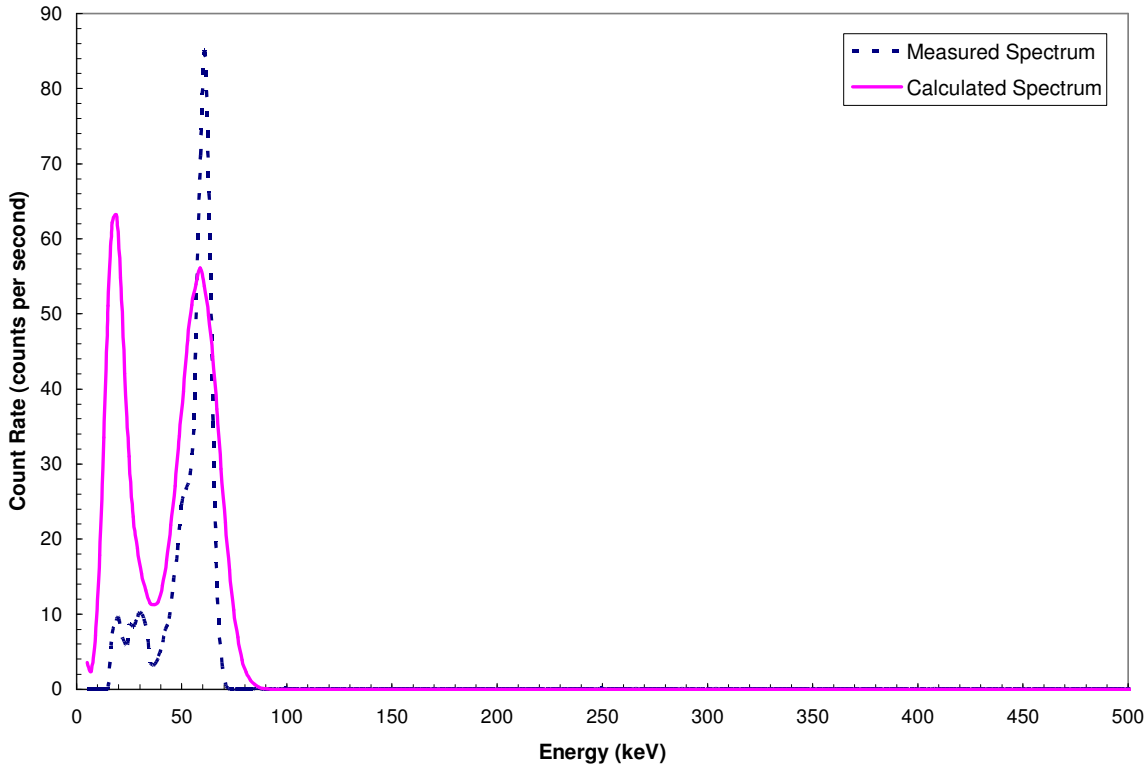

Figure B.1 Measured and calculated spectra for Am-241 with 0 mm PMMA

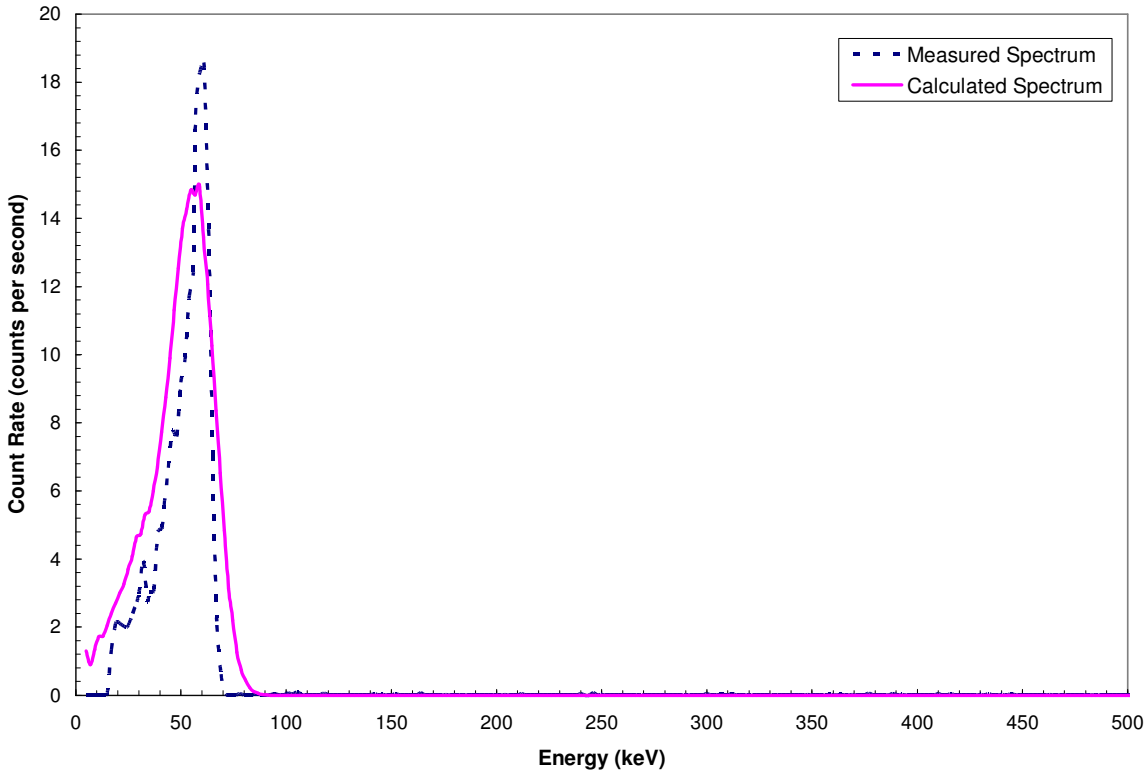

Figure B.2 Measured and calculated spectra for Am-241 with 60 mm PMMA

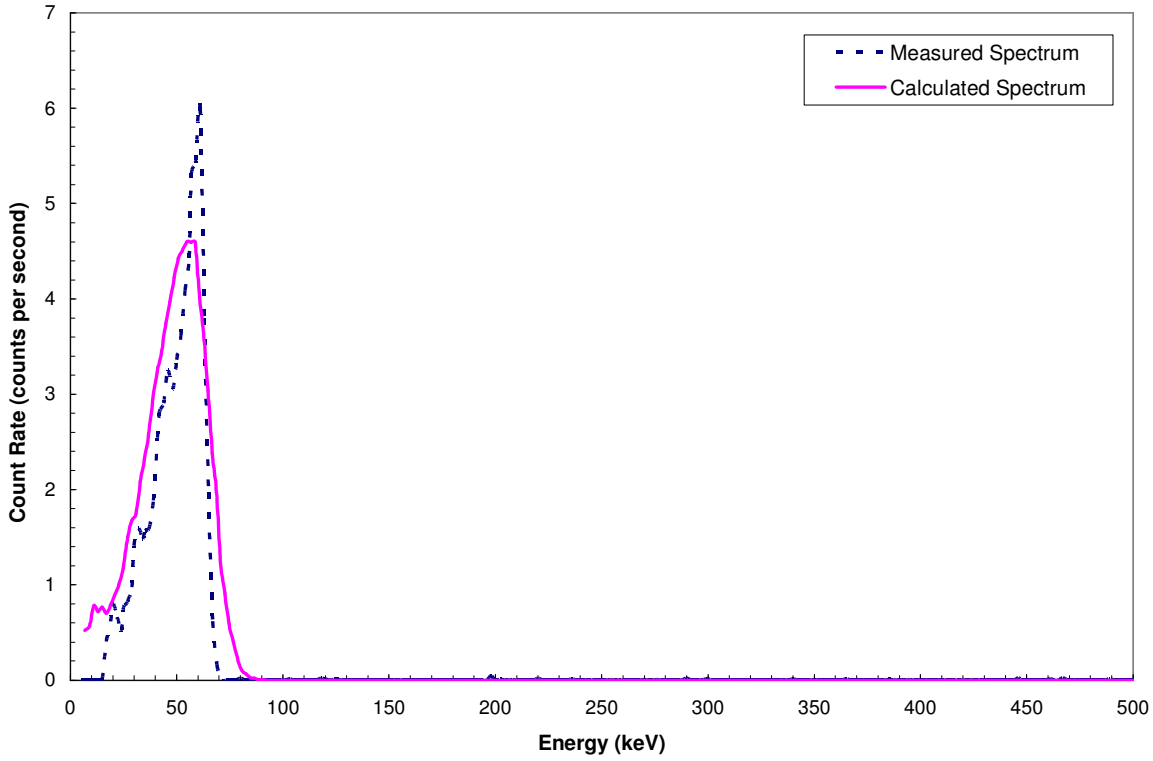

Figure B.3 Measured and calculated spectra for Am-241 with 108 mm PMMA

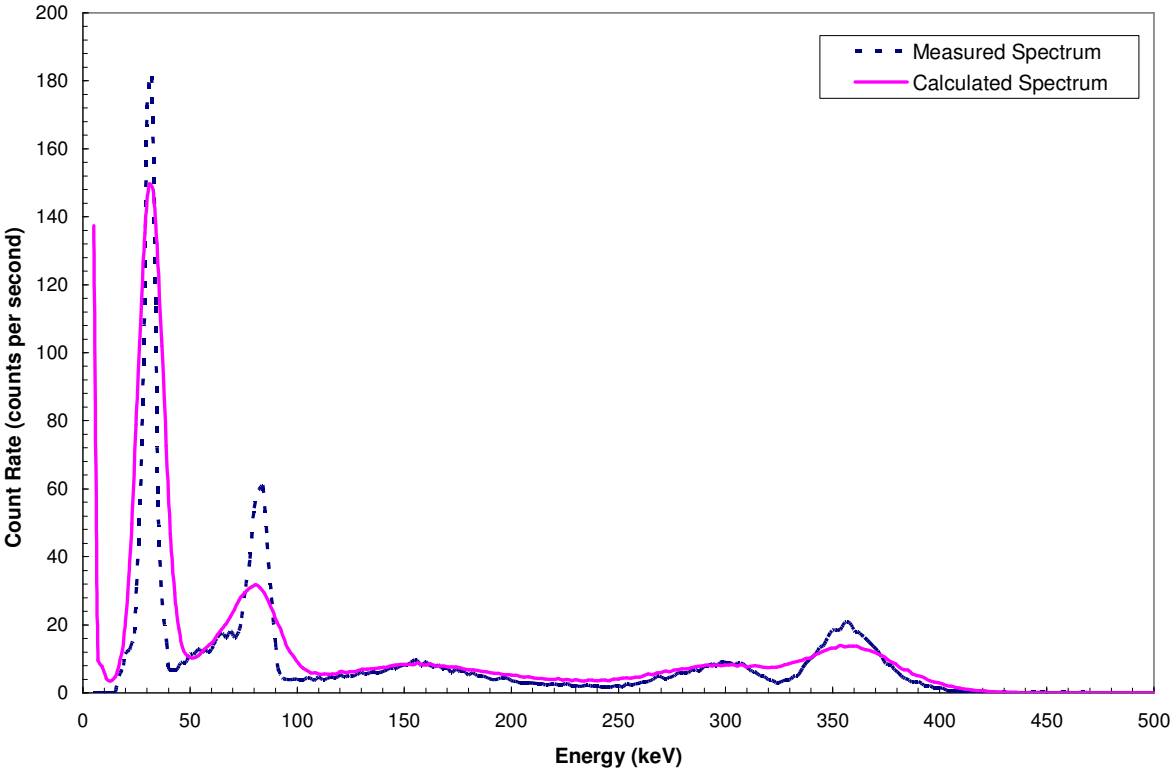

Figure B.4 Measured and calculated spectra for Ba-133 with 0 mm PMMA

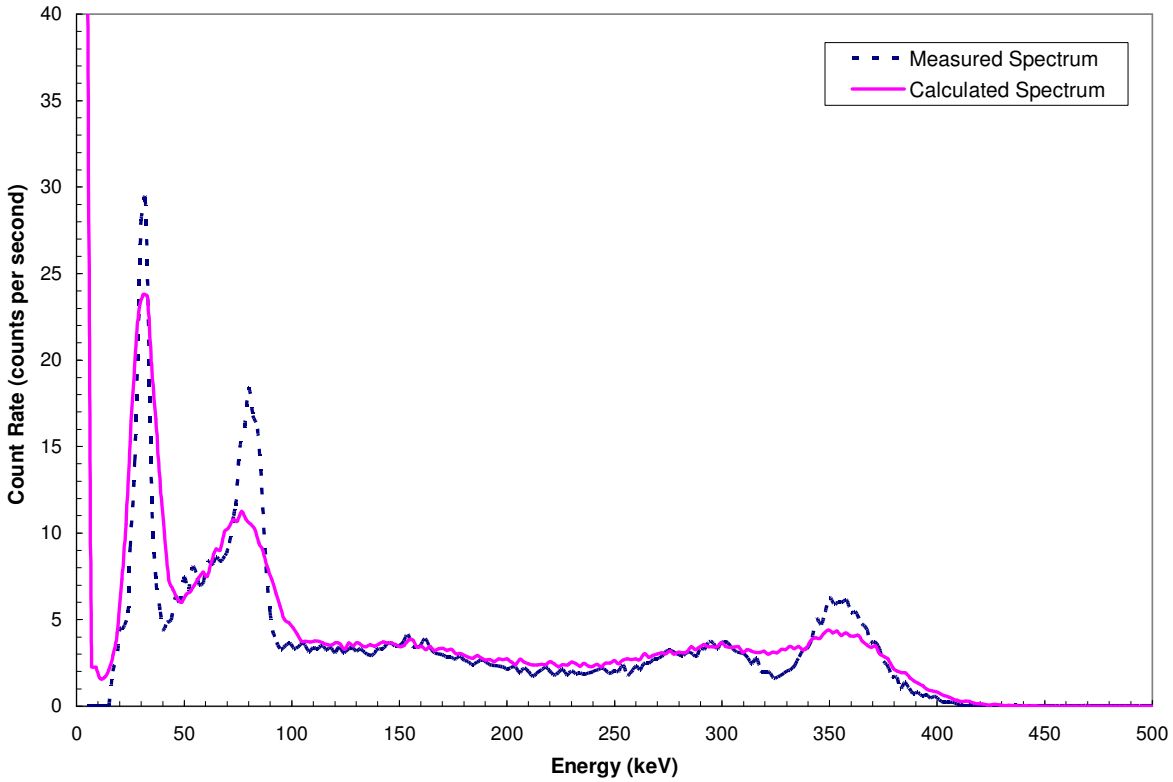

Figure B.5 Measured and calculated spectra for Ba-133 with 60 mm PMMA

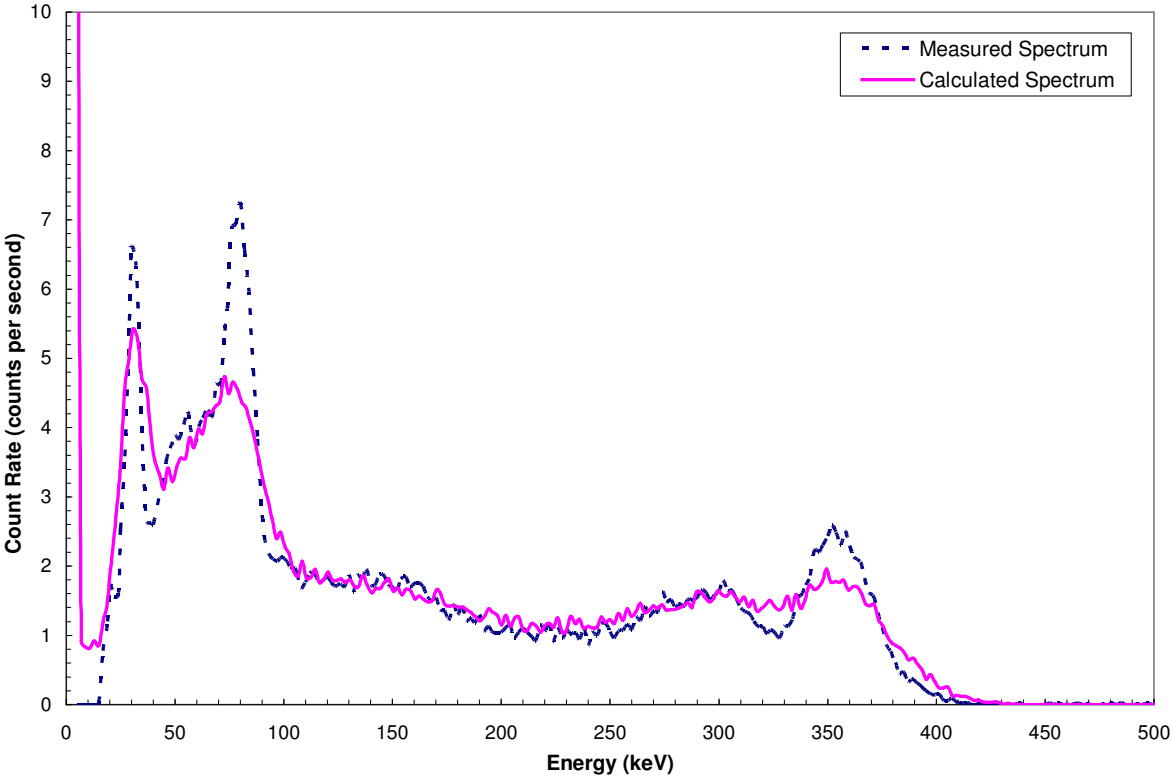

Figure B.6 Measured and calculated spectra for Ba-133 with 108 mm PMMA

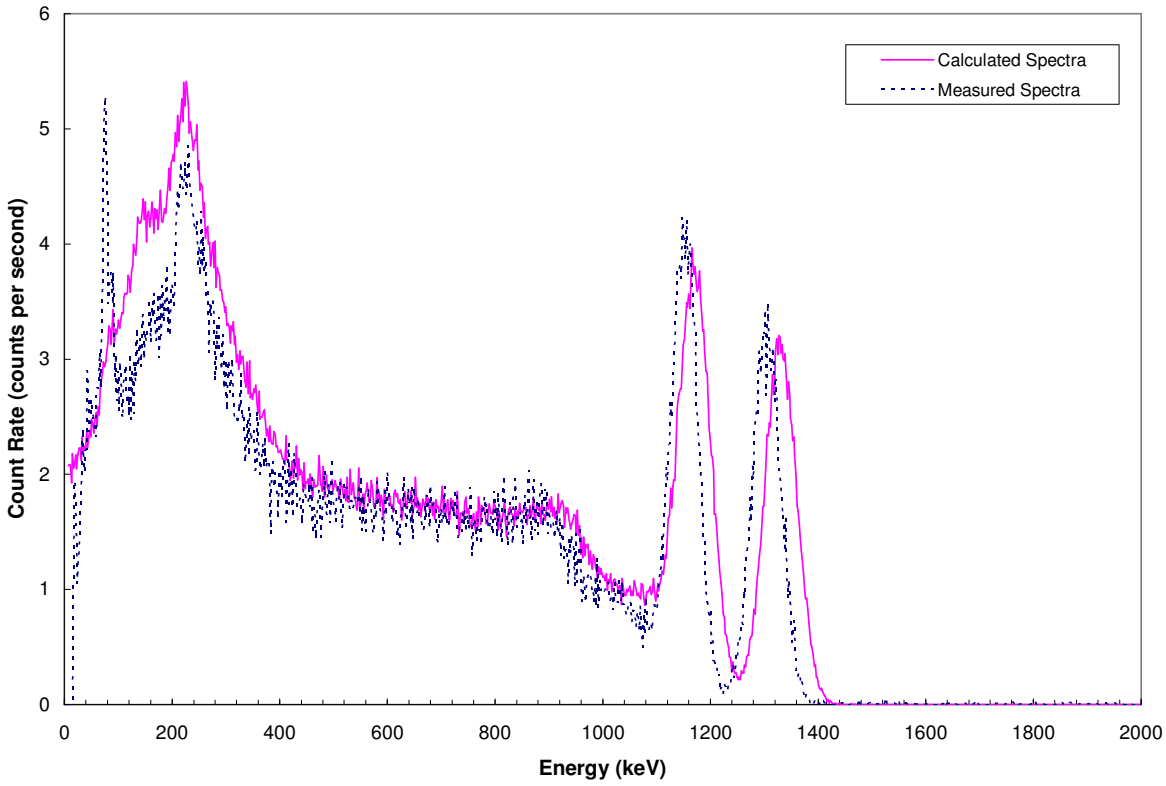

Figure B.7 Measured and calculated spectra for Co-60 with 0 mm PMMA

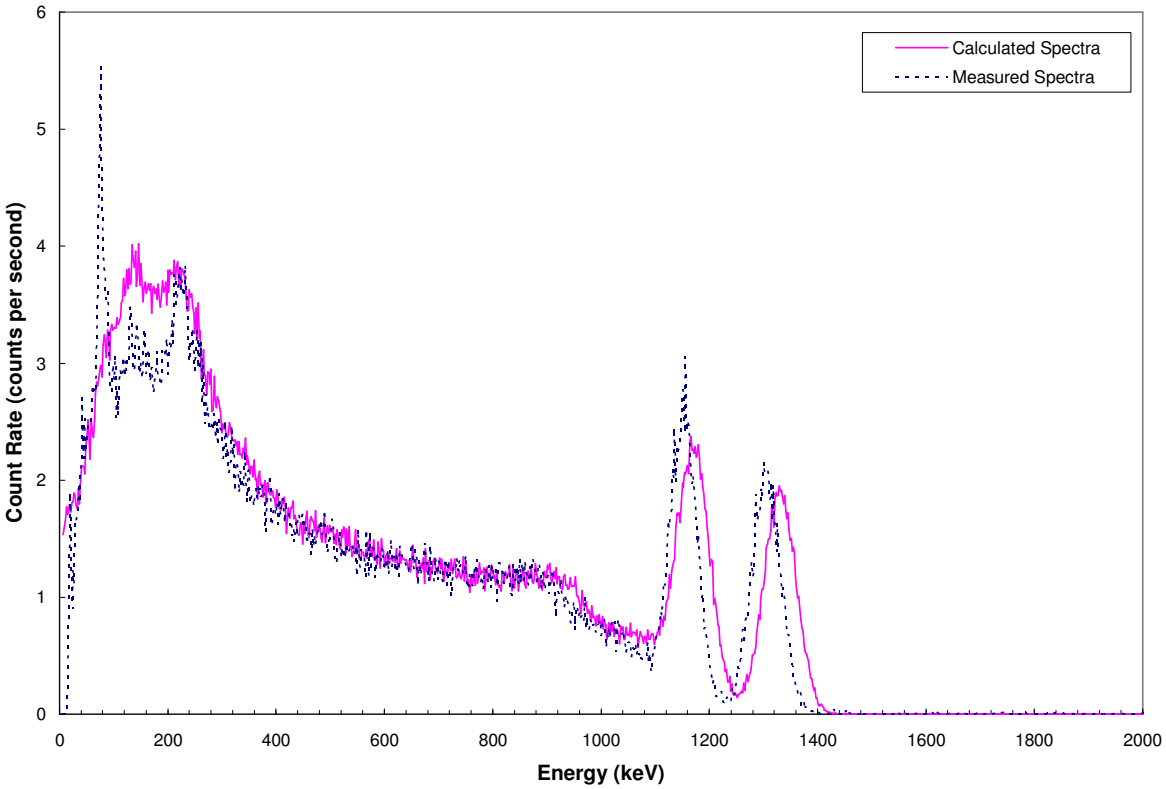

Figure B.8 Measured and calculated spectra for Co-60 with 60 mm PMMA

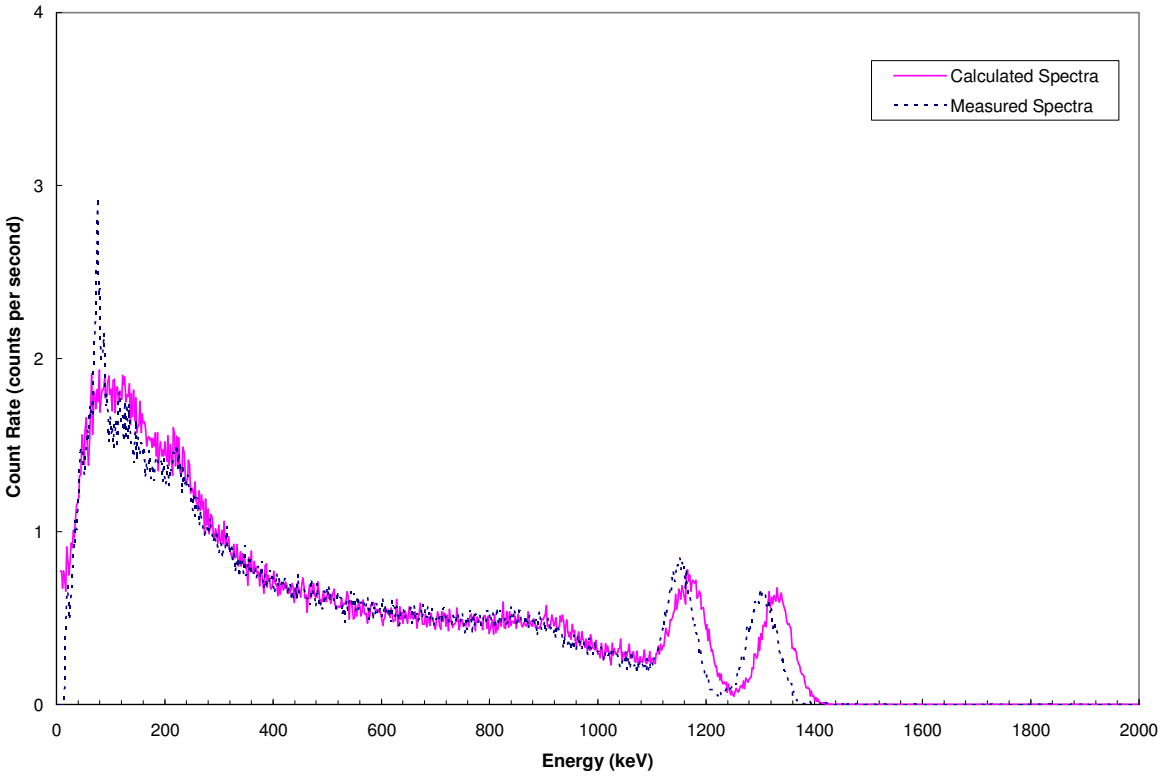

Figure B.9 Measured and calculated spectra for Co-60 with 108 mm PMMA

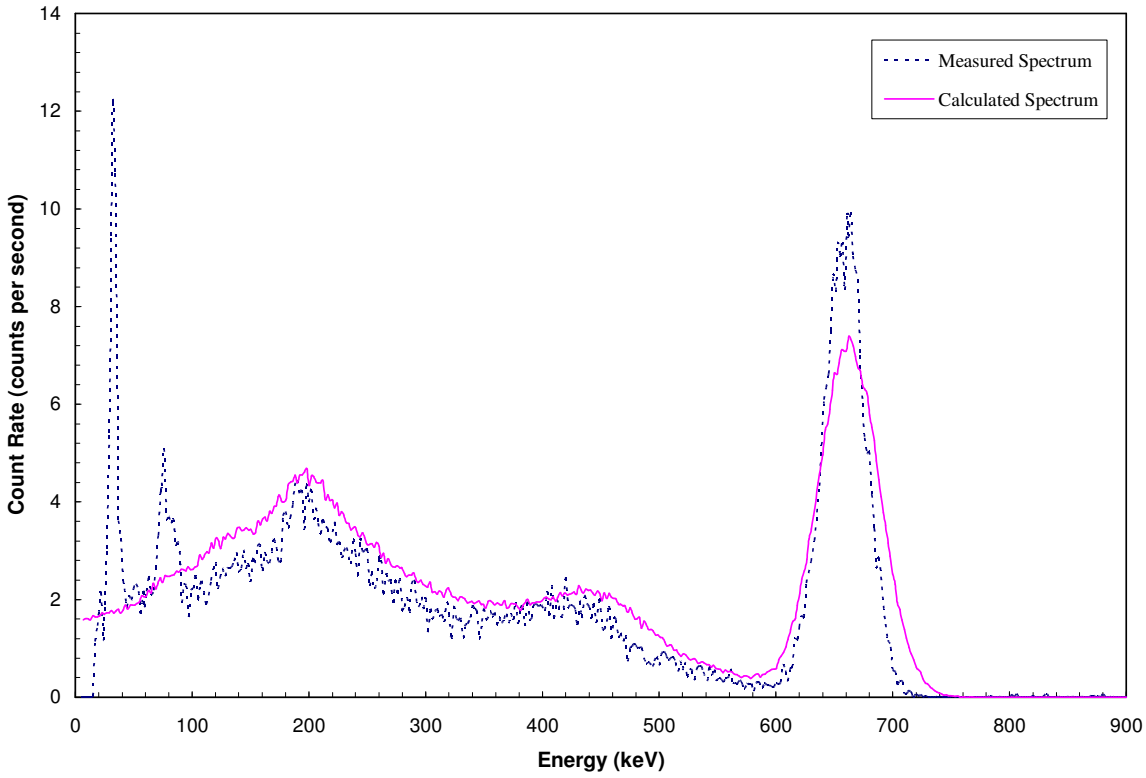

Figure B.10 Measured and calculated spectra for Cs-137 with 0 mm PMMA

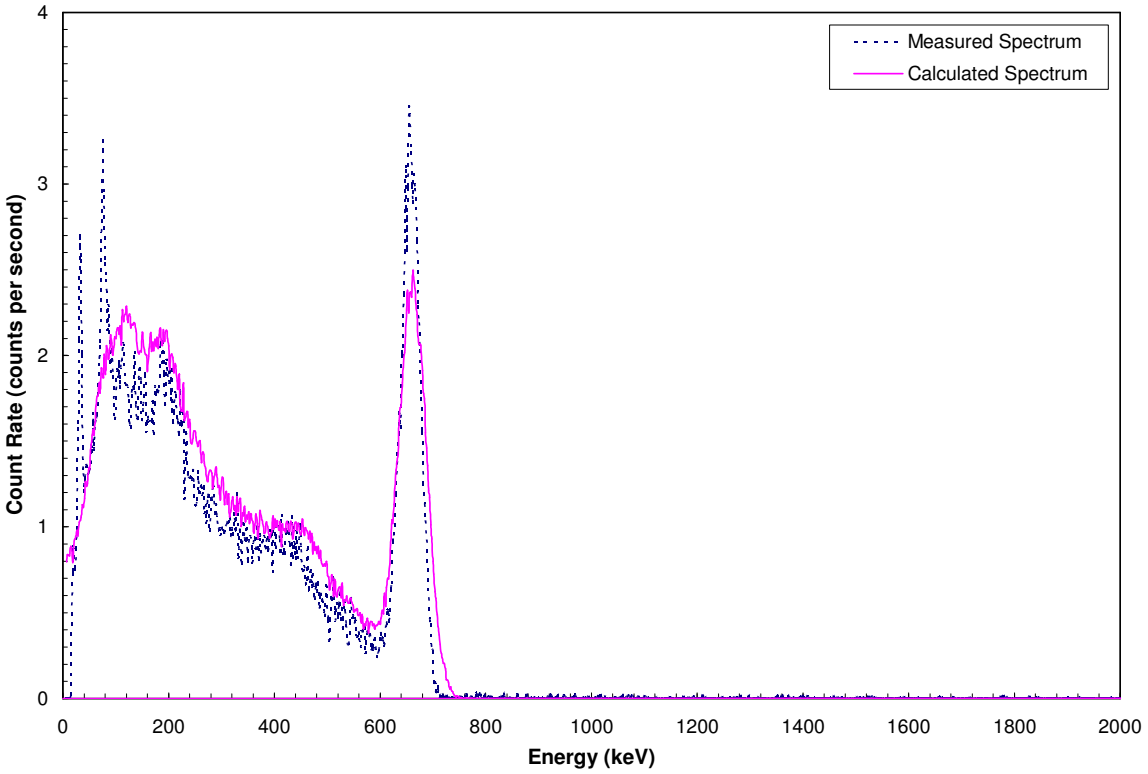

Figure B.11 Measured and calculated spectra for Cs-137 with 60 mm PMMA

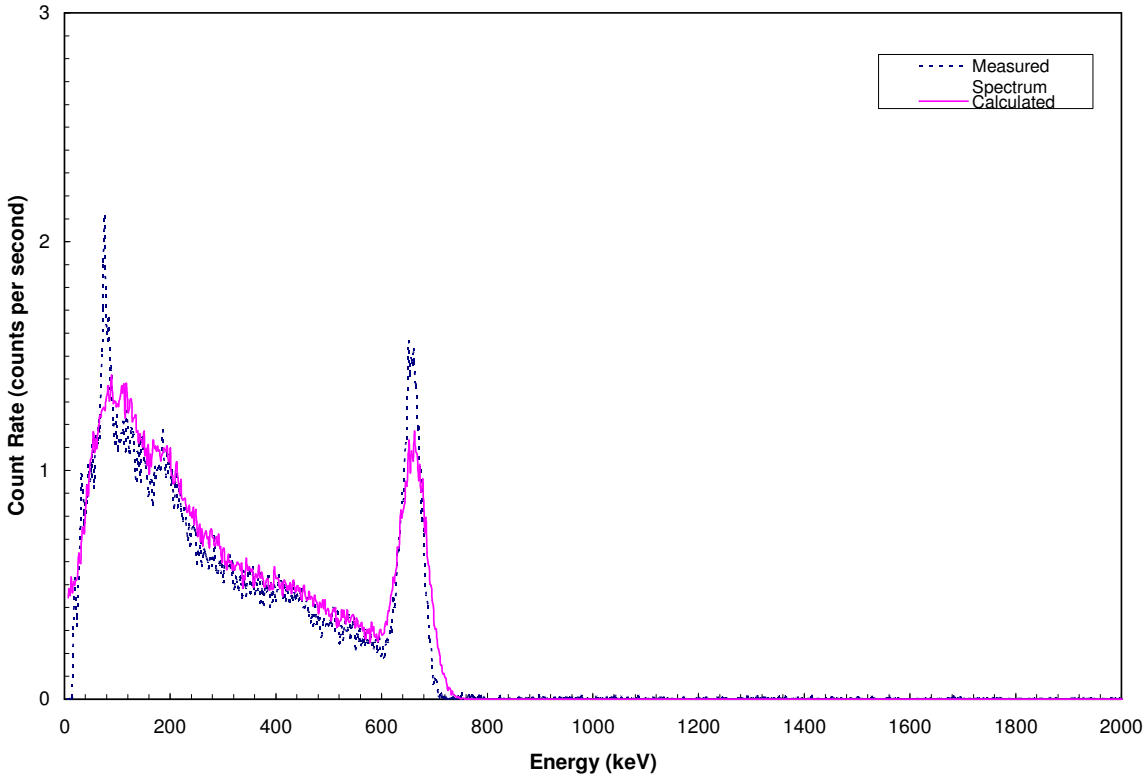

Figure B.12 Measured and calculated spectra for Cs-137 with 108 mm PMMA

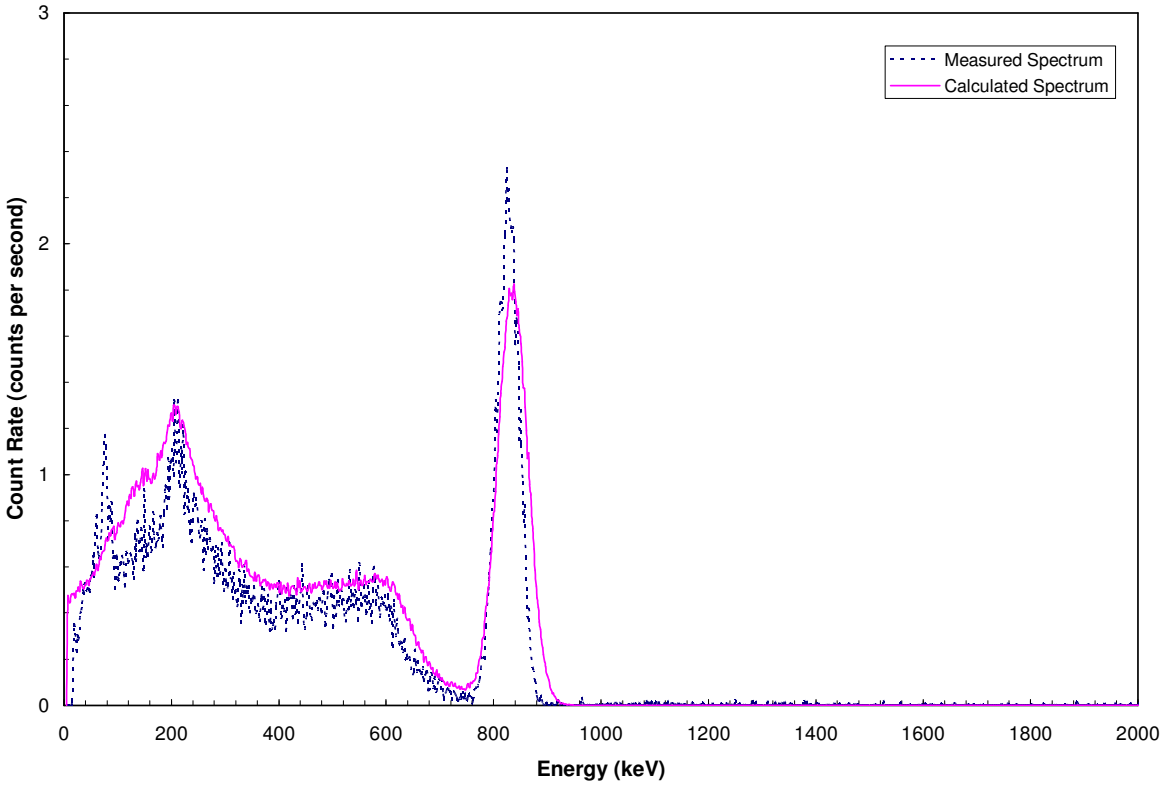

Figure B.13 Measured and calculated spectra for Mn-54 with 0 mm PMMA

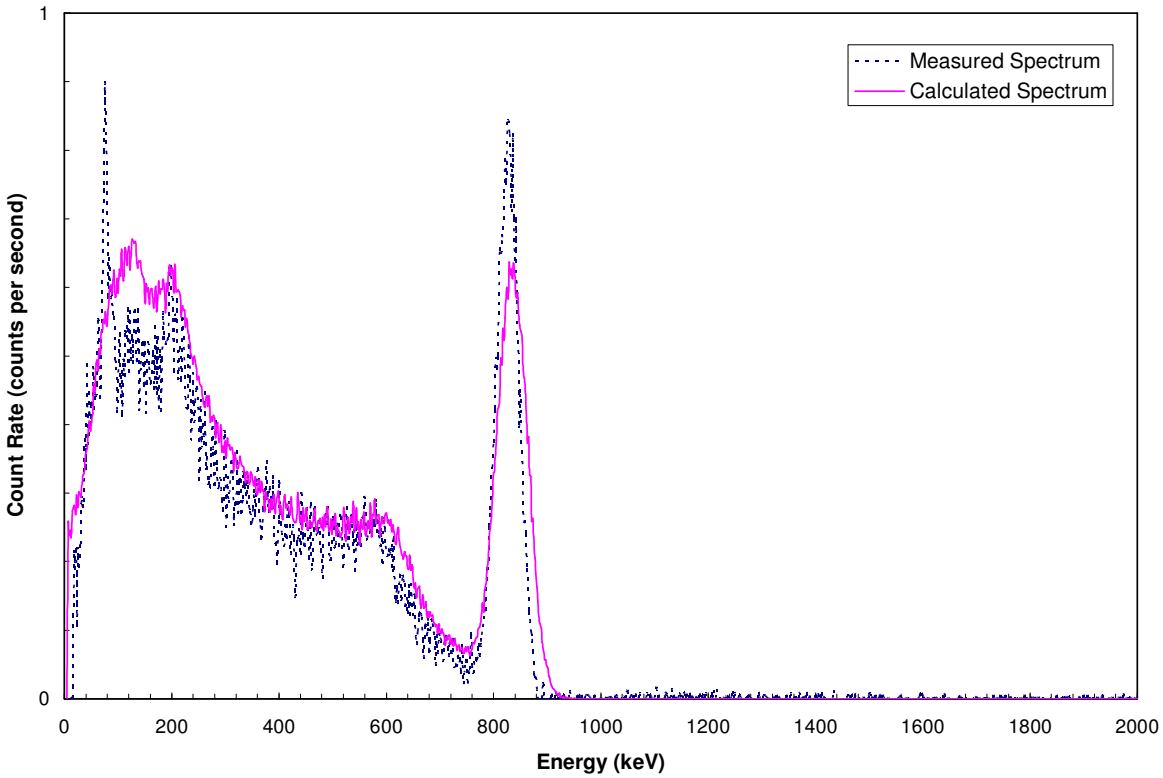

Figure B.14 Measured and calculated spectra for Mn-54 with 60 mm PMMA

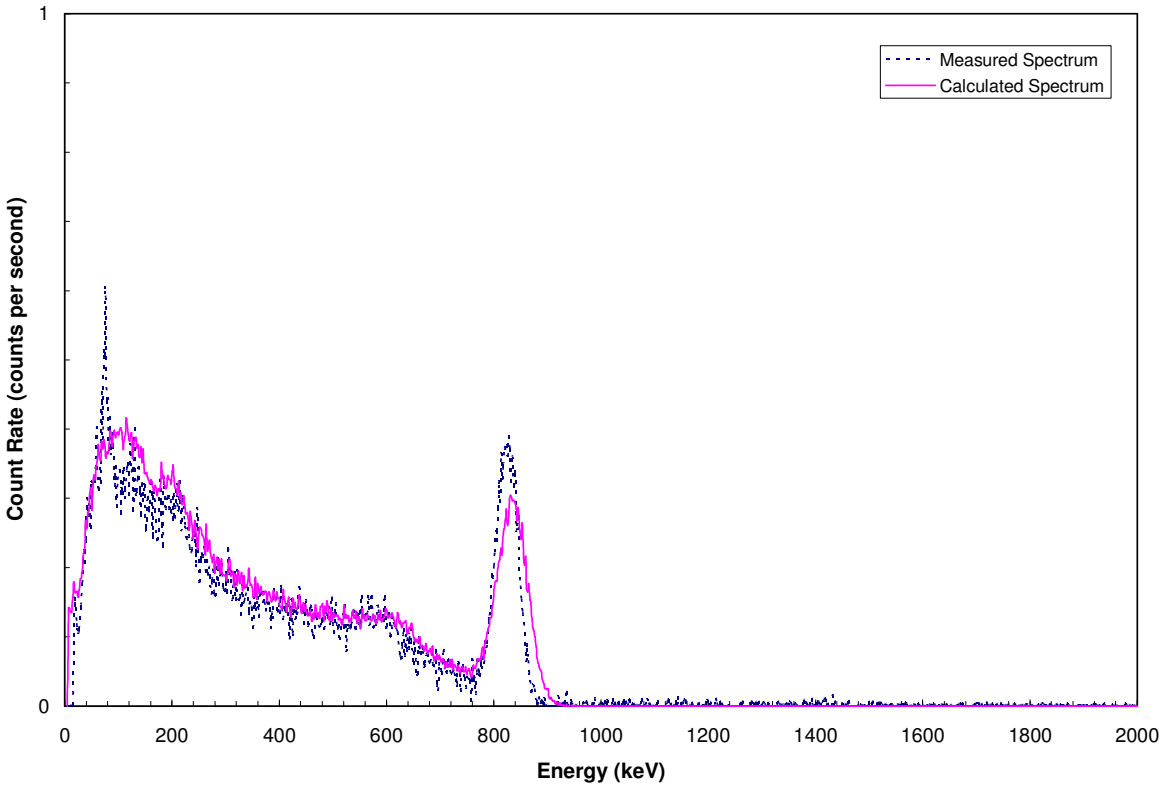

Figure B.15 Measured and calculated spectra for Mn-54 with 108 mm PMMA

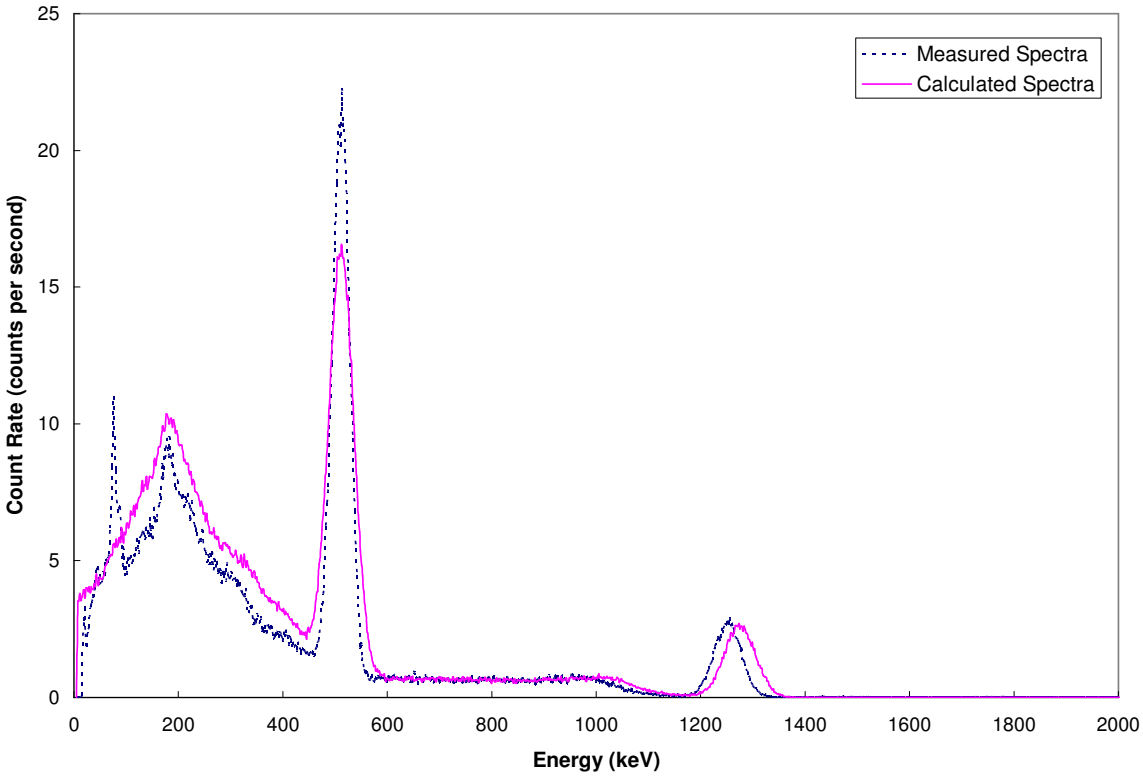

Figure B.16 Measured and calculated spectra for Na-22 with 0 mm PMMA

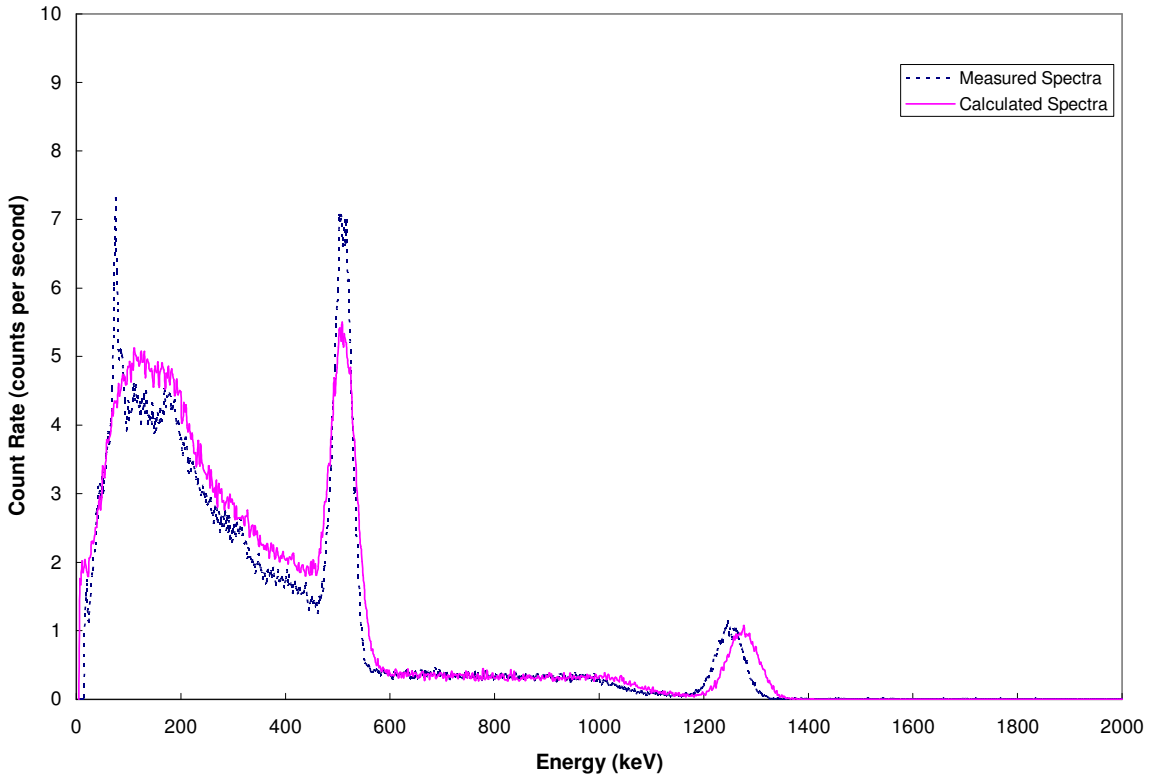

Figure B.17 Measured and calculated spectra for Na-22 with 60 mm PMMA

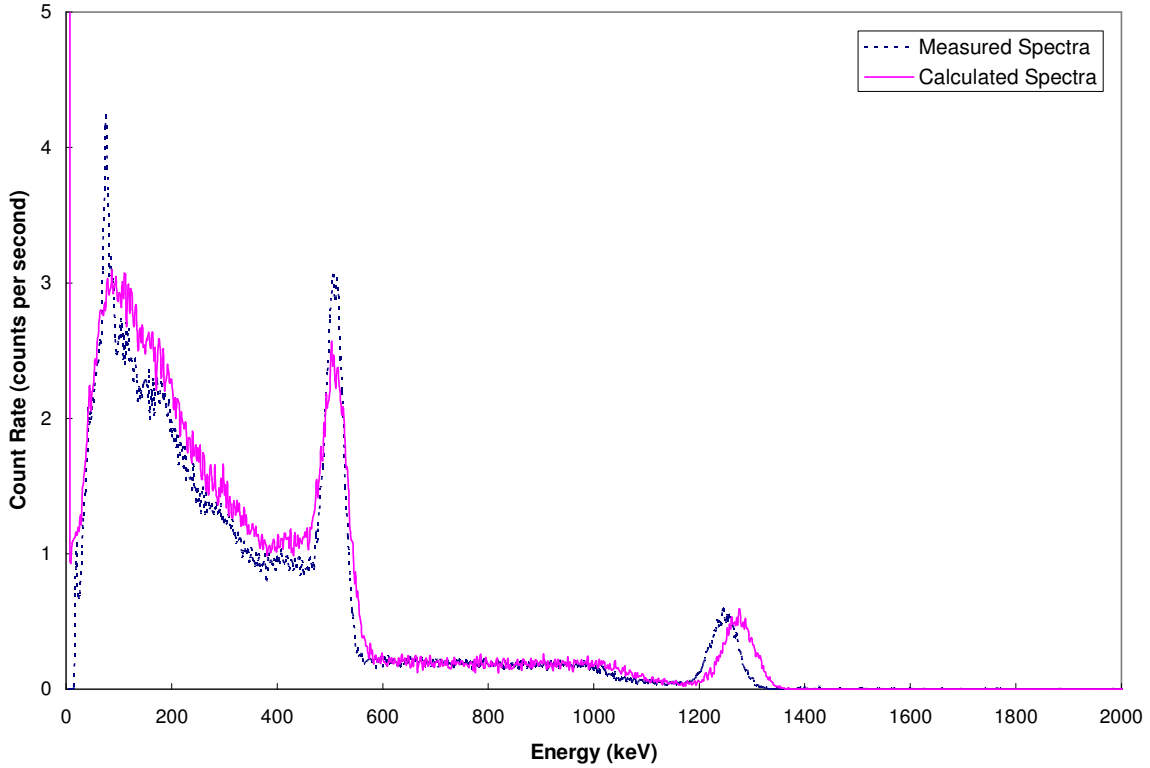

Figure B.18 Measured and calculated spectra for Na-22 with 108 mm PMMA

APPENDIX C

CONDENSED MIRD PHANTOM MCNP INPUT FILE

Male Phantom contaminated with Cs-137

```
1    1 -.001293    -1 (607:-37:606) (-606:601:35) (600:-35) &
                   (-615:37:-43:44:4:-616) (37:-608:609) &
                   (37:-608:610) 900 901 902 903
2    2 -0.2958     ((-2 -4 3):(-2 4)) 5                          $ left lung
3    3 -0.9869     -7 51 -6 (-8:32) 84 101 #2 #24 #28 #58 #59
                   (113:115) (114:115) #62 #700                  $ torso insd ribs/lvrtop-shldr
4    3 -0.9869     -7 8 -32 117 113 114 #15 #16 #17 #18 #19 #20 #700
                   (-4:-9:116:118:-119) (-4:-9:116:120:-121)     $torso
5    3 -0.9869     -7 8 -117 51 113 114 #9 #13 #14 #700          $ torso
6    3 -0.9869     -7 50 -51 56 84 96 105 106 113 114 #10 #11 #12
                   #27 #32 #43 #44 #47 #700                      $ torso
7    3 -0.9869     -7 97 -50 (83:-86:87:-88) 113 114 #30 #33 #38 #39
                   #63 #64 #65 #700                              $ torso abdoman
8    3 -0.9869     -7 37 -97 95 113 114 #31 #33 #38 #65 #66 #700  $ torso abdoman
9    4 -1.4862     8 -9 5 -10                                    $ rib
10   4 -1.4862     8 -9 11 -12                                   $ rib
11   4 -1.4862     8 -9 13 -14                                   $ rib
12   4 -1.4862     8 -9 15 -16                                   $ rib
13   4 -1.4862     8 -9 17 -18                                   $ rib
14   4 -1.4862     8 -9 19 -20                                   $ rib
15   4 -1.4862     8 -9 21 -22                                   $ rib
16   4 -1.4862     8 -9 23 -24                                   $ rib
17   4 -1.4862     8 -9 25 -26                                   $ rib
18   4 -1.4862     8 -9 27 -28                                   $ rib
19   4 -1.4862     8 -9 29 -30                                   $ rib
20   4 -1.4862     8 -9 31 -32                                   $ rib
21   3 -0.9869     ((35 -34):(-33 6 -35)) 102 (84:85)
                   #37 #60 #61 #62 #700                          $ head
22   3 -0.9869     -37 38 -39 103 #700                           $ left leg
23   3 -0.9869     -37 38 -40 104 #22 #700                       $ right leg
24   2 -0.2958     ((-41 -4 42):(-41 4)) 5                       $ right lung
25   3 -0.9869     715 -37 43 -44 -4 716 39 40 72 73 #700 #600   $ genitalia
26   3 -0.9869     -47                                           $ brain
27   3 -0.9869     50 -51 -48 -49 #10 #11 #12                    $ liver
28   3 -0.9869     (-52 54):(-53 -54 55)                         $ heart
29   3 -0.9869     -56                                           $ stomach
30   3 -0.9869     138 -57 58 -59                                $ Ascending Colon Wall
31   3 -0.9869     (-63 141 65 -61):(-64 142 37 -65)             $ Sigmoid Colon Wall
32   3 -0.9869     -62 139 66 -67 59                             $ Transverse Colon Wall
33   3 -0.9869     -60 140 61 -59 -83                            $ Descending Colon Wall
35   3 -0.9869     -72                                           $ testicle
36   3 -0.9869     -73                                           $ testicle
37   3 -0.9869     -74 75 -76 6 -77                              $ thyroid
38   4 -1.4862     -82 83 37 -78 80 (79:-81)                     $ pelvis
39   4 -1.4862     -84 78 -85 102                                $ spine
40   3 -0.9869     -83 86 -50 88 -87 #30 #32 #33 #63 #64 #65     $ small int.
41   1 -0.001293   -107 606 -4                                   $ air
42   1 -0.001293   -108 606 -4                                   $ air
43   3 -0.9869     -92 65                                        $ kidney
44   3 -0.9869     -93 -94                                       $ kidney
45   3 -0.9869     -95                                           $ bladder
46   3 -0.9869     -96                                           $ spleen
47   3 -0.9869     -98 99 (-65:100)                              $ pancreas
48   3 -0.9869     -101                                          $ thymus
49   4 -1.4862     47 -102 #60 #61                               $ skull
```

```
50    4 -1.4862     -103 38 -37                                  $ leg bone
51    4 -1.4862     -104 38 -37                                  $ leg bone
52    3 -0.9869     -105 92                                     $ adrenal
53    3 -0.9869     -106 93                                     $ adrenal
54    4 -1.4862     37 -115 -113                                  $ arm bone
55    4 -1.4862     37 -115 -114                                  $ arm bone
56    4 -1.4862     4 9 -32 -116 117 -118 119                          $ scapulae
57    4 -1.4862     4 9 -32 -116 117 -120 121                          $ scapulae
58    4 -1.4862     -4 -122 -123 124                              $ clavicle
59    4 -1.4862     -4 -122 -125 126                              $ clavicle
60    3 -0.9869     -33 128 129 -130 133 -134 -4 #700                  $ eye lense
61    3 -0.9869     -33 128 -131 132 133 -134 -4 #700                  $ eye lense
62    3 -0.9869     -77 -137 51                                 $ oesophagus
63    3 -0.9869     -138 58 -59                                 $ Ascending Colon Interior
64    3 -0.9869     -139 66 -67                                 $ Transvers Colon Interior
65    3 -0.9869     -140 61 -59 -83                               $ Decending Colon Interior
66    3 -0.9869     (-141 65 -61) : (-142 37 -65)                      $ Sigmoid Colon Interior
600   0           -600 35 34 902 : -601 33 -35 606 902 : &             $ Head & Neck
                  -606 6 33 -607 902: -607 7 -6 37 900 901 902 : &   $ Shoulders & Torso
  (((-46 616) (43 -44) (615 -37)):((615 -45)(610 609)(46 -4)(43 -44))): & $ Genitalia
                  -610 40 -37 38 : -609 39 -37 38 903: &             $ Legs
                  -708 608 -609 : -708 608 -610 : &                $ Feet
                  -38 708 -610 40 : -38 708 -609 39
700   5 -1.04       700 35 102 -34 : 701 -33 -35 6 : &                $ Head & Neck
                  706 -6 701 -707 : 707 -7 -6 37 114 113 : &          $ Shoulders & Torso
  (((46 -716)(43 -44)(609 610)(715 -37)):((-715 45)(610 609)(46 -4)(43 -44))): & $ Genitalia
                  -40 710 -37 38 : -39 709 -37 38 : &                $ Legs
                  -38 708 -39 : -38 708 -40                        $ Feet
900   1 -.001293    -900 7 515 514 505 504
901   1 -.001293    -901 7 535 534 525 524
902   1 -.001293    -902 6 33 34 555 554 545 544
903   1 -.001293    -903 39 575 574 565 564
c Detector in box 900
502   502   -3.67     -501                          $ NaI crystal
503   503   -7.82      (-505 504):(-514 513): -515       $ Steel
504   506   -2.7       501 510 -502                   $ Aluminum
505   501   -0.00012  -503                           $ Vacuum
506   501   -0.0012   -507                           $ Air in coll
507   503   -7.82     (507 -506)                     $ Inner St Liner
508   508   -11.4     (-504 506):(-513 506 508 512 516)  $ Pb innards
509   501  -.0012    -513 512 -516                     $ air in back
510   509   -8.4      (-510 511):(-508 509)            $ Brass Ring
511   501   -0.0012   502 506 -511                    $ Air ret ring
512   501   -0.0012  -509 502 503 510 511                $ Air in brs tube
513   510  -11.4     -512 508                        $ Pure Led sheet
c Detector in box 901
522   502   -3.67     -521                          $ NaI crystal
523   503   -7.82      (-525 524):(-534 533): -535       $ Steel
524   506   -2.7       521 530 -522                   $ Aluminum
525   501   -0.00012  -523                           $ Vacuum
526   501   -0.0012   -527                           $ Air in coll
527   503   -7.82     (527 -526)                     $ Inner St Liner
528   508   -11.4     (-524 526):(-533 526 528 532 536)  $ Pb innards
529   501  -.0012    -533 532 -536                     $ air in back
530   509   -8.4      (-530 531):(-528 529)            $ Brass Ring
531   501   -0.0012   522 526 -531                    $ Air ret ring
```

```
532   501   -0.0012  -529 522 523 530 531              $ Air in brs tube
533   510  -11.4     -532 528                          $ Pure Led sheet
c Detector in box 902
542   502   -3.67     -541                             $ NaI crystal
543   503   -7.82      (-545 544):(-554 553): -555      $ Steel
544   506   -2.7       541 550 -542                     $ Aluminum
545   501   -0.00012  -543                             $ Vacuum
546   501   -0.0012   -547                             $ Air in coll
547   503   -7.82     (547 -546)                       $ Inner St Liner
548   508   -11.4     (-544 546):(-553 546 548 552 556)  $ Pb innards
549   501   -.0012    -553 552 -556                    $ air in back
550   509   -8.4      (-550 551):(-548 549)            $ Brass Ring
551   501   -0.0012   542 546 -551                     $ Air ret ring
552   501   -0.0012  -549 542 543 550 551              $ Air in brs tube
553   510  -11.4     -552 548                          $ Pure Led sheet
c Detector in box 903
562   502   -3.67     -561                             $ NaI crystal
563   503   -7.82      (-565 564):(-574 573): -575      $ Steel
564   506   -2.7       561 570 -562                     $ Aluminum
565   501   -0.00012  -563                             $ Vacuum
566   501   -0.0012   -567                             $ Air in coll
567   503   -7.82     (567 -566)                       $ Inner St Liner
568   508   -11.4     (-564 566):(-573 566 568 572 576)  $ Pb innards
569   501   -.0012    -573 572 -576                    $ air in back
570   509   -8.4      (-570 571):(-568 569)            $ Brass Ring
571   501   -0.0012   562 566 -571                     $ Air ret ring
572   501   -0.0012  -569 562 563 570 571              $ Air in brs tube
573   510  -11.4     -572 568                          $ Pure Led sheet
67    0            1

*********************************************************************************
SURFACES
*********************************************************************************

C     2 concentric elliptical cylinders and planes to define eye lenses
127   SQ  100 64 0 0 0 0 -6400 0 0 0
128   SQ  88.36 40.96 0 0 0 0 -3619.2256 0 0 0
129   PX  2
130   PX  4
131   PX  -2
132   PX  -4
133   PZ  82.5
134   PZ  84.5
C     segmenting planes for RBM regions in leg and arm bones
135   PZ  -22.8
136   PZ  52.6
C     Oesophagus
137   SQ 0.16 1.0 0 0 0 0 -0.16 0.5 2.5 0                $ Oesophagus Exterior
C     Colon Wall
138   SQ 1 1 0 0 0 0 -3.209 -8.5 -2.36 0                 $ Ascending Colon Interior
139   SQ 0 0.9467 3.8927 0 0 0 -3.6854 0 -2.36 25.5
140   GQ 1.796 2.496 0.0674 0 0.818 -0.066 -30.75 -7.12 -0.602 132.2
141   TY 3 0 8.72 5.72 0.91 0.91                         $ Upper Sigmoid Interior
142   TY 3 0 0 3 0.91 0.91                               $ Lower Sigmoid Interior
C Boxes for Detectors
900 900 BOX 0.39 10.9607 38.36   -17.78 0 0 &
```

```
      0 50.8 0      0 0 17.78
901 901 BOX 0.39 -10.9609 38.35  -17.78 0 0 &
      0 -50.8 0     0 0 17.80
902 BOX -8.89 -10 70.01  17.78 0 0  0 -50.8 0   0 0 17.78
903 903 BOX 19.98 -8.89 0  50.8 0 0  0 17.78 0  0 0 -17.78
c
c c
c Detector in Box 900
501 501   rcc -21.5051 0 0 5.08 0 0 2.54            $ NaI Crystal
502 501   rcc -21.5051 0 0 5.1308 0 0 2.824         $ Al Housing
503 501   rcc -34.7893 0 0 13.2842 0 0 2.921        $ PMT Tubes space
504 501   trc -11.5824 0 0 11.5824 0 0 4.445 5.3975   $ Outer Detector Housing ID
505 501   trc -11.5824 0 0 11.5824 0 0 4.7625 5.715   $ Outer Detector Housing OD
506 501   trc -15.7393 0 0 15.7393 0 0 2.7344 4.8018  $ Inner Steel Liner
507 501   trc -15.7393 0 0 15.7393 0 0 2.5344 4.6018  $ Air in collimator
508 501   rcc -40.8223 0 0 25.083 0 0 3.505         $ Inner Tube OD around PMT
509 501   rcc -40.8223 0 0 25.083 0 0 3.175         $ Inner Tube ID
510 501   rcc -16.3743 0 0 0.635 0 0 3.175          $ Retaining Ring OD
511 501   rcc -16.3743 0 0 0.635 0 0 2.565          $ Retaining Ring ID (air)
512 501   rcc -40.8223 0 0 14.9225 0 0 3.823        $ Detector Side Shield (Pb)
513 501   rcc -40.8223 0 0 29.2399 0 0 4.445        $ Cyl Detector Housing ID
514 501   rcc -40.8223 0 0 29.2399 0 0 4.7625       $ Cyl Detector Housing OD
515 501   rcc -41.8223 0 0 1.0 0 0 4.7625           $ Back end cap
516 501   px -25.8998                          $ air plane!
c Detector in Box 901
521 502   rcc -21.5051 0 0 5.08 0 0 2.54            $ NaI Crystal
522 502   rcc -21.5051 0 0 5.1308 0 0 2.824         $ Al Housing
523 502   rcc -34.7893 0 0 13.2842 0 0 2.921        $ PMT Tubes space
524 502   trc -11.5824 0 0 11.5824 0 0 4.445 5.3975   $ Outer Detector Housing ID
525 502   trc -11.5824 0 0 11.5824 0 0 4.7625 5.715   $ Outer Detector Housing OD
526 502   trc -15.7393 0 0 15.7393 0 0 2.7344 4.8018  $ Inner Steel Liner
527 502   trc -15.7393 0 0 15.7393 0 0 2.5344 4.6018  $ Air in collimator
528 502   rcc -40.8223 0 0 25.083 0 0 3.505         $ Inner Tube OD around PMT
529 502   rcc -40.8223 0 0 25.083 0 0 3.175         $ Inner Tube ID
530 502   rcc -16.3743 0 0 0.635 0 0 3.175          $ Retaining Ring OD
531 502   rcc -16.3743 0 0 0.635 0 0 2.565          $ Retaining Ring ID (air)
532 502   rcc -40.8223 0 0 14.9225 0 0 3.823        $ Detector Side Shield (Pb)
533 502   rcc -40.8223 0 0 29.2399 0 0 4.445        $ Cyl Detector Housing ID
534 502   rcc -40.8223 0 0 29.2399 0 0 4.7625       $ Cyl Detector Housing OD
535 502   rcc -41.8223 0 0 1.0 0 0 4.7625           $ Back end cap
536 502   px -25.8998                          $ air plane!
c Detector in Box 902
541 503   rcc -21.5051 0 0 5.08 0 0 2.54            $ NaI Crystal
542 503   rcc -21.5051 0 0 5.1308 0 0 2.824         $ Al Housing
543 503   rcc -34.7893 0 0 13.2842 0 0 2.921        $ PMT Tubes space
544 503   trc -11.5824 0 0 11.5824 0 0 4.445 5.3975   $ Outer Detector Housing ID
545 503   trc -11.5824 0 0 11.5824 0 0 4.7625 5.715   $ Outer Detector Housing OD
546 503   trc -15.7393 0 0 15.7393 0 0 2.7344 4.8018  $ Inner Steel Liner
547 503   trc -15.7393 0 0 15.7393 0 0 2.5344 4.6018  $ Air in collimator
548 503   rcc -40.8223 0 0 25.083 0 0 3.505         $ Inner Tube OD around PMT
549 503   rcc -40.8223 0 0 25.083 0 0 3.175         $ Inner Tube ID
550 503   rcc -16.3743 0 0 0.635 0 0 3.175          $ Retaining Ring OD
551 503   rcc -16.3743 0 0 0.635 0 0 2.565          $ Retaining Ring ID (air)
552 503   rcc -40.8223 0 0 14.9225 0 0 3.823        $ Detector Side Shield (Pb)
553 503   rcc -40.8223 0 0 29.2399 0 0 4.445        $ Cyl Detector Housing ID
554 503   rcc -40.8223 0 0 29.2399 0 0 4.7625       $ Cyl Detector Housing OD
```

```
555 503   rcc -41.8223 0 0 1.0 0 0 4.7625            $ Back end cap
556 503   px -25.8998                          $ air plane!
c Detector in Box 903
561 504   rcc -21.5051 0 0 5.08 0 0 2.54            $ NaI Crystal
562 504   rcc -21.5051 0 0 5.1308 0 0 2.824          $ Al Housing
563 504   rcc -34.7893 0 0 13.2842 0 0 2.921         $ PMT Tubes space
564 504   trc -11.5824 0 0 11.5824 0 0 4.445 5.3975   $ Outer Detector Housing ID
565 504   trc -11.5824 0 0 11.5824 0 0 4.7625 5.715   $ Outer Detector Housing OD
566 504   trc -15.7393 0 0 15.7393 0 0 2.7344 4.8018  $ Inner Steel Liner
567 504   trc -15.7393 0 0 15.7393 0 0 2.5344 4.6018  $ Air in collimator
568 504   rcc -40.8223 0 0 25.083 0 0 3.505          $ Inner Tube OD around PMT
569 504   rcc -40.8223 0 0 25.083 0 0 3.175          $ Inner Tube ID
570 504   rcc -16.3743 0 0 0.635 0 0 3.175           $ Retaining Ring OD
571 504   rcc -16.3743 0 0 0.635 0 0 2.565           $ Retaining Ring ID (air)
572 504   rcc -40.8223 0 0 14.9225 0 0 3.823         $ Detector Side Shield (Pb)
573 504   rcc -40.8223 0 0 29.2399 0 0 4.445         $ Cyl Detector Housing ID
574 504   rcc -40.8223 0 0 29.2399 0 0 4.7625        $ Cyl Detector Housing OD
575 504   rcc -41.8223 0 0 1.0 0 0 4.7625            $ Back end cap
576 504   px  -25.8998                         $ air plane!

C Data Cards
*****************************************************************************************
TRANSFORMATIONS
*****************************************************************************************

IMP:P 1 118R 0
C
C Sources
SDEF  PAR=2  ERG=D1  CEL=D2  RAD=fcel=D3  &
     POS=fcel=D4  EXT=fcel=D5  AXS=fcel=D6
SI1 L 0.662 0.0332 0.0318
SP1 0.898 0.0392 0.0213
C Left Lung, Right Lung, Stomach, Small Int., Heart, Ascending Colon,
C Sigmoid Colon, Transvers Colon, Descending Colon, Bladder,
C Body Tissue (3, 4, 5, 6, 7, 8, 21, 22, 23, 25)
SI2 L 2 24 29 40 28 30 31 32 33 45 3 4 5 6 7 8 21 22 23 25
SP2 D 1 1  1  1  1  1  1  1  1  1  1 1 1 1 1 1 1  1  1  1
DS3 S 7 8 9 10 11 12 13 14 15 16 17 18 19 20 21 22 23 24 25 26
DS4 L 8.5 0 43.4   -8.5 0 43.4   8 -4 35   0 -3.8 11.3   -1 -3 51   &
     -8.5 -2.36 14.35   5 0 -0.1   -10.6 -2.36 25.5   8.72 0 8.52  &
     0 -4.5 8   0 0 42.9   0 0 50.8   0 0 42.9   0 0 26.9          &
     0 0 11.9   0 0 -0.1   0 0 69.9   10.5 0 -80.1   -10.5 0 -80.1 &
     0 -8 -4.9
DS5 S 30 31 0 32 0 33 34 35 36 0 37 38 39 40 41 42 43 44 45 46
DS6 L 0 0 1   0 0 1   0 0 0   0 0 1   0 0 0   0 0 1   0 0 1 &
     1 0 0   0 0 1   0 0 0   0 0 1   0 0 1   0 0 1   0 0 1 &
     0 0 1   0 0 1   0 0 1   0 0 1   0 0 1   0 0 1
SI7  0 7.6
SP7  -21 1
SI8  0 7.6
SP8  -21 1
SI9  0 8.2
SP9  -21 2
SI10 0 11.4
SP10 -21 1
SI11 0 8.2
```

```
SP11 -21 2
SI12 0 2.6
SP12 -21 1
SI13 0 7.1
SP13 -21 1
SI14 0 3.85
SP14 -21 1
SI15 0 4
SP15 -21 1
SI16 0 5.2
SP16 -21 2
SI17 0 20.2
SP17 -21 1
SI18 0 20.3
SP18 -21 1
SI19 0 20.3
SP19 -21 1
SI20 0 20.3
SP20 -21 1
SI21 0 20.3
SP21 -21 1
SI22 0 20.3
SP22 -21 1
SI23 0 10.1
SP23 -21 1
SI24 0 11
SP24 -21 1
SI25 0 11
SP25 -21 1
SI26 0 8.1
SP26 -21 1
SI27 0 16.6
SP27 -21 1
SI30 0 24.6
SP30 -21 0
SI31 0 24.6
SP31 -21 0
SI32 0 10.2
SP32 -21 0
SI33 0 9.75
SP33 -21 0
SI34 0 8.92
SP34 -21 0
SI35 0 21.2
SP35 -21 0
SI36 0 16
SP36 -21 0
SI37 0 27.2
SP37 -21 0
SI38 0 16.6
SP38 -21 0
SI39 0 8.1
SP39 -21 0
SI40 0 16.2
SP40 -21 0
SI41 0 15.2
```

```
SP41 -21 0
SI42 0 12.2
SP42 -21 0
SI43 0 24.2
SP43 -21 0
SI44 0 80.2
SP44 -21 0
SI45 0 80.2
SP45 -21 0
SI46 0 5
SP46 -21 0
C
C Tally Cards
c Back Right Lung
F8:P 502
E8 0 1e-8 0.005 1024i 2.046
FT8 SCX 2  GEB -0.00298579 0.0925102 -0.4
c Front Right Lung
F18:P 522
E18 0 1e-8 0.005 1024i 2.046
FT18 SCX 2 GEB -0.00298579 0.0925102 -0.4
c Front Neck Under Chin
F28:P 542
E28 0 1e-8 0.005 1024i 2.046
FT28 SCX 2 GEB -0.00298579 0.0925102 -0.4
c Outer Left Leg
F38:P 562
E38 0 1e-8 0.005 1024i 2.046
FT38 SCX 2 GEB -0.00298579 0.0925102 -0.4
C
C Material Cards
C       THIS IS THE COMPOSITION FOR AIR
M1    7014 -.7558 8016 -.2314 18000 -.0128
C      THIS IS THE COMPOSITION FOR LUNG TISSUE
M2    1001 -.1021
      6012 -.1001
      7014 -.0280
      8016 -.7596
     11023 -.0019
     15031 -.0008
     16032 -.0023
     17000 -.0027
     19000 -.0020
     20000 -.0001
     26000 -.0004
C       THE COMPOSITION FOR TOTAL BODY MINUS SKELETON AND LUNGS
M3    1001 -.1047
      6012 -.2302
      7014 -.0234
      8016 -.6321
     11023 -.0013
     12000 -.0002
     15031 -.0024
     16032 -.0022
     17000 -.0014
     19000 -.0021
```

```
C      THE COMPOSITION FOR SKELETAL TISSUE
M4    1001 -.0704
      6012 -.2279
      8016 -.4856
      7014 -.0387
     11023 -.0032
     12000 -.0011
     15031 -.0694
     16032 -.0017
     17000 -.0014
     19000 -.0015
     20000 -.0991
c      Adult Tissues (Density = 1.04 g/cc)
M5       1001  -0.10454
         6012  -0.22663
         7014  -0.02490
         8016  -0.63525
        11023  -0.00112
        12000  -0.00013
        14000  -0.00030
        15031  -0.00134
        16032  -0.00204
        17000  -0.00133
        19000  -0.00208
        20000  -0.00024
        26000  -0.00005
        30000  -0.00003
        37085  -0.000007217
        37087  -0.000002783
        40000  -0.00001
c Detectors Materials
c Material Card for Air (NIST DRY AIR)
m501  8016.             -0.232
      7014.             -0.755
      6012              -1.20E-4
      18000.42c         -1.28E-2
c Material Card for Sodium Iodide
m502  11000.04p           0.5
      53000.04p           0.5
c Material Card for grain controlled mild steel
m503  26054             -0.05821
      26056             -0.9137
      26057             -0.0211
      26058             -0.00281
       6012             -0.0006
      25055             -0.0035
      15031             -0.00004
      16000             -0.00005
c Material Card for Aluminum
m506  13027.  1
c Material Card for Antimonial Lead
m508  82000   0.96
      51000   0.04
c Material Card for High Brass
m509  29000    0.65
      30000    0.35
```

```
c Material Card for Pure Lead
m510  82000   1
lost 50
c STOP NPS 1E8 F38 0.01
NPS 4E9
RAND GEN=2 SEED=1561615651
PHYS:P 4J 1
PRINT
MODE P
```

APPENDIX D

MIRD PHANTOM RESULTS FOR Cs-137, Co-60, Am-241, I-131, Ir-192

Table D.1 Count rate per Bq calculated for the Male phantom contaminated with Cs-137

		Back Right Lung	Front Right Lung	Neck	Thigh
		cpm per Bq	cpm per Bq	cpm per Bq	cpm per Bq
Days following exposure	0	1.85E-04	1.77E-04	1.51E-05	1.31E-06
	1	4.29E-04	4.63E-04	5.07E-04	2.47E-04
	2	4.11E-04	4.48E-04	5.20E-04	2.54E-04
	3	3.94E-04	4.30E-04	5.08E-04	2.49E-04
	4	3.83E-04	4.19E-04	4.99E-04	2.44E-04
	5	3.76E-04	4.11E-04	4.91E-04	2.40E-04
	6	3.71E-04	4.05E-04	4.84E-04	2.37E-04
	7	3.66E-04	4.00E-04	4.79E-04	2.35E-04
	8	3.63E-04	3.97E-04	4.74E-04	2.32E-04
	9	3.60E-04	3.93E-04	4.70E-04	2.30E-04
	10	3.57E-04	3.90E-04	4.66E-04	2.28E-04
	20	3.33E-04	3.64E-04	4.36E-04	2.13E-04
	30	3.13E-04	3.42E-04	4.09E-04	2.00E-04

Table D.2 Count rate per Bq calculated for the Female phantom contaminated with Cs-137

		Back Right Lung	Neck	Thigh
		cpm per Bq	cpm per Bq	cpm per Bq
Days following exposure	0	1.73E-04	1.49E-05	1.59E-06
	1	5.41E-04	6.39E-04	2.37E-04
	2	5.29E-04	6.56E-04	2.43E-04
	3	5.09E-04	6.42E-04	2.39E-04
	4	4.97E-04	6.30E-04	2.34E-04
	5	4.88E-04	6.20E-04	2.30E-04
	6	4.81E-04	6.12E-04	2.27E-04
	7	4.76E-04	6.05E-04	2.25E-04
	8	4.71E-04	5.99E-04	2.23E-04
	9	4.67E-04	5.94E-04	2.21E-04
	10	4.63E-04	5.89E-04	2.19E-04
	20	4.33E-04	5.50E-04	2.05E-04
	30	4.06E-04	5.16E-04	1.92E-04

Table D.3 Count rate per Bq calculated for the Adipose Male phantom contaminated with Cs-137

		Back Right Lung	Neck	Thigh
		cpm per Bq	cpm per Bq	cpm per Bq
Days following exposure	0	1.22E-04	1.03E-05	6.41E-07
	1	3.67E-04	5.80E-04	2.29E-04
	2	3.58E-04	5.96E-04	2.36E-04
	3	3.45E-04	5.84E-04	2.31E-04
	4	3.36E-04	5.73E-04	2.27E-04
	5	3.30E-04	5.64E-04	2.23E-04
	6	3.26E-04	5.56E-04	2.20E-04
	7	3.22E-04	5.50E-04	2.18E-04
	8	3.19E-04	5.45E-04	2.16E-04
	9	3.16E-04	5.40E-04	2.14E-04
	10	3.14E-04	5.36E-04	2.12E-04
	20	2.93E-04	5.01E-04	1.98E-04
	30	2.75E-04	4.70E-04	1.86E-04

Table D.4 Count rate per Bq calculated for the Adipose Female phantom contaminated with Cs-137

		Back Right Lung	Neck	Thigh
		cpm per Bq	cpm per Bq	cpm per Bq
Days following exposure	0	1.29E-04	1.14E-05	9.44E-07
	1	4.21E-04	5.63E-04	3.30E-04
	2	4.12E-04	5.78E-04	3.40E-04
	3	3.97E-04	5.66E-04	3.33E-04
	4	3.88E-04	5.55E-04	3.27E-04
	5	3.81E-04	5.46E-04	3.21E-04
	6	3.76E-04	5.39E-04	3.17E-04
	7	3.71E-04	5.33E-04	3.14E-04
	8	3.68E-04	5.28E-04	3.11E-04
	9	3.64E-04	5.23E-04	3.08E-04
	10	3.62E-04	5.19E-04	3.06E-04
	20	3.38E-04	4.85E-04	2.86E-04
	30	3.17E-04	4.55E-04	2.68E-04

Table D.5 Count rate per Bq calculated for the Post-Menopausal Adipose Female phantom contaminated with Cs-137

		Back Right Lung	Neck	Thigh
		cpm per Bq	cpm per Bq	cpm per Bq
Days following exposure	0	2.09E-05	7.59E-06	8.40E-07
	1	1.10E-04	1.55E-04	5.54E-05
	2	1.10E-04	1.58E-04	5.68E-05
	3	1.06E-04	1.55E-04	5.57E-05
	4	1.04E-04	1.52E-04	5.46E-05
	5	1.02E-04	1.49E-04	5.37E-05
	6	1.01E-04	1.48E-04	5.31E-05
	7	9.98E-05	1.46E-04	5.25E-05
	8	9.89E-05	1.44E-04	5.20E-05
	9	9.80E-05	1.43E-04	5.15E-05
	10	9.72E-05	1.42E-04	5.11E-05
	20	9.08E-05	1.33E-04	4.77E-05
	30	8.52E-05	1.25E-04	4.48E-05

Table D.6 Count rate per Bq calculated for the Child phantom contaminated with Cs-137

		Back Right Lung	Neck	Thigh
		cpm per Bq	cpm per Bq	cpm per Bq
Days following exposure	0	2.28E-04	1.90E-05	0.00E+00
	1	7.00E-04	7.43E-04	3.86E-04
	2	6.82E-04	7.62E-04	3.98E-04
	3	6.57E-04	7.45E-04	3.90E-04
	4	6.41E-04	7.31E-04	3.83E-04
	5	6.29E-04	7.20E-04	3.77E-04
	6	6.21E-04	7.10E-04	3.72E-04
	7	6.13E-04	7.03E-04	3.68E-04
	8	6.07E-04	6.96E-04	3.64E-04
	9	6.02E-04	6.90E-04	3.61E-04
	10	5.97E-04	6.84E-04	3.58E-04
	20	5.58E-04	6.39E-04	3.35E-04
	30	5.24E-04	6.00E-04	3.14E-04

Table D.7 Count Rate per Bq calculated for the Male phantom contaminated with Co-60

		Back Right Lung	Front Right Lung	Neck	Thigh
		cpm per Bq	cpm per Bq	cpm per Bq	cpm per Bq
Days following exposure	0	2.76E-04	2.65E-04	6.39E-05	6.55E-06
	1	1.30E-04	1.33E-04	5.24E-05	2.04E-05
	2	1.06E-04	1.08E-04	4.85E-05	2.02E-05
	3	9.57E-05	9.63E-05	4.53E-05	1.83E-05
	4	9.04E-05	9.07E-05	4.30E-05	1.70E-05
	5	8.72E-05	8.74E-05	4.13E-05	1.60E-05
	6	8.49E-05	8.50E-05	3.99E-05	1.53E-05
	7	8.30E-05	8.31E-05	3.87E-05	1.48E-05
	8	8.14E-05	8.14E-05	3.77E-05	1.43E-05
	9	7.99E-05	7.99E-05	3.68E-05	1.39E-05
	10	7.85E-05	7.84E-05	3.59E-05	1.35E-05
	20	6.82E-05	6.80E-05	3.07E-05	1.14E-05
	30	6.15E-05	6.15E-05	2.84E-05	1.07E-05

Table D.8 Count Rate per Bq calculated for the Female phantom contaminated with Co-60

		Back Right Lung	Neck	Thigh
		cpm per Bq	cpm per Bq	cpm per Bq
Days following exposure	0	2.63E-04	6.44E-05	7.69E-06
	1	1.29E-04	6.30E-05	2.09E-05
	2	1.08E-04	6.09E-05	2.04E-05
	3	9.77E-05	5.76E-05	1.85E-05
	4	9.24E-05	5.49E-05	1.71E-05
	5	8.92E-05	5.27E-05	1.61E-05
	6	8.68E-05	5.09E-05	1.54E-05
	7	8.48E-05	4.93E-05	1.48E-05
	8	8.30E-05	4.79E-05	1.44E-05
	9	8.14E-05	4.67E-05	1.39E-05
	10	7.99E-05	4.56E-05	1.36E-05
	20	6.93E-05	3.89E-05	1.15E-05
	30	6.27E-05	3.61E-05	1.08E-05

Table D.9 Count Rate per Bq calculated for the Adipose Male Phantom contaminated with Co-60

		Back Right Lung	Neck	Thigh
		cpm per Bq	cpm per Bq	cpm per Bq
Days following exposure	0	1.92E-04	4.73E-05	3.98E-06
	1	9.29E-05	5.11E-05	1.81E-05
	2	7.81E-05	5.11E-05	1.85E-05
	3	7.11E-05	4.89E-05	1.71E-05
	4	6.73E-05	4.68E-05	1.59E-05
	5	6.50E-05	4.50E-05	1.51E-05
	6	6.32E-05	4.34E-05	1.44E-05
	7	6.18E-05	4.20E-05	1.39E-05
	8	6.05E-05	4.08E-05	1.34E-05
	9	5.93E-05	3.97E-05	1.30E-05
	10	5.83E-05	3.87E-05	1.27E-05
	20	5.05E-05	3.30E-05	1.07E-05
	30	4.57E-05	3.07E-05	1.01E-05

Table D.10 Count rate per Bq calculated for the Adipose Female phantom contaminated with Co-60

		Back Right Lung	Neck	Thigh
		cpm per Bq	cpm per Bq	cpm per Bq
Days following exposure	0	1.98E-04	5.08E-05	5.14E-06
	1	9.92E-05	5.24E-05	2.23E-05
	2	8.39E-05	5.18E-05	2.37E-05
	3	7.64E-05	4.94E-05	2.25E-05
	4	7.23E-05	4.72E-05	2.13E-05
	5	6.97E-05	4.54E-05	2.02E-05
	6	6.78E-05	4.38E-05	1.94E-05
	7	6.62E-05	4.24E-05	1.87E-05
	8	6.48E-05	4.12E-05	1.81E-05
	9	6.36E-05	4.01E-05	1.75E-05
	10	6.24E-05	3.92E-05	1.71E-05
	20	5.40E-05	3.34E-05	1.44E-05
	30	4.90E-05	3.10E-05	1.36E-05

Table D.11 Count rate per Bq calculated for the Post-Menopausal Adipose Female phantom contaminated with Co-60

		Back Right Lung	Neck	Thigh
		cpm per Bq	cpm per Bq	cpm per Bq
Days following exposure	0	2.03E-04	5.33E-05	4.94E-06
	1	9.89E-05	5.60E-05	1.59E-05
	2	8.29E-05	5.58E-05	1.58E-05
	3	7.52E-05	5.34E-05	1.45E-05
	4	7.11E-05	5.11E-05	1.34E-05
	5	6.86E-05	4.91E-05	1.27E-05
	6	6.68E-05	4.74E-05	1.21E-05
	7	6.52E-05	4.59E-05	1.17E-05
	8	6.39E-05	4.45E-05	1.13E-05
	9	6.26E-05	4.34E-05	1.09E-05
	10	6.15E-05	4.23E-05	1.07E-05
	20	5.33E-05	3.60E-05	9.01E-06
	30	4.82E-05	3.35E-05	8.47E-06

Table D.12 Count rate per Bq calculated for the Child phantom contaminated with Co-60

		Back Right Lung	Neck	Thigh
		cpm per Bq	cpm per Bq	cpm per Bq
Days following exposure	0	3.36E-04	6.67E-05	1.91E-05
	1	1.65E-04	7.32E-05	3.00E-05
	2	1.38E-04	6.96E-05	2.75E-05
	3	1.25E-04	6.53E-05	2.44E-05
	4	1.18E-04	6.19E-05	2.24E-05
	5	1.14E-04	5.93E-05	2.11E-05
	6	1.11E-04	5.72E-05	2.02E-05
	7	1.08E-04	5.54E-05	1.95E-05
	8	1.06E-04	5.38E-05	1.89E-05
	9	1.04E-04	5.23E-05	1.84E-05
	10	1.02E-04	5.11E-05	1.79E-05
	20	8.85E-05	4.35E-05	1.53E-05
	30	8.01E-05	4.05E-05	1.42E-05

Table D.13 Count rate per Bq calculated for the Male phantom contaminated with Am-241

		Back Right Lung	Front Right Lung	Neck	Thigh
		cpm per Bq	cpm per Bq	Cpm per Bq	cpm per Bq
Days following exposure	0	7.16E-05	6.84E-05	4.75E-07	0.00E+00
	1	3.19E-05	2.59E-05	1.45E-06	6.48E-07
	2	2.65E-05	2.04E-05	1.02E-06	4.42E-07
	3	2.46E-05	1.82E-05	8.57E-07	3.35E-07
	4	2.38E-05	1.73E-05	8.00E-07	2.91E-07
	5	2.35E-05	1.68E-05	7.81E-07	2.75E-07
	6	2.34E-05	1.66E-05	7.77E-07	2.70E-07
	7	2.33E-05	1.63E-05	7.79E-07	2.70E-07
	8	2.32E-05	1.61E-05	7.83E-07	2.72E-07
	9	2.31E-05	1.59E-05	7.87E-07	2.74E-07
	10	2.31E-05	1.58E-05	7.92E-07	2.76E-07
	20	2.26E-05	1.42E-05	8.33E-07	2.97E-07
	30	2.23E-05	1.29E-05	8.62E-07	3.12E-07

Table D.14 Count rate per Bq calculated for the Female phantom contaminated with Am-241

		Back Right Lung	Neck	Thigh
		cpm per Bq	cpm per Bq	cpm per Bq
Days following exposure	0	6.49E-05	5.64E-07	0.00E+00
	1	3.27E-05	1.53E-06	6.99E-07
	2	2.83E-05	1.08E-06	4.75E-07
	3	2.67E-05	9.09E-07	3.54E-07
	4	2.62E-05	8.49E-07	3.02E-07
	5	2.60E-05	8.29E-07	2.84E-07
	6	2.60E-05	8.24E-07	2.78E-07
	7	2.60E-05	8.26E-07	2.78E-07
	8	2.60E-05	8.30E-07	2.79E-07
	9	2.60E-05	8.34E-07	2.81E-07
	10	2.61E-05	8.39E-07	2.84E-07
	20	2.66E-05	8.79E-07	3.05E-07
	30	2.72E-05	9.08E-07	3.20E-07

Table D.15 Count rate per Bq calculated for the Adipose Male phantom contaminated with Am-241

		Back Right Lung	Neck	Thigh
		cpm per Bq	cpm per Bq	cpm per Bq
Days following exposure	0	4.15E-05	4.52E-07	4.52E-07
	1	2.10E-05	1.38E-06	1.38E-06
	2	1.82E-05	9.69E-07	9.69E-07
	3	1.72E-05	8.17E-07	8.17E-07
	4	1.68E-05	7.62E-07	7.62E-07
	5	1.67E-05	7.45E-07	7.45E-07
	6	1.67E-05	7.41E-07	7.41E-07
	7	1.67E-05	7.43E-07	7.43E-07
	8	1.67E-05	7.46E-07	7.46E-07
	9	1.68E-05	7.50E-07	7.50E-07
	10	1.68E-05	7.55E-07	7.55E-07
	20	1.71E-05	7.94E-07	7.94E-07
	30	1.76E-05	8.21E-07	8.21E-07

Table D.16 Count rate per Bq calculated for the Adipose Female phantom contaminated with Am-241

		Back Right Lung	Neck	Thigh
		cpm per Bq	cpm per Bq	cpm per Bq
Days following exposure	0	5.13E-05	5.26E-07	1.33E-09
	1	2.55E-05	1.43E-06	1.17E-06
	2	2.19E-05	1.00E-06	8.01E-07
	3	2.07E-05	8.48E-07	6.39E-07
	4	2.02E-05	7.92E-07	5.76E-07
	5	2.01E-05	7.73E-07	5.54E-07
	6	2.00E-05	7.69E-07	5.49E-07
	7	2.00E-05	7.70E-07	5.51E-07
	8	2.01E-05	7.74E-07	5.55E-07
	9	2.01E-05	7.78E-07	5.59E-07
	10	2.01E-05	7.82E-07	5.64E-07
	20	2.04E-05	8.20E-07	6.06E-07
	30	2.08E-05	8.47E-07	6.38E-07

Table D.17 Count rate per Bq calculated for the Post-Menopausal Adipose Female phantom contaminated with Am-241

		Back Right Lung	Neck	Thigh
		cpm per Bq	cpm per Bq	cpm per Bq
Days following exposure	0	4.49E-05	5.74E-07	0.00E+00
	1	2.29E-05	1.51E-06	5.28E-07
	2	1.98E-05	1.06E-06	3.59E-07
	3	1.88E-05	8.98E-07	2.66E-07
	4	1.84E-05	8.38E-07	2.27E-07
	5	1.83E-05	8.18E-07	2.13E-07
	6	1.83E-05	8.14E-07	2.09E-07
	7	1.83E-05	8.16E-07	2.09E-07
	8	1.83E-05	8.19E-07	2.10E-07
	9	1.84E-05	8.24E-07	2.11E-07
	10	1.84E-05	8.28E-07	2.13E-07
	20	1.88E-05	8.68E-07	2.29E-07
	30	1.93E-05	8.95E-07	2.40E-07

Table D.18 Count rate per Bq calculated for the Child phantom contaminated with Am-241

		Back Right Lung	Neck	Thigh
		cpm per Bq	cpm per Bq	cpm per Bq
Days following exposure	0	1.11E-04	1.87E-06	0.00E+00
	1	5.02E-05	3.39E-06	1.15E-06
	2	4.18E-05	2.41E-06	7.54E-07
	3	3.87E-05	2.04E-06	5.17E-07
	4	3.75E-05	1.91E-06	4.15E-07
	5	3.70E-05	1.86E-06	3.76E-07
	6	3.67E-05	1.85E-06	3.63E-07
	7	3.66E-05	1.85E-06	3.60E-07
	8	3.65E-05	1.86E-06	3.61E-07
	9	3.64E-05	1.87E-06	3.63E-07
	10	3.63E-05	1.87E-06	3.66E-07
	20	3.57E-05	1.94E-06	3.92E-07
	30	3.53E-05	1.98E-06	4.12E-07

Table D.19 Count rate per Bq calculated for the Male phantom contaminated with I-131

		Back Right Lung	Front Right Lung	Neck	Thigh
		cpm per Bq	cpm per Bq	cpm per Bq	cpm per Bq
Days following exposure	0	2.86E-04	2.75E-04	2.42E-06	1.90E-07
	1	3.35E-05	3.28E-05	8.61E-05	1.02E-06
	2	1.11E-05	1.16E-05	8.14E-05	6.12E-07
	3	4.69E-06	5.36E-06	7.48E-05	8.07E-07
	4	2.71E-06	3.41E-06	6.86E-05	9.83E-07
	5	2.15E-06	2.82E-06	6.28E-05	1.11E-06
	6	2.02E-06	2.65E-06	5.76E-05	1.20E-06
	7	2.01E-06	2.60E-06	5.27E-05	1.26E-06
	8	2.02E-06	2.57E-06	4.83E-05	1.29E-06
	9	2.02E-06	2.52E-06	4.42E-05	1.29E-06
	10	1.99E-06	2.46E-06	4.05E-05	1.28E-06
	20	1.26E-06	1.46E-06	1.65E-05	8.20E-07
	30	6.10E-07	6.91E-07	6.67E-06	3.97E-07

Table D.20 Count rate per Bq calculated for the Female phantom contaminated with I-131

		Back Right Lung	**Neck**	**Thigh**
		cpm per Bq	**cpm per Bq**	**cpm per Bq**
Days following exposure	0	2.66E-04	2.38E-06	2.51E-07
	1	3.17E-05	7.16E-05	9.49E-07
	2	1.09E-05	6.75E-05	5.65E-07
	3	4.99E-06	6.21E-05	7.42E-07
	4	3.26E-06	5.71E-05	9.03E-07
	5	2.80E-06	5.24E-05	1.02E-06
	6	2.73E-06	4.81E-05	1.10E-06
	7	2.75E-06	4.41E-05	1.15E-06
	8	2.77E-06	4.05E-05	1.18E-06
	9	2.77E-06	3.71E-05	1.19E-06
	10	2.73E-06	3.40E-05	1.18E-06
	20	1.72E-06	1.40E-05	7.53E-07
	30	8.28E-07	5.69E-06	3.64E-07

Table D.21 Count rate per Bq calculated for the Adipose Male phantom contaminated with I-131

		Back Right Lung	Neck	Thigh
		cpm per Bq	cpm per Bq	cpm per Bq
Days following exposure	0	1.83E-04	1.77E-06	1.07E-07
	1	2.18E-05	7.53E-05	9.03E-07
	2	7.44E-06	7.13E-05	5.42E-07
	3	3.39E-06	6.55E-05	7.19E-07
	4	2.18E-06	6.01E-05	8.77E-07
	5	1.86E-06	5.51E-05	9.94E-07
	6	1.81E-06	5.05E-05	1.07E-06
	7	1.82E-06	4.63E-05	1.12E-06
	8	1.83E-06	4.24E-05	1.15E-06
	9	1.82E-06	3.88E-05	1.16E-06
	10	1.80E-06	3.55E-05	1.15E-06
	20	1.13E-06	1.45E-05	7.34E-07
	30	5.45E-07	5.87E-06	3.56E-07

Table D.22 Count rate per Bq calculated for the Adipose Female phantom contaminated with I-131

		Back Right Lung	Neck	Thigh
		cpm per Bq	cpm per Bq	cpm per Bq
Days following exposure	0	1.99E-04	1.85E-06	1.76E-07
	1	2.39E-05	6.05E-05	1.37E-06
	2	8.20E-06	5.71E-05	8.45E-07
	3	3.79E-06	5.26E-05	1.12E-06
	4	2.48E-06	4.83E-05	1.37E-06
	5	2.13E-06	4.44E-05	1.55E-06
	6	2.07E-06	4.07E-05	1.68E-06
	7	2.08E-06	3.74E-05	1.75E-06
	8	2.09E-06	3.43E-05	1.79E-06
	9	2.09E-06	3.14E-05	1.80E-06
	10	2.06E-06	2.88E-05	1.79E-06
	20	1.29E-06	1.19E-05	1.14E-06
	30	6.20E-07	4.82E-06	5.54E-07

Table D.23 Count rate per Bq calculated for the Post-Menopausal Adipose Female phantom contaminated with I-131

		Back Right Lung	Neck	Thigh
		cpm per Bq	cpm per Bq	cpm per Bq
Days following exposure	0	1.94E-04	2.01E-06	1.63E-07
	1	2.32E-05	6.84E-05	6.89E-07
	2	7.94E-06	6.46E-05	4.05E-07
	3	3.64E-06	5.94E-05	5.29E-07
	4	2.35E-06	5.46E-05	6.42E-07
	5	2.00E-06	5.01E-05	7.25E-07
	6	1.93E-06	4.60E-05	7.82E-07
	7	1.93E-06	4.22E-05	8.18E-07
	8	1.94E-06	3.87E-05	8.37E-07
	9	1.93E-06	3.55E-05	8.41E-07
	10	1.90E-06	3.26E-05	8.34E-07
	20	1.18E-06	1.34E-05	5.33E-07
	30	5.67E-07	5.46E-06	2.58E-07

Table D.24 Count rate per Bq for the Child phantom contaminated with I-131

		Back Right Lung	Neck	Thigh
		cpm per Bq	cpm per Bq	cpm per Bq
Days following exposure	0	3.65E-04	2.22E-06	8.02E-07
	1	4.48E-05	5.43E-05	1.20E-06
	2	1.54E-05	5.06E-05	7.16E-07
	3	7.28E-06	4.71E-05	8.96E-07
	4	4.88E-06	4.38E-05	1.07E-06
	5	4.24E-06	4.06E-05	1.19E-06
	6	4.13E-06	3.77E-05	1.28E-06
	7	4.14E-06	3.49E-05	1.33E-06
	8	4.15E-06	3.23E-05	1.36E-06
	9	4.13E-06	2.98E-05	1.37E-06
	10	4.06E-06	2.75E-05	1.35E-06
	20	2.51E-06	1.20E-05	8.57E-07
	30	1.21E-06	4.98E-06	4.14E-07

Table D.25 Count Rate per Bq for the Male Phantom Contaminated with I-192

		Back Right Lung	Front Right Lung	Neck	Thigh
		cpm per Bq	cpm per Bq	cpm per Bq	cpm per Bq
Days following exposure	0	3.45E-04	3.31E-04	3.07E-06	1.73E-07
	1	1.35E-04	1.30E-04	1.76E-05	9.62E-06
	2	1.08E-04	1.04E-04	1.82E-05	9.45E-06
	3	9.71E-05	9.38E-05	1.80E-05	8.88E-06
	4	9.19E-05	8.88E-05	1.78E-05	8.58E-06
	5	8.89E-05	8.59E-05	1.77E-05	8.43E-06
	6	8.67E-05	8.38E-05	1.77E-05	8.36E-06
	7	8.48E-05	8.20E-05	1.76E-05	8.31E-06
	8	8.31E-05	8.04E-05	1.75E-05	8.28E-06
	9	8.15E-05	7.88E-05	1.74E-05	8.25E-06
	10	7.99E-05	7.73E-05	1.74E-05	8.22E-06
	20	6.64E-05	6.44E-05	1.68E-05	8.01E-06
	30	5.59E-05	5.43E-05	1.63E-05	7.77E-06

Table D.26 Count rate per Bq for the Female phantom contaminated with I-192

		Back Right Lung	Neck	Thigh
		cpm per Bq	cpm per Bq	cpm per Bq
Days following exposure	0	3.21E-04	3.14E-06	2.19E-07
	1	1.30E-04	1.84E-05	8.94E-06
	2	1.05E-04	1.90E-05	8.73E-06
	3	9.47E-05	1.88E-05	8.16E-06
	4	8.98E-05	1.87E-05	7.86E-06
	5	8.70E-05	1.85E-05	7.72E-06
	6	8.50E-05	1.85E-05	7.65E-06
	7	8.32E-05	1.84E-05	7.61E-06
	8	8.16E-05	1.83E-05	7.58E-06
	9	8.01E-05	1.82E-05	7.55E-06
	10	7.86E-05	1.82E-05	7.52E-06
	20	6.59E-05	1.76E-05	7.32E-06
	30	5.60E-05	1.70E-05	7.10E-06

Table D.27 Count rate per Bq for the Adipose Male phantom contaminated with I-192

		Back Right Lung	Neck	Thigh
		cpm per Bq	cpm per Bq	cpm per Bq
Days following exposure	0	2.23E-04	2.41E-06	7.28E-08
	1	8.97E-05	1.60E-05	8.57E-06
	2	7.24E-05	1.65E-05	8.44E-06
	3	6.53E-05	1.64E-05	7.94E-06
	4	6.19E-05	1.63E-05	7.67E-06
	5	6.00E-05	1.62E-05	7.55E-06
	6	5.86E-05	1.61E-05	7.48E-06
	7	5.73E-05	1.61E-05	7.44E-06
	8	5.62E-05	1.60E-05	7.41E-06
	9	5.52E-05	1.59E-05	7.38E-06
	10	5.42E-05	1.59E-05	7.36E-06
	20	4.54E-05	1.54E-05	7.17E-06
	30	3.85E-05	1.49E-05	6.95E-06

Table D.28 Count rate per Bq for the Adipose Female phantom contaminated with I-192

		Back Right Lung	Neck	Thigh
		cpm per Bq	cpm per Bq	cpm per Bq
Days following exposure	0	2.45E-04	2.37E-06	1.69E-07
	1	9.91E-05	1.56E-05	1.24E-05
	2	8.01E-05	1.61E-05	1.27E-05
	3	7.23E-05	1.60E-05	1.23E-05
	4	6.86E-05	1.59E-05	1.20E-05
	5	6.65E-05	1.58E-05	1.19E-05
	6	6.49E-05	1.57E-05	1.18E-05
	7	6.36E-05	1.57E-05	1.18E-05
	8	6.23E-05	1.56E-05	1.17E-05
	9	6.12E-05	1.55E-05	1.17E-05
	10	6.00E-05	1.55E-05	1.17E-05
	20	5.04E-05	1.50E-05	1.14E-05
	30	4.28E-05	1.45E-05	1.10E-05

Table D.29 Count rate per Bq for the Post-Menopausal Adipose Female phantom contaminated with I-192

		Back Right Lung	Neck	Thigh
		cpm per Bq	cpm per Bq	cpm per Bq
Days following exposure	0	2.40E-04	2.66E-06	7.67E-08
	1	9.63E-05	1.75E-05	6.71E-06
	2	7.77E-05	1.82E-05	6.43E-06
	3	7.00E-05	1.80E-05	5.90E-06
	4	6.64E-05	1.79E-05	5.63E-06
	5	6.43E-05	1.78E-05	5.51E-06
	6	6.28E-05	1.77E-05	5.45E-06
	7	6.14E-05	1.76E-05	5.42E-06
	8	6.02E-05	1.76E-05	5.39E-06
	9	5.91E-05	1.75E-05	5.37E-06
	10	5.80E-05	1.74E-05	5.36E-06
	20	4.86E-05	1.69E-05	5.21E-06
	30	4.12E-05	1.64E-05	5.06E-06

Table D.30 Count rate per Bq for the Child phantom contaminated with I-192

		Back Right Lung	Neck	Thigh
		cpm per Bq	cpm per Bq	cpm per Bq
Days following exposure	0	4.41E-04	4.31E-06	5.75E-07
	1	1.80E-04	3.12E-05	1.09E-05
	2	1.45E-04	3.23E-05	1.04E-05
	3	1.31E-04	3.20E-05	9.55E-06
	4	1.25E-04	3.17E-05	9.12E-06
	5	1.21E-04	3.16E-05	8.93E-06
	6	1.18E-04	3.14E-05	8.83E-06
	7	1.16E-04	3.13E-05	8.77E-06
	8	1.13E-04	3.12E-05	8.73E-06
	9	1.11E-04	3.10E-05	8.70E-06
	10	1.09E-04	3.09E-05	8.67E-06
	20	9.19E-05	3.00E-05	8.43E-06
	30	7.83E-05	2.90E-05	8.16E-06

REFERENCES

1. Anigstein, R., Erdman, M., King, S., Mauro, J., Miller, K., and Olsher, R. (2007). Use of Radiation Detection, Measuring, and Imaging Instruments to Assess Internal Contamination from Inhaled Radionuclides, Part I and Part II. S. Cohen & Associates, Contract Number 200-2002-00367

2. Argonne National Laboratory, (2002) Radiological Dispersal Device: Human Health Fact Sheet

3. Attix, F.H. (1986) Introduction to Radiological Physics and Radiation Dosimetry. (John Wiley and Sons, New York)

4. Capintec, Inc. Captus 3000 Thyroid Uptake System User's Manual. (2007)

5. Capintec, Inc. Website: www.capintec.com (Last accessed March, 2008)

6. DOE/NRC Interagency Working Group on Radiological Dispersal Devices. Radiological Dispersal Devices: An Initial Study To Identify Radioactive Materials of Greatest Concern And Approaches To Their Tracking, Tagging, And Disposition. Report to the Nuclear Regulatory Commission and the Secretary of Energy, May 2003.

7. Eckerman, K.F., Cristy, M., Ryman, J.C., The ORNL Mathematical Phantom Series, Oak Ridge National Laboratory, http://homer.hsr.gov/VLab/VLabPhan.html. (1996)

8. Eckerman, K.F., Sjoreen, A.L., Radiological Toolbox. ORNL/TM-2004/27R1.

9. Eckerman, K.F., et al, Dose and Risk Calculation Software. ORML/TM-2001/190.

10. International Commission on Radiological Protection (ICRP) (1975). Report of the Task Group on Reference Man. ICRP Publication 23.

11. International Commission on Radiological Protection (ICRP) (1977). Recommendations of the ICRP. ICRP Publication 26. Annals of the ICRP, Volume 3, No. 1-4.

12. International Commission on Radiological Protection (ICRP). (1979). Limits for Intakes by Workers. ICRP Publication 30, Part 1, Pergamon Press, Oxford.

13. International Commission on Radiological Protection (ICRP). (1983). Radionuclide Transformations Energy and Intensity of Emission. ICRP Publication 38, Pergamon Press, Oxford.

14. International Commission on Radiological Protection (ICRP). 1989. Age-Dependent Doses to Members of the Public from Intake of Radionuclides, Part 1. ICRP Publication 56, Pergamon Press, Oxford.

15. International Commission on Radiological Protection (ICRP) (1991). Recommendations of the ICRP. ICRP Publication 60. Annals of the ICRP, Volume 21, No 1-3.

16. International Commission on Radiological Protection (ICRP). (1993). Age-Dependent Doses to Members of the Public from Intake of Radionuclides, Part 2. ICRP Publication 67, Pergamon Press, Oxford.

17. International Commission on Radiological Protection (ICRP). (1994a). Human Respiratory Tract Model for Radiological Protection. ICRP Publication 66, Pergamon Press, Oxford.

18. International Commission on Radiological Protection (ICRP). (1994b). Dose Coefficients for Intakes of Radionuclides by Workers. ICRP Publication 68, Pergamon Press, Oxford.

19. International Commission on Radiological Protection (ICRP). (1995a). Age-Dependent Doses to Members of the Public from Intake of Radionuclides, Part 3. ICRP Publication 69, Pergamon Press, Oxford.

20. International Commission on Radiological Protection (ICRP). (1995b). Age-Dependent Doses to Members of the Public from Intake of Radionuclides, Part 4. ICRP Publication 71, Pergamon Press, Oxford.

21. International Commission on Radiological Protection (ICRP) (1996) 91 Age-dependent dose to members of the public from intake of radionuclides: Part 5 compilation of ingestion and inhalation dose coefficients. Annals of the ICRP, Volume 26, Issue 1

22. International Commission on Radiation Units and Measurements (ICRU). (1992). Phantoms and Computational Models in Therapy, Diagnosis, and Protection. ICRU Report 48. Bethesda, MD.

23. Knoll, G.F. (2000). Radiation Detection and Measurement, Third Edition. (John Wiley and Sons, New York).

24. Lorio, R. A. Feasibility of Determining Radioactivity in Lungs Using A Thyroid Uptake Counter: A Thesis Presented to the Faculty. Georgia Institute of Technology (2005).

25. Lugar, R.G. (2005) The Lugar Survey on Proliferation Threats and Responses. http://lugar.senate.gov/reports/NPSurvey.pdf. (Accessed February, 2008)

26. AISI 1000: Material composition of mild grain controlled steel. www.Matls.com (Accessed June, 2007).

27. Marcus, C.S., Siegel, J.A. Medical Management of Internally Radiocontaminated Patients. (2006)

28. Mathematica Version 6. Wolfram Research, Inc., 2007.

29. MCNP A General Monte Carlo N-Particle Transport Code Version 5, Volumes I, II, and III: User's Guide. LA-CP-03-0245. LANL x-5 Monte Carlo Team, April 2003.

30. National Council on Radiation Protection (NCRP) (1980). Management of Persons Accidentally Contaminated with Radionuclides, NCRP Report 65. Washington, DC.

31. NIOSH Dose Reconstruction Project. ORAUT-0TIB-0002, ORAUT-TKBS-0010-5, ORAUT-TKBS-0049, ORAUT-TKBS-003605.

32. NIST Standard Reference Materials. http://nist.gov/srm. (Accessed June, 2007)

33. Oliveira, C., Lourenco, M., Dantas, B., Lucena, E., Design and Operation of a Whole-body Monitoring System for the Goiania Radiation Accident. Health Physics. 60(1):51-55, January 1991.

34. Personal Communication with Dr. Armin Ansari. February 18, 2008.

35. Saint-Gobain Crystals NaI(Tl) Scintillation Material Properties Sheet. (2005)

36. Sandia National Laboratories. An Initial Study to Identify Materials of Greatest Concern for Use in a Radiological Dispersal Device. (2002)

37. Simpkins, R. Hertel, N. (2003) Neutron Organ Dose and the Influence of Adipose Tissue. American Nuclear Society, Radiation Protection and Shielding Division 12th Biennial Topical Meeting presentation

38. Smith, J., Ansari, A., Harper, F. (2005) Hospital Management of Mass Radiological Casualties: Reassessing Exposures from Contaminated Victims of an Exploded Radiological Dispersal Device. Health Physics. 89(5):513-520.

39. Sohier, A., Hardeman, F. (2006) Radiological Dispersion Devices: are we prepared? Journal of Environmental Radioactivity 85 pp 171-181.

40. Strom, D. (1998) False Alarms, True Alarms, and Statistics: Correct Usage of Decision Level and Minimum Detectable Amount. Health Physics Society, Continuing Education Lecture, Minneapolis, Minnesota, July 15, 1998.

41. Turner, J.E. (1995). Atoms, Radiation, and Radiation Protection, Second Edition. (John Wiley and Sons, New York).

42. Ueda, Normal Volume of the Thyroid Gland in Children. (1990) Journal of Clinical Ultrasound, Volume 18, Issue 6, pg 455-462.

43. Wang, Z, Hertel N. (2005) Determination of dosimetric characteristics of OptiSeed a plastic brachytherapy Pd-103 source. Applied Radiation and Isotopes, 63 (2005) pp 311-321.

44. White Rock Science (2004). Bodybuilder, http://www.whiterockscience.com/bodybuilder/bodybuilder.html.

45. X-5 Monte Carlo Team. (2003). MCNP – A General Monte Carlo N-Particle Transport Code, Version 5. LA-UR-03-1987.

46. X-5 Monte Carlo Team. (2003). VisEd Version 19L, November 2005.